

In Zusammenarbeit mit

THE UNIVERSITY *of York*

Advanced Array Signal Processing Techniques for Beamforming and Direction Finding

Masterarbeit

zur Erlangung des akademischen Grades Master of Science

vorgelegt von:	Jens Steinwandt
Matrikelnummer:	39733
geboren:	14. März 1986 in Leinefelde
Studiengang:	Elektrotechnik und Informationstechnik
Studienrichtung:	Informationstechnik und Kommunikationstechnik
Anfertigung im Fachgebiet:	Nachrichtentechnik Fakultät für Elektrotechnik und Informationstechnik
verantwortlicher Professor:	Univ.-Prof. Dr.-Ing. Martin Haardt
Erster wissenschaftlicher Betreuer:	Dr. Rodrigo C. de Lamare
Zweiter wissenschaftlicher Betreuer:	Univ.-Prof. Dr.-Ing. Martin Haardt
Datum:	9. Mai 2011

ACKNOWLEDGEMENTS

Firstly, I would like to express my sincere gratitude to Prof. Martin Haardt for giving me the chance to work on such an interesting topic under his supervision. His constant support of fresh ideas, comments and questions have encouraged me to go beyond what I believed would be my limits.

Secondly, I am very grateful to Dr. Rodrigo C. de Lamare for his help, valuable supervision and useful advice for my research, without which most of this work would not have been possible.

Further thanks go to all members of the Communications Research Group at the University of York and the members of the Communications Research Laboratory at Ilmenau University of Technology, for their support throughout my master's research.

I would like to thank my family, especially my mother, for constantly supporting me in many ways over the last year in York. I would not have made it to this point if you had not believed in me and encouraged me to discover my full potential.

Finally, I want to thank Lola for being there for me and for being the source of my strength.

ABSTRACT

Beamforming and direction of arrival estimation are areas of array signal processing devoted to extracting information of interest from signals received over the spatial aperture of an antenna array. The need for these techniques is encountered in a broad range of important engineering applications, including radar, sonar, wireless communications, radio astronomy and biomedicine, and is still a vital area of research.

In the first part, we focus on the development of widely-linear adaptive beamforming algorithms designed according to the constrained minimum variance (CMV) principle for strictly non-circular sources. Specifically, we devise three adaptive algorithms based on the Krylov subspace, applying the auxiliary vector filtering (AVF), the conjugate gradient (CG), and the modified conjugate gradient (MCG) algorithms, which avoid the covariance matrix inversion required by the constraint. The proposed adaptive algorithms fully exploit the second-order statistics of the strictly non-circular data and achieve significant performance gains.

The second part is concerned with direction finding algorithms in the beamspace domain. It is demonstrated that operation in beamspace substantially reduces the computational complexity while providing increased estimation performance compared to the element space. Therefore, two Krylov subspace-based algorithms, employing the AVF and the CG algorithm developed for direction finding, are extended to the beamspace processing. The development is followed by an extensive performance evaluation, highlighting their superior resolution performance for closely-spaced sources at a low SNR and a small sample size.

In the last part, we introduce a new strategy of incorporating prior knowledge for direction finding to improve the estimation performance of unknown signal sources. The novel approach is developed for situations with a limited data record and is based on an enhanced covariance matrix estimate obtained by linearly combining the sample covariance matrix and a prior known covariance matrix in an automatic fashion. As a result, knowledge-aided MUSIC-type and ESPRIT-type direction finding algorithms are devised and evaluated. Extensive studies to assess the performance illustrate that the exploitation of prior knowledge is translated into a significantly better estimation performance.

CONTENTS

Acknowledgements	i
Abstract	ii
Contents	iii
List of Figures	vi
List of Tables	viii
1. Introduction	1
1.1 Adaptive beamforming	1
1.2 Direction of arrival estimation	3
1.3 Overview and contributions	4
1.4 List of publications	5
2. System Model	7
2.1 Data model for direction of arrival estimation	7
2.2 Signal subspace estimation	9
2.2.1 True signal subspace	9
2.2.2 Direct data approach	10
2.2.3 Covariance approach	10
2.3 Data model for CMV beamforming	11
3. Widely-linear adaptive beamforming using Krylov-based algorithms	13
3.1 Introduction	13
3.2 LCMV beamforming	15
3.3 Non-circularity and WL-CMV beamforming	16
3.3.1 Non-circularity of signal sources	17
3.3.2 WL-CMV beamforming assuming strict non-circularity	17
3.4 Widely-linear beamforming based on the AVF algorithm	19
3.5 Widely-linear beamforming based on the CG algorithm	21
3.6 Widely-linear beamforming based on the MCG algorithm	24
3.7 Computational complexity	27
3.7.1 Complexity of LCMV algorithms	28
3.7.2 Complexity of WL-CMV algorithms	29
3.8 Simulation results	30
3.8.1 Performance in stationary scenarios	30
3.8.2 Performance in non-stationary scenarios	32

3.9	Conclusions	33
4.	Beamspace direction finding using Krylov subspace-based algorithms . .	35
4.1	Introduction	35
4.2	Beamspace processing	37
4.3	Beamspace transformation matrix	39
4.3.1	Discrete Fourier transform (DFT) beamspace	39
4.3.2	Discrete prolate spheroidal sequences (DPSS) beamspace	40
4.3.3	Comparison of the DFT and DPSS spatial filters	41
4.4	Beamspace direction finding based on the CG algorithm	41
4.5	Beamspace direction finding based on the AVF algorithm	43
4.6	Computational complexity	46
4.6.1	Subspace estimation via SVD	46
4.6.2	Subspace estimation via EVD	48
4.7	Simulation results	50
4.7.1	Comparison of the proposed algorithms in the DFT beamspace	50
4.7.2	Comparison of the DFT and DPSS beamspace	54
4.8	Conclusions	56
5.	Knowledge-aided direction of arrival estimation	57
5.1	Introduction	57
5.2	Enhanced covariance matrix estimation	59
5.2.1	Computation of the <i>a priori</i> covariance matrix	59
5.2.2	Problem statement	60
5.2.3	Computation of the optimal weight factors	61
5.2.4	Estimation of the optimal weight factors	65
5.2.5	Improved estimation of the optimal weight factors	65
5.3	General knowledge-aided direction of arrival estimation scheme	67
5.3.1	Structure of KA DOA estimation	68
5.3.2	Computational complexity	69
5.4	Knowledge-aided ESPRIT-type direction of arrival estimation	70
5.4.1	KA-ESPRIT	70
5.4.2	Unitary KA-ESPRIT	73
5.5	Knowledge-aided MUSIC-type direction of arrival estimation	78
5.5.1	KA-MUSIC	78
5.5.2	KA-Root-MUSIC	80
5.6	Simulations with accurate <i>a priori</i> knowledge	83
5.6.1	Comparison of LC1 and LC2 using KA-ESPRIT	83
5.6.2	Comparison of the proposed KA DOA estimation algorithms	88
5.6.3	Closely-spaced signal sources	92
5.6.4	Widely-spaced signal sources	92
5.6.5	Correlated signal sources	93
5.7	Simulations with inaccurate <i>a priori</i> knowledge	94
5.8	Conclusion	95
6.	Summary and future work	97

Appendix A. Derivations	99
A.1 Proof of equation (3.8)	99
A.2 Real-valued source symbols for strict non-circularity	100
A.3 Proof of equation (3.23)	101
A.4 Proof of equation (3.43)	101
A.5 Proof of equation (5.30)	102
Acronyms	103
Symbols and Notation	105
Bibliography	106
Theses	110
Erklärung	111

LIST OF FIGURES

2.1	Generic model of a ULA	7
2.2	Block diagram of a narrowband beamformer	11
3.1	Contour lines of complex Gaussian random variables with different ρ . .	17
3.2	Structure of the WL-AVF algorithm	19
3.3	Structure of the WL-CG algorithm	22
3.4	Structure of the WL-MCG algorithm	25
3.5	Computational complexity of LCMV and WL-CMV algorithms	28
3.6	Output SINR versus the snapshot number in a stationary scenario . . .	31
3.7	Output SINR versus the input SNR in a stationary scenario	31
3.8	Output SINR versus the snapshot number in a non-stationary scenario	32
4.1	Diagram of the beamspace environment	37
4.2	Comparison of the DFT and DPSS spatial filters	41
4.3	Complexity in terms of arithmetic operations applying the SVD	48
4.4	Complexity in terms of arithmetic operations applying the EVD	50
4.5	Probability of resolution versus the SNR in the DFT beamspace	52
4.6	Probability of resolution versus the snapshots in the DFT beamspace . .	52
4.7	RMSE versus the SNR in the DFT beamspace	53
4.8	Comparison of the DFT and DPSS beamspace regarding the probability of resolution versus the SNR	54
4.9	Comparison of the DFT and DPSS beamspace regarding the probability of resolution versus the snapshot number	55
4.10	Comparison of the DFT and DPSS beamspace regarding the RMSE versus the SNR	55
5.1	Block diagram of the KA DOA estimation scheme	68
5.2	Comparison of the LC_1 and LC_2 regarding the RMSE versus the SNR . .	84
5.3	Combination factors of the LC_1 and LC_2 versus the SNR	84
5.4	Comparison of the LC_1 and LC_2 regarding the RMSE versus the snapshots	85
5.5	Combination factors of the LC_1 and LC_2 versus the snapshot number . .	85

5.6	RMSE versus the SNR of KA-ESPRIT and forward-backward averaging	87
5.7	RMSE versus the snapshot number of KA-ESPRIT and forward-backward averaging	87
5.8	Comparison of KA-ESPRIT-type algorithms	89
5.9	Comparison of Unitary KA-ESPRIT-type algorithms	89
5.10	Comparison of all the proposed KA algorithms	90
5.11	Comparison of KA-MUSIC-type and constrained MUSIC-type algorithms	91
5.12	Comparison of the proposed KA algorithms for closely-spaced sources .	92
5.13	Comparison of the proposed KA algorithms for widely-spaced sources .	93
5.14	Comparison of the proposed KA algorithms for correlated sources . . .	94
5.15	Comparison of the proposed KA algorithms with inaccurate knowledge	95

LIST OF TABLES

3.1	The proposed WL-AVF algorithm	21
3.2	The proposed WL-CG algorithm	24
3.3	The proposed WL-MCG algorithm	27
3.4	Computational complexity of LCMV beamforming algorithms	29
3.5	Computational complexity of WL-CMV beamforming algorithms	29
4.1	The proposed DFT BS CG algorithm	43
4.2	The proposed DFT BS AVF algorithm	45
4.3	Number of additions applying the SVD	47
4.4	Number of multiplications applying the SVD	47
4.5	Number of additions applying the EVD	49
4.6	Number of multiplications applying the EVD	49
5.1	Computational complexity of the proposed versions of the KA scheme	69
5.2	The proposed KA-ESPRIT algorithm	72
5.3	The proposed Unitary KA-ESPRIT algorithm	77
5.4	The proposed KA-MUSIC algorithm	80
5.5	The proposed KA-Root-MUSIC algorithm	82

1. INTRODUCTION

Array signal processing is an active area of research in the broad field of signal processing, and focuses on the problem of estimating signal parameters from data collected over the spatial aperture of an antenna array, where the sensors are placed at distinct spatial locations. The given estimation task is usually associated with the extraction of desired information from impinging signals in the presence of noise and interference. The antenna array addresses the estimation problem by exploiting the spatial separation of the sensor elements to capture the propagating wavefronts, which originate from energy-radiating sources. Common signal parameters of interest to be estimated are the signal content itself, the directions of arrival of the signals, and their power. To obtain this information, the sensor array data is processed using statistical and adaptive signal processing techniques. These schemes include parameter estimation and adaptive filtering applied to array signal processing. The underlying set of principles and techniques for sensor array signal processing is applicable in many versatile areas [1, 2], including wireless communications, radar, sonar, biomedicine, seismology and astronomy.

Among the most relevant topics within array signal processing are beamforming [1] and direction of arrival estimation [1], which present inevitable challenges when designing wireless communications systems. As this thesis focuses on the advancement of these techniques for communications, the main problems to be solved are interference suppression, source localization, source tracking, complexity reduction and general performance improvements. For the sake of simplicity, the novel strategies developed in this work rely on the use of a uniform linear sensor array. An extension to arbitrary array geometries will be addressed in future work.

1.1 Adaptive beamforming

A ubiquitous task in array signal processing is the extraction of desired information from propagating signals originating from a certain direction by employing an antenna array equipped with multiple sensors. The array records the radiating wavefronts and produces an observation vector at a given time instant, which is processed to obtain the

information of interest. The most straightforward strategy to achieve this objective is the weighted linear combination of the signals received at multiple spatially separated sensor elements. By selecting the appropriate weights, signals from a particular direction can be emphasized while attenuating interfering signals from other directions. This weighting process is referred to as beamforming or spatial filtering [2, 3]. Generally, the steering of beams into specific angles by constructing the weights is equivalent to designing a frequency-selective finite impulse response (FIR) filter for temporal signals. The weighting applied to the received signal at each sensor element can either be fixed and data-independent, or continuously adapted to track changes in the system and to reject interference. The latter approach, termed adaptive beamforming, evidently provides a better performance and is the focus of this thesis.

The adaptive algorithms used to adjust the weights for each sensor element are designed by optimizing certain criteria according to the given properties. One of the most relevant design criteria in practice is the constrained minimum variance (CMV) approach [4], which does not require the transmission of a known training sequence and only implies knowledge of the array geometry and the angle of the desired signal. The CMV optimality criterion minimizes the total beamformer output power while constraining the array response in the direction of the desired signal to be constant. Due to its simplicity and effectiveness much effort has been devoted over the past few decades to devise efficient adaptive algorithms in order to realize a practical beamformer design [1, 3, 5]. Among the existing adaptive algorithms, the least mean squares (LMS) method [5] as a representative of the low-complexity stochastic gradient techniques adopts gradient vectors for the iterative computation of the weights and yields an acceptable performance in many applications. However, its efficacy strongly depends on the step size and the eigenvalue spread of the covariance matrix, resulting in an insufficient convergence performance for certain scenarios [3]. An alternative method is the recursive least squares (RLS) algorithm [5], which is independent of the eigenvalue spread and thus attains a fast convergence speed. Nevertheless, its main drawbacks are numerical instability and a relatively high complexity. An attractive trade-off between the performance and the complexity of the LMS method and the RLS technique is achieved by the conjugate gradient (CG) algorithm [6, 7] originally derived to solve a linear system of equations. It forms successive residual vectors within a number of iterations in order to update the beamforming weight vector, requiring a lower computational cost compared to the RLS method for few iterations and providing a faster convergence rate than the LMS approach. A modified version of the CG (MCG) algorithm derived to obtain further reduction of the complexity while maintaining the same performance level was proposed in [8]. Another adaptive algorithm

that has received considerable interest is the auxiliary vector filtering (AVF) technique [9]. Similarly to the CG method, it utilizes an iterative procedure to update the weight vector by adopting auxiliary vectors to approach the optimal solution. The AVF algorithm was shown to outperform the performance of the RLS method with regard to the convergence speed and the steady-state level, and to be the state-of-the-art algorithm for adaptive beamforming [9].

1.2 Direction of arrival estimation

A second problem, which is extensively studied as part of the general field of array signal processing, is the estimation of the direction of arrival (DOA). The objective is to determine the angle of arrival of a given spatially propagating signal relative to the antenna array. To this end, the spatial separation of multiple sensor elements is exploited to obtain the location of the energy-radiating source. The result of the estimation procedure is subsequently used for the beamforming design described in the previous section to steer the beam towards this specific direction, in order to capture or radiate maximal power. With the field of applications involving DOA estimation constantly expanding, numerous direction finding techniques have been devised over the past few decades [1, 10]. The most well-known parameter estimation strategies discussed here can be classified into three main categories, namely conventional [11], subspace-based [12–17], and maximum likelihood (ML) methods [18].

The concept of the conventional DOA estimation algorithms relies on the beamforming principle. These techniques successively steer the main beam in all possible look directions and measure the output power [10], which is recorded in the form of a pseudo spectrum over the angle range. The largest peaks in the pseudo spectrum are associated with the DOA estimates. The most prominent approach within this class is Capon's method [11] based on the CMV criterion [4]. It minimizes the power induced by interfering signals and noise while keeping the gain towards the look direction fixed. Although the implementation of the conventional techniques is simple, they suffer from a lack of angular resolution and require a large number of sensors to achieve a higher resolution.

The class of subspace-based methods exploits a spectral decomposition of the covariance matrix to achieve high-resolution DOA estimates. Among the most relevant techniques are the multiple signal classification (MUSIC) [12], its extension Root-MUSIC [13], the estimation of signal parameters via rotational invariance techniques (ESPRIT) [14], its enhancement Unitary ESPRIT [15] and the recently proposed auxiliary vector filtering (AVF) [16] and conjugate gradient (CG) [17] algorithms developed for direction

finding. The MUSIC-type and the ESPRIT-type algorithms exploit the eigen-structure of the covariance matrix, allowing a decomposition of the observation space into a signal subspace and a complementary noise subspace. Specifically, MUSIC scans over the possible angle range and makes use of the orthogonality of the subspaces to obtain a pseudo spectrum with increased resolution. The extension Root-MUSIC for uniform linear arrays avoids the exhaustive search for peaks by applying a polynomial rooting technique. The ESPRIT-type algorithms avoid the exhaustive peak search by dividing the sensor array into two identical subarrays and benefit from the uniform displacement of the subarrays. The Unitary ESPRIT additionally takes advantage of the fact that the phase factors representing the displacement lie on the unit circle. The recently developed AVF and CG algorithms iteratively generate an extended non-eigen-based signal subspace containing the true signal subspace and the scanning vector itself. The DOA estimates are determined by the search for the collapse of the extended signal subspace as the scanning vector belongs to it. Whereas the AVF algorithm adopts auxiliary vectors to form the extended signal subspace, the CG method applies residual vectors and can be considered as an extension of the AVF technique. Both approaches provide high-resolution estimates at a low signal-to-noise ratio, and a small sample size.

ML-type methods are based on a parametric approach. They effectively exploit the underlying data model, resulting in sufficiently high accuracy superior to the conventional and subspace-based methods. However, the efficiency is at the expense of the computational intensity as a multidimensional search is required. An iterative approach to limit the computational effort is the alternating projection technique [18], which transforms the optimization problem into a sequence of one-dimensional optimization problems.

1.3 Overview and contributions

In this work, we deal with the advancement of array signal processing algorithms for the applications of beamforming and direction finding, which are of significant relevance in wireless communications.

Chapter 2 introduces the system model for array signal processing, focusing on the subspace estimation for direction finding and the CMV criterion-based design for adaptive beamforming.

Chapter 3 is concerned with the first major contribution, which is the development of adaptive beamforming methods using Krylov-based algorithms for non-circular

sources. By exploiting the widely-linear property that some of the signal sources are non-circular, an improved performance can be achieved. Three efficient widely-linear adaptive algorithms based on the AVF, the CG and the MCG algorithms, which avoid the computation of the inverse of the covariance matrix are derived according to the CMV criterion. Furthermore, their performance compared to the linear versions is investigated and the complexity analyzed.

Chapter 4 deals with the extension of the Krylov subspace-based DOA estimation algorithms to the operation in beamspace, which is the second major contribution. The operation in the beamspace domain allows for a significant reduction of the complexity while substantially increasing the estimation performance. The AVF and CG-based direction finding techniques are developed for two different beamspace designs, providing improved performance over their counterparts in element space. Complexity and performance assessments are also conducted.

Chapter 5 addresses the third contribution, focusing on knowledge-aided DOA estimation. By exploiting *a priori* knowledge of some of the DOAs to be estimated, the estimation accuracy of the unknown signal directions can be significantly enhanced. A novel way of incorporating the prior knowledge for situations of a limited data record and a low signal-to-noise ratio is developed. The proposed scheme is applied to ESPRIT-type and MUSIC-type algorithms and the impact of the knowledge on the estimation performance is extensively studied.

Chapter 6 concludes the key properties covered in this work, emphasizing the relevance for the scientific community and discussing possible topics for future work.

1.4 List of publications

Some of the research work outlined in this thesis has already been published. A list of the conference papers is provided below.

Conference Papers

1. J. Steinwandt, R. C. de Lamare, L. Wang, N. Song, and M. Haardt, "Widely linear adaptive beamforming algorithm based on the conjugate gradient method," *International ITG Workshop on Smart Antennas (WSA)*, (Aachen, Germany), Feb. 2011.

-
2. J. Steinwandt, R. C. de Lamare, and M. Haardt, "Beamspace direction finding based on the conjugate gradient algorithm," *International ITG Workshop on Smart Antennas (WSA)*, (Aachen, Germany), Feb. 2011.
 3. N. Song, J. Steinwandt, L. Wang, R. C. de Lamare, and M. Haardt, "Non-data-aided adaptive beamforming algorithm based on the widely linear auxiliary vector filter," *IEEE International Conference on Acoustics, Speech, and Signal Processing (ICASSP)*, (Prague, Czech Republic), May 2011.

2. SYSTEM MODEL

This chapter presents the system model of the antenna array output at the receiver, which provides the basis for the development of array signal processing algorithms. Although the problems of adaptive beamforming and DOA estimation are different, the fundamental model used for them is very similar. As stated earlier, the developments throughout this work are based on the use of a uniform linear array (ULA). Hence, the introduced system model is only valid for this class of array geometries.

2.1 Data model for direction of arrival estimation

Considering a spherical coordinate system, the DOA of an incident wavefront can be determined by estimating the azimuth angle θ and the elevation angle ϕ . For the sake of simplicity, we limit this model to the one-dimensional case, assuming that the wavefront impinges on the sensor array in the horizontal plane, i.e. $\phi = \pi/2$, so that the azimuth angle θ entirely specifies the DOA. Corresponding to the schematic array structure in Figure 2.1, additional assumptions to describe the system model are to be made:

- The propagating wavefronts are assumed to be radiated by point sources.
- The sources are considered to be in the far field and the wavefronts are approximately planar.

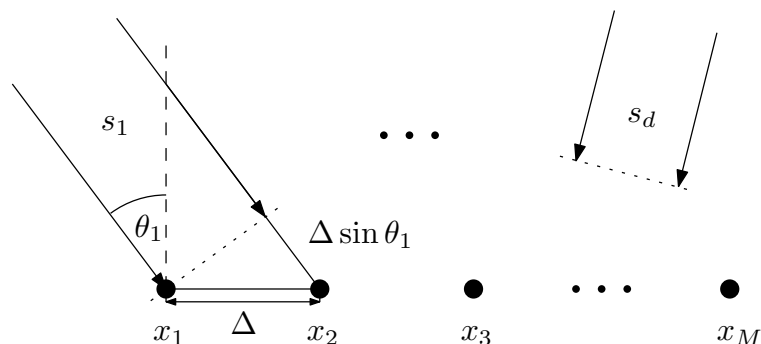


Fig. 2.1: Generic model of a ULA.

- The signals are narrowband signals, so that a time delay corresponds to a phase shift.
- The sensors are omni-directional, there is no coupling between them and the array is perfectly calibrated.

Let us suppose that an M -element sensor array receives d ($d < M$) propagating wavefronts with the distinct DOAs $\boldsymbol{\theta} = [\theta_1, \dots, \theta_d]^T$ relative to the broad side of the array. The i th of N available data snapshots of the $(M \times 1)$ -dimensional array output vector can be modeled as

$$\mathbf{x}(i) = \begin{bmatrix} \mathbf{a}(\theta_1) & \cdots & \mathbf{a}(\theta_d) \end{bmatrix} \begin{bmatrix} \mathbf{s}_1(i) \\ \vdots \\ \mathbf{s}_d(i) \end{bmatrix} + \mathbf{n}(i) = \mathbf{A}(\boldsymbol{\theta})\mathbf{s}(i) + \mathbf{n}(i), \quad i = 1, \dots, N, \quad (2.1)$$

where $\mathbf{A}(\boldsymbol{\theta}) \in \mathbb{C}^{M \times d}$ is the array steering matrix, whose columns are functions of the unknown DOAs. The zero-mean vector $\mathbf{s}(i) \in \mathbb{C}^{d \times 1}$ represents the impinging complex waveforms of the d signals and $\mathbf{n}(i) \in \mathbb{C}^{M \times 1}$ is the additive vector of white circularly symmetric complex Gaussian noise with zero mean and variance σ_n^2 .

Considering a ULA equipped with equally spaced sensors as shown in Figure 2.1, the $(M \times 1)$ steering vectors $\mathbf{a}(\theta_n)$ corresponding to the n th source, $n = 1, \dots, d$, can be expressed as

$$\mathbf{a}(\theta_n) = \left[1 \quad e^{j2\pi \frac{\Delta}{\lambda_c} \sin \theta_n} \quad \cdots \quad e^{j2\pi(M-1) \frac{\Delta}{\lambda_c} \sin \theta_n} \right]^T, \quad (2.2)$$

where Δ denotes the distance of adjacent sensors of the ULA and λ_c is the signal wavelength. In order to avoid spatial aliasing, Δ is restricted to $\Delta \leq \lambda_c/2$ in which case the DOAs are limited to the interval $-90^\circ < \theta_n < 90^\circ$. Defining the spatial frequencies $\mu_n \in [-\pi, \pi]$ as a result of the geometry in Figure 2.1 as

$$\mu_n = 2\pi \frac{\Delta}{\lambda_c} \sin \theta_n, \quad (2.3)$$

the model stated in (2.1) can be written as

$$\mathbf{x}(i) = \begin{bmatrix} 1 & 1 & \cdots & 1 \\ e^{j\mu_1} & e^{j\mu_2} & \cdots & e^{j\mu_d} \\ \vdots & \vdots & & \vdots \\ e^{j(M-1)\mu_1} & e^{j(M-1)\mu_2} & \cdots & e^{j(M-1)\mu_d} \end{bmatrix} \mathbf{s}(i) + \mathbf{n}(i), \quad (2.4)$$

where the array steering matrix $\mathbf{A}(\boldsymbol{\theta})$ exhibits the Vandermonde structure. Given the entire data of the N snapshots, (2.4) can also be expressed compactly as

$$\mathbf{X} = [\mathbf{x}_1 \ \cdots \ \mathbf{x}_N] = \mathbf{A}(\boldsymbol{\theta})\mathbf{S} + \mathbf{N} \in \mathbb{C}^{M \times N}. \quad (2.5)$$

2.2 Signal subspace estimation

The DOA estimation techniques considered in this work belong to the class of subspace-based algorithms. Therefore, a brief review of the fundamental properties is covered in this section.

2.2.1 True signal subspace

Due to the fact that the source data $\mathbf{s}(i)$ and the noise vector $\mathbf{n}(i)$ are modeled as uncorrelated random variables, the covariance matrix of the noise-corrupted zero-mean array output $\mathbf{x}(i)$ is calculated by

$$\mathbf{R} = \mathbb{E}\{\mathbf{x}(i)\mathbf{x}^H(i)\} = \mathbf{A}(\boldsymbol{\theta})\mathbf{R}_{ss}\mathbf{A}^H(\boldsymbol{\theta}) + \sigma_n^2\mathbf{I}_M \in \mathbb{C}^{M \times M}, \quad (2.6)$$

where $\mathbf{R}_{ss} = \mathbb{E}\{\mathbf{s}(i)\mathbf{s}^H(i)\}$ is the signal covariance matrix, which is diagonal if the sources are uncorrelated and nondiagonal for partially correlated sources. The noise covariance matrix $\mathbb{E}\{\mathbf{n}(i)\mathbf{n}^H(i)\} = \sigma_n^2\mathbf{I}_M$, where \mathbf{I}_M denotes the $M \times M$ identity matrix.

The eigenvalue decomposition (EVD) of the covariance matrix \mathbf{R} can be expressed as

$$\mathbf{R} = [\mathbf{U}_s \ \mathbf{U}_n] \left(\begin{bmatrix} \boldsymbol{\Lambda}_d & \mathbf{0} \\ \mathbf{0} & \mathbf{0} \end{bmatrix} + \sigma_n^2\mathbf{I}_M \right) \begin{bmatrix} \mathbf{U}_s^H \\ \mathbf{U}_n^H \end{bmatrix} \quad (2.7)$$

where the diagonal matrix $\boldsymbol{\Lambda}_d = \text{diag}\{\lambda_n\}_{n=1}^d$ consists of the nonzero eigenvalues, and \mathbf{U}_s and \mathbf{U}_n represent the orthogonal eigenvectors corresponding to the d largest eigenvalues and the $M - d$ smallest eigenvalues, respectively. The matrix \mathbf{U}_s is often referred to as signal subspace \mathcal{S} and its orthogonal complement \mathbf{U}_n is termed noise subspace. Without additive noise, i.e., $\sigma_n^2 = 0$, it is evident from

$$\mathbf{R} = \mathbf{A}(\boldsymbol{\theta})\mathbf{R}_{ss}\mathbf{A}^H(\boldsymbol{\theta}) = \mathbf{U}_s\boldsymbol{\Lambda}_d\mathbf{U}_s^H \quad (2.8)$$

that $\mathbf{A}(\boldsymbol{\theta})$ and \mathbf{U}_s span the same signal subspace \mathcal{S} of dimension d , i.e.,

$$\mathcal{S} = \text{span}\{\mathbf{A}(\boldsymbol{\theta})\} = \text{span}\{\mathbf{U}_s\}. \quad (2.9)$$

2.2.2 Direct data approach

In the direct data approach, a singular value decomposition (SVD) of the array output matrix \mathbf{X} is performed to estimate the signal and the noise subspace. Assuming that the number of sources d , i.e., the rank, is known, \mathbf{X} can be written as

$$\mathbf{X} = \begin{bmatrix} \hat{\mathbf{U}}_s & \hat{\mathbf{U}}_n \end{bmatrix} \begin{bmatrix} \hat{\mathbf{\Sigma}}_s & \mathbf{0} \\ \mathbf{0} & \hat{\mathbf{\Sigma}}_n \end{bmatrix} \begin{bmatrix} \hat{\mathbf{V}}_s^H \\ \hat{\mathbf{V}}_n^H \end{bmatrix} \quad (2.10)$$

$$= \hat{\mathbf{U}}_s \hat{\mathbf{\Sigma}}_s \hat{\mathbf{V}}_s^H + \hat{\mathbf{U}}_n \hat{\mathbf{\Sigma}}_n \hat{\mathbf{V}}_n^H, \quad (2.11)$$

where the diagonal matrices $\hat{\mathbf{\Sigma}}_s$ and $\hat{\mathbf{\Sigma}}_n$ contain the d largest singular values and the $M - d$ smallest singular values, respectively. The estimated signal subspace $\hat{\mathbf{U}}_s \in \mathbb{C}^{M \times d}$ comprises the singular vectors corresponding to $\hat{\mathbf{\Sigma}}_s$ and the noise subspace $\hat{\mathbf{U}}_n \in \mathbb{C}^{M \times (M-d)}$ is associated with $\hat{\mathbf{\Sigma}}_n$. If only the signal subspace is to be estimated a rank- d approximation of the SVD can be applied.

2.2.3 Covariance approach

In practical applications, the true covariance matrix \mathbf{R} is unknown and needs to be estimated. A widely used estimator for \mathbf{R} is a sample-averaged approach, termed sample covariance matrix, which is given by

$$\hat{\mathbf{R}} = \frac{1}{N} \sum_{i=1}^N \mathbf{x}(i) \mathbf{x}^H(i) = \frac{1}{N} \mathbf{X} \mathbf{X}^H \in \mathbb{C}^{M \times M}. \quad (2.12)$$

Again, assuming the rank d is known, the EVD of the sample covariance matrix $\hat{\mathbf{R}}$ yields

$$\tilde{\mathbf{R}} = \begin{bmatrix} \hat{\mathbf{U}}_s & \hat{\mathbf{U}}_n \end{bmatrix} \begin{bmatrix} \hat{\mathbf{\Lambda}}_s & \mathbf{0} \\ \mathbf{0} & \hat{\mathbf{\Lambda}}_n \end{bmatrix} \begin{bmatrix} \hat{\mathbf{U}}_s^H \\ \hat{\mathbf{U}}_n^H \end{bmatrix} \quad (2.13)$$

$$= \hat{\mathbf{U}}_s \hat{\mathbf{\Lambda}}_s \hat{\mathbf{U}}_s^H + \hat{\mathbf{U}}_n \hat{\mathbf{\Lambda}}_n \hat{\mathbf{U}}_n^H, \quad (2.14)$$

where the diagonal matrices $\hat{\mathbf{\Lambda}}_s$ and $\hat{\mathbf{\Lambda}}_n$ contain the d largest eigenvalues and the $M - d$ smallest eigenvalues, respectively. The estimated signal subspace $\hat{\mathbf{U}}_s \in \mathbb{C}^{M \times d}$ is composed of the eigenvectors corresponding to $\hat{\mathbf{\Lambda}}_s$ and the noise subspace $\hat{\mathbf{U}}_n \in \mathbb{C}^{M \times (M-d)}$ complies with $\hat{\mathbf{\Lambda}}_n$. If only the signal subspace is to be estimated a rank- d approximation of the EVD can be applied. Both the direct data approach and the covariance approach are theoretically equivalent.

2.3 Data model for CMV beamforming

In order to describe adaptive beamforming techniques according to the constrained minimum variance (CMV) principle, the same assumptions on the impinging wavefronts as in the previous section are presumed. However, for the system model, we do not restrict the sensor array to be a ULA as this property is not required by the adaptive algorithms. Furthermore, we use a slightly different notation to distinguish between the problems of DOA estimation and adaptive beamforming.

Assume that d narrowband signals from sources in the far field are impinging on an arbitrarily formed array of M ($M \geq d$) sensor elements with the DOAs $\boldsymbol{\theta} = [\theta_1, \dots, \theta_d]^T$. The i th of N available data snapshots of the $(M \times 1)$ -dimensional array output vector can be modeled as

$$\mathbf{r}(i) = \mathbf{A}(\boldsymbol{\theta})\mathbf{P}^{1/2}\mathbf{s}(i) + \mathbf{n}(i), \quad i = 1, \dots, N, \quad (2.15)$$

where the zero-mean vector $\mathbf{s}(i) = [s_1(i), \dots, s_d(i)]^T \in \mathbb{C}^{d \times 1}$ represents the complex signal waveforms, $\mathbf{P} = \text{diag}\{\sigma_1^2, \dots, \sigma_d^2\}$ contains the signal powers on its diagonal, $\mathbf{n}(i) \in \mathbb{C}^{M \times 1}$ is the vector of white circularly symmetric complex Gaussian noise with zero mean and variance σ_n^2 , and the matrix $\mathbf{A}(\boldsymbol{\theta}) = [\mathbf{a}(\theta_1), \dots, \mathbf{a}(\theta_d)] \in \mathbb{C}^{M \times d}$ consists of the array steering vectors corresponding to the d sources.

Corresponding to Figure 2.2, the output of the adaptive beamformer is generated by appropriately weighting the sum of the signals at each sensor element. Then, the output signal is sent back to the adaptive processor to update the weights subject to the optimization of a cost function. The weighting process can be mathematically

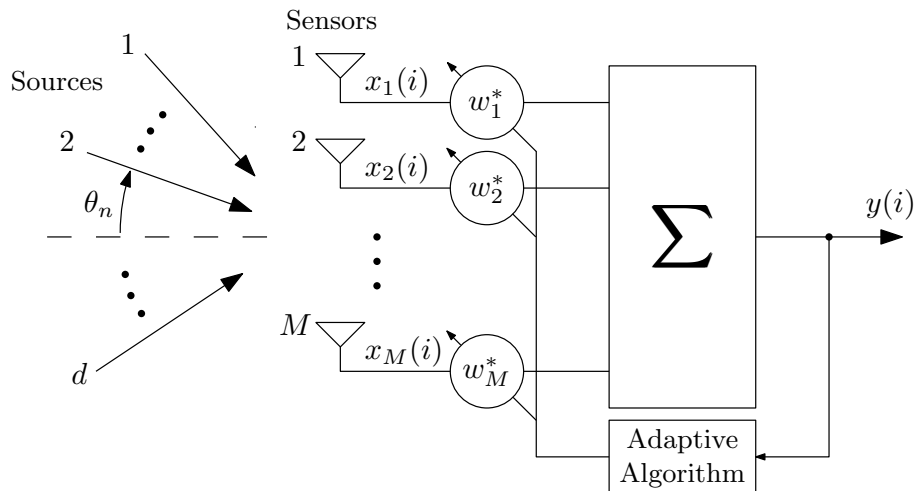


Fig. 2.2: Block diagram of a narrowband beamformer.

expressed as

$$y(i) = \mathbf{w}^H \mathbf{r}(i), \quad (2.16)$$

where $\mathbf{w} = [w_1, \dots, w_M]^T \in \mathbb{C}^{M \times 1}$ is the complex beamforming weight vector to be designed. After estimating the DOAs in the environment and selecting a particular source of interest with the signal direction θ_1 , the beamformer output in (2.16) can be expanded as

$$y(i) = \sqrt{\sigma_1^2} \mathbf{w}^H \mathbf{a}(\theta_1) s_1(i) + \mathbf{w}^H \left(\sum_{k=2}^K \sqrt{\sigma_k^2} \mathbf{a}(\theta_k) s_k(i) + \mathbf{n}(i) \right) \quad (2.17)$$

$$= \sqrt{\sigma_1^2} \mathbf{w}^H \mathbf{a}(\theta_1) s_1(i) + \mathbf{w}^H \mathbf{u}(i), \quad (2.18)$$

where $\mathbf{u}(i)$ is the vector containing the interferers and the additive noise. The objective is to keep the gain in the direction of the desired user fixed, i.e., $\mathbf{w}^H \mathbf{a}(\theta_1) = \gamma$ and the gain of the interferers small $\mathbf{w}^H \mathbf{u}(i) \approx 0$. This can be achieved by CMV beamforming, which formulates the objective as the constrained optimization problem

$$\begin{aligned} \mathbf{w}_{\text{opt}} = \underset{\mathbf{w}}{\text{argmin}} \quad & \mathbb{E} \{ |y(i)|^2 \} = \mathbb{E} \{ |\mathbf{w}^H \mathbf{r}(i)|^2 \} = \mathbf{w}^H \mathbf{R} \mathbf{w} \\ \text{subject to} \quad & \mathbf{w}^H \mathbf{a}(\theta_1) = \gamma, \end{aligned} \quad (2.19)$$

where the covariance matrix \mathbf{R} is estimated by the sample covariance matrix $\hat{\mathbf{R}}$ defined in (2.12). The goal of (2.19) is to minimize the array output variance while maintaining the response in the direction of the SOI.

Applying the method of Lagrange multipliers, the optimal solution for the minimization problem is

$$\mathbf{w}_{\text{opt}} = \frac{\gamma \mathbf{R}^{-1} \mathbf{a}(\theta_1)}{\mathbf{a}^H(\theta_1) \mathbf{R}^{-1} \mathbf{a}(\theta_1)}. \quad (2.20)$$

Setting the constant $\gamma = 1$ yields the so-called minimum variance distortionless response (MVDR). Note that the CMV criterion requires the knowledge of the DOA θ_1 of the desired user and the array geometry to form the steering vector $\mathbf{a}(\theta_1)$. Further details and a classification into linear CMV (LCMV) and widely-linear CMV (WLCMV) will be discussed in the next chapter.

3. WIDELY-LINEAR ADAPTIVE BEAMFORMING USING KRYLOV-BASED ALGORITHMS

In this chapter, we develop three widely-linear constrained adaptive beamforming algorithms based on the Krylov subspace, which are designed according to the minimum variance principle. The proposed algorithms apply either the auxiliary vector filtering (AVF) algorithm, the conjugate gradient (CG) algorithm or the modified conjugate gradient (MCG) algorithm to iteratively update the beamforming weight vector. By exploiting the non-circularity of impinging signals via a widely-linear processing technique, the output performance of these adaptive algorithms can be significantly improved.

3.1 Introduction

Adaptive beamforming is an essential approach for estimating the properties of a signal of interest at the sensor array output by weighting and combining the received signals to filter the desired user and to reject interference. The key advantage of the adaptive architecture is its ability to automatically adjust its weights to suit differences in the observed scenario. This includes tracking of moving interferers, or adaptation to leaving or entering signal sources in the system. Given its vast importance in multiple fields such as radar, sonar, biomedicine and wireless communications, adaptive beamforming has received considerable attention in the last few decades and numerous algorithms have been reported [5]. One of the most popular criteria for designing a beamformer is the linearly constrained minimum variance (LCMV) concept [4], which minimizes the variance at the array output while maintaining a desired response in the direction of the source of interest (SOI). This design criterion only requires the knowledge of the steering vector of the desired signal.

In most existing estimation and filtering algorithms, it is often assumed that the received vector $\mathbf{r}(i)$ is second-order circular as for quadrature phase-shift keying (QPSK)-

modulated signals, where the conventional covariance matrix

$$\mathbf{R} = \mathbb{E} \left\{ \mathbf{r}(i) \mathbf{r}^H(i) \right\} \in \mathbb{C}^{M \times M} \quad (3.1)$$

fully describes the second-order statistics. However, in many modern telecommunications and satellite systems based on binary phase-shift keying (BPSK)-modulated or amplitude-shift keying (ASK)-modulated signals, the observation signal $\mathbf{r}(i)$ features second-order non-circularity, i.e., the complementary covariance matrix

$$\mathbf{C} = \mathbb{E} \left\{ \mathbf{r}(i) \mathbf{r}^T(i) \right\} \neq \mathbf{0} \in \mathbb{C}^{M \times M} \quad (3.2)$$

and thus needs to be considered to optimally characterize the statistical properties of the signals [19]. It was recently shown that fully exploiting the second-order statistics, referred to as widely-linear (WL) processing, substantially improves the output performance compared to that in the linear processing [19–21]. Consequently, several widely-linear adaptive beamforming algorithms comprising the WL minimum variance distortionless response (WL-MVDR) algorithm [21] and the WL recursive least squares (WL-RLS) algorithm [22] have been devised. These approaches are either based on the assumption of weak non-circularity [21] or strict non-circularity [22] of the signals. A slight drawback associated with the strategy of widely-linear processing is the increased complexity due to the extended dimensions as both the originally observed data vector $\mathbf{r}(i)$ and its complex conjugate $\mathbf{r}^*(i)$ need to be processed. As the filtered data ordinarily occupies a large sample size and also, largely equipped sensor arrays are utilized in practice, the widely-linear processing scheme further slows down the convergence speed of the adaptive algorithms.

Among the well-established linearly constrained adaptive algorithms are the least mean squares (LMS) approach [5], which requires a low computational complexity but exhibits a slow convergence, and the recursive least squares (RLS) algorithm [5] that converges fast but suffers from a high computational burden. Two more recently developed adaptive beamforming algorithms, namely the auxiliary vector filtering (AVF) algorithm [9] and the conjugate gradient (CG) algorithm [8] [23], rely on the Krylov subspace and iteratively update the filter weights in a stochastic gradient fashion. The AVF algorithm is known to yield a high convergence speed and to outperform the LMS and the RLS techniques. The iterative method based on the CG algorithm can provide an attractive trade-off between the convergence performance and the computational complexity. Similarly to the AVF algorithm, it avoids the computation of \mathbf{R}^{-1} required by the constraint, saving significant computational resources. However, it does not attain the performance level of the RLS algorithm. Despite the benefits

of these Krylov-based methods, they require several iterations per data snapshot in order to converge. Thus, a modified version of the CG algorithm employing only one iteration per data update was developed in [23]. By making use of a degenerated scheme, meaning that its residual vectors are not requested to be orthogonal to the spanned Krylov subspace, the computational cost is further reduced while maintaining the performance.

Motivated by the convergence speed-enhancing and complexity-reducing performance of the Krylov-based adaptive algorithms, this chapter is concerned with the development of these algorithms combined with the strategy of widely-linear processing to overcome the issues of the increased complexity and the convergence speed limitations. The resulting novel algorithms devised for strictly non-circular sources are referred to as the WL-AVF, the WL-CG and the WL-MCG beamforming methods and are designed according to the widely LCMV (WL-CMV) criterion. Requiring only the *a priori* knowledge of the signal direction of the desired user, the proposed techniques fully exploit the second-order statistics of the strictly non-circular signals in the system and, at the same time, ensure the benefits of the Krylov-based algorithms. In connection with the development of the WL-AVF, the WL-CG, and the WL-MCG methods, an analysis of their computational complexity is performed and their convergence capabilities are studied. For comparison purposes, their performance is contrasted with the previously developed WL-LMS and the WL-RLS algorithms.

3.2 LCMV beamforming

We start by shortly reviewing the LCMV concept for adaptive beamforming. Adopting the definition of the received vector $\mathbf{r}(i)$ stated in Section 2.3, the output of an adaptive narrowband beamformer is given by

$$y(i) = \mathbf{w}^H \mathbf{r}(i), \quad (3.3)$$

where

$$\mathbf{w} = [w_1, \dots, w_M]^T \in \mathbb{C}^{M \times 1} \quad (3.4)$$

is the beamforming vector to be designed, which contains the complex weights that multiply the signals at each sensor element. The adaptation of the weight vector according to the LCMV optimality criterion is defined as the minimization of the total output variance while simultaneously keeping the gain of the array into a desired signal direction θ_1 fixed. This formulation is equivalent to the reduction of the output variance by suppressing the interference. Mathematically, the optimal weights \mathbf{w}_{opt} are

computed by solving the constrained optimization problem

$$\begin{aligned} \mathbf{w}_{\text{opt}} = \underset{\mathbf{w}}{\operatorname{argmin}} \quad & \mathbb{E} \left\{ |y(i)|^2 \right\} = \mathbb{E} \left\{ |\mathbf{w}^H \mathbf{r}(i)|^2 \right\} = \mathbf{w}^H \mathbf{R} \mathbf{w} \\ \text{subject to} \quad & \mathbf{w}^H \mathbf{a}(\theta_1) = \gamma, \end{aligned} \quad (3.5)$$

where \mathbf{R} is the $M \times M$ covariance matrix defined in (3.1), $\mathbf{a}(\theta_1)$ is the array steering vector of the desired user with the DOA θ_1 , and γ is an arbitrary constant. Solving the minimization problem by using the method of Lagrange multipliers, the optimal solution for the calculation of the weights is obtained by

$$\mathbf{w}_{\text{opt}} = \frac{\gamma \mathbf{R}^{-1} \mathbf{a}(\theta_1)}{\mathbf{a}^H(\theta_1) \mathbf{R}^{-1} \mathbf{a}(\theta_1)}. \quad (3.6)$$

Setting the constant $\gamma = 1$ yields the so-called MVDR beamformer, meaning that the desired signal is undistorted due to the gain of 1 and the output signal exhibits minimum variance. Note that the LCMV criterion requires the knowledge of the DOA of the SOI and the exact array geometry to form the steering vector $\mathbf{a}(\theta_1)$.

In order to assess the effectiveness of an adaptive beamformer, the signal-to-interference-plus-noise ratio (SINR) for the particular signal direction θ_1 at each snapshot i is analyzed. The expression of the SINR is given by

$$\text{SINR}(i) = \frac{\sigma_1^2 |\mathbf{w}^H(i) \mathbf{a}(\theta_1)|^2}{\mathbb{E} \left\{ |\mathbf{w}^H(i) \mathbf{v}(i)|^2 \right\}} = \frac{\sigma_1^2 |\mathbf{w}^H(i) \mathbf{a}(\theta_1)|^2}{\mathbf{w}^H(i) \mathbf{R}_u \mathbf{w}(i)}, \quad (3.7)$$

where σ_1^2 is the power of the SOI and \mathbf{R}_u is the $M \times M$ covariance matrix of the interference plus noise. The maximum output SINR according to the LCMV criterion can be derived as

$$\text{SINR}_{\text{max}}^{\text{LCMV}} = \frac{\sigma_1^2 \mathbf{a}^H(\theta_1) \mathbf{R}^{-1} \mathbf{a}(\theta_1)}{1 - \sigma_1^2 \mathbf{a}^H(\theta_1) \mathbf{R}^{-1} \mathbf{a}(\theta_1)}. \quad (3.8)$$

The proof of equation (3.8) was moved to the Appendix A.1.

3.3 Non-circularity and WL-CMV beamforming

As the objective of this chapter is to develop WL adaptive beamforming algorithms for non-circular sources, we first review the properties of non-circularity and then make use of the resulting characteristics to design the WL-CMV optimization criterion to generate the beamforming weight vectors.

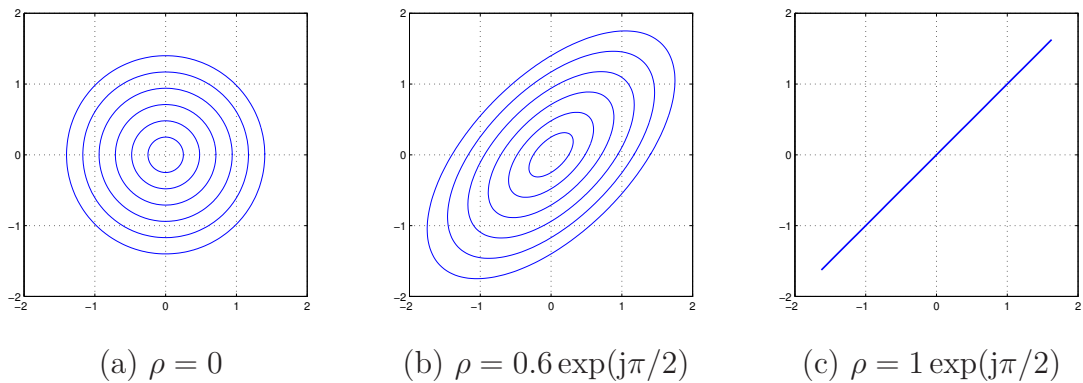


Fig. 3.1: Contour lines of complex Gaussian random variables with different ρ .

3.3.1 Non-circularity of signal sources

A signal is termed non-circular if the real and the imaginary part of its source symbols are dependent, such that the lines of equal probability in the joint density function are not circles anymore [24, 25]. Consequently, a signal is referred to as circular if the opposite fact holds. For mathematical purposes, the non-circularity coefficient

$$\rho = \frac{\mathbb{E}\{s^2(i)\}}{\mathbb{E}\{|s(i)|^2\}} = |\rho|e^{j\psi} \quad (3.9)$$

is defined to provide a measure for the deviation from the circular symmetry. Thus, the non-circularity coefficient is $\rho = 0$ if the signal is circular. Assuming a signal in the system to be non-circular is not a distinct condition. Furthermore, it is essential to distinguish between weak non-circularity and strict non-circularity. The requirement for a weakly non-circular signal is $0 < |\rho| < 1$ and a strictly non-circular signal implies a non-circularity coefficient of $|\rho| = 1$. The contour lines of constant probability density for the three cases depending on ρ are depicted in Figure 3.1. Note that the lines for non-circular sources can have an arbitrary orientation $\psi/2$, which is determined by the angle of (3.9) [24]. In the following development of the WL Krylov-based beamforming algorithms, we assume the property of strict non-circularity of all the signals in the system.

3.3.2 WL-CMV beamforming assuming strict non-circularity

In order to exploit the strict non-circularity of signals impinging on the sensor array, the second-order statistics fully described by the covariance matrix $\mathbf{R} = \mathbb{E}\{\mathbf{r}(i)\mathbf{r}^H(i)\}$ and the complementary covariance matrix $\mathbf{C} = \mathbb{E}\{\mathbf{r}(i)\mathbf{r}^T(i)\}$ need to be taken into account. Thus, to make use of the additional information contained in \mathbf{C} , the received vector $\mathbf{r}(i)$

and its complex conjugate $\mathbf{r}^*(i)$ are processed by applying a bijective transformation \mathcal{T} such that

$$\mathbf{r}(i) \xrightarrow{\mathcal{T}} \tilde{\mathbf{r}}(i) : \quad \tilde{\mathbf{r}}(i) = [\mathbf{r}^T(i), \mathbf{r}^H(i)]^T \in \mathbb{C}^{2M \times 1}, \quad (3.10)$$

where $\tilde{\mathbf{r}}(i)$ is the augmented received vector. It is utilized by the designed beamformer to design the augmented weight vector $\tilde{\mathbf{w}} \in \mathbb{C}^{2M \times 1}$ and to generate the output $y(i) = \tilde{\mathbf{w}}^H \tilde{\mathbf{r}}(i)$, which is termed widely-linear beamforming. In what follows, all the widely-linear quantities are denoted by an over tilde. Expanding the augmented vector after the bijective transformation, and taking into account the entire data block, yields

$$\tilde{\mathbf{X}} = \begin{bmatrix} \mathbf{X} \\ \mathbf{X}^* \end{bmatrix} = \begin{bmatrix} \mathbf{A}(\boldsymbol{\theta})\mathbf{S} \\ \mathbf{A}^*(\boldsymbol{\theta})\mathbf{S}^* \end{bmatrix} + \begin{bmatrix} \mathbf{N} \\ \mathbf{N}^* \end{bmatrix} \in \mathbb{C}^{2M \times N}, \quad (3.11)$$

where we used \mathbf{X} to denote the array output matrix for beamforming to avoid confusions with the covariance matrix \mathbf{R} . As a result of the strict non-circularity assumption with $|\rho| = 1$, the source symbols in \mathbf{S} are real-valued and (3.11) can be rewritten as

$$\tilde{\mathbf{X}} = \begin{bmatrix} \mathbf{A}(\boldsymbol{\theta}) \\ \mathbf{A}^*(\boldsymbol{\theta}) \end{bmatrix} \mathbf{S} + \begin{bmatrix} \mathbf{N} \\ \mathbf{N}^* \end{bmatrix}. \quad (3.12)$$

A proof of the implication of real-valued symbols when presuming a non-circularity coefficient of $|\rho| = 1$ is shown in Appendix A.2.

Applying the bijective transformation \mathcal{T} to the LCMV optimization problem in (3.5), we obtain a new optimization problem referred to as WL-CMV design criterion, which is formulated as

$$\begin{aligned} \tilde{\mathbf{w}}_{\text{opt}} = \underset{\tilde{\mathbf{w}}}{\text{argmin}} \quad & \mathbb{E} \{ |y(i)|^2 \} = \mathbb{E} \{ |\tilde{\mathbf{w}}^H \tilde{\mathbf{r}}(i)|^2 \} = \tilde{\mathbf{w}}^H \tilde{\mathbf{R}} \tilde{\mathbf{w}} \\ \text{subject to} \quad & \tilde{\mathbf{w}}^H \tilde{\mathbf{a}}(\theta_1) = \gamma, \end{aligned} \quad (3.13)$$

where $\tilde{\mathbf{a}}(\theta_1) = \mathcal{T}\{\mathbf{a}(\theta_1)\}$ is the augmented steering vector of the SOI and $\tilde{\mathbf{R}} = \mathbb{E}\{\tilde{\mathbf{r}}(i)\tilde{\mathbf{r}}^H(i)\} \in \mathbb{C}^{2M \times 2M}$ is the augmented covariance matrix of the structure

$$\tilde{\mathbf{R}} = \begin{bmatrix} \mathbf{R} & \mathbf{C} \\ \mathbf{C}^* & \mathbf{R}^* \end{bmatrix}, \quad (3.14)$$

where the covariance matrix \mathbf{R} and the complementary covariance matrix \mathbf{C} appear in conjugate pairs. Solving the widely-linear minimization problem using the Lagrange

multiplier yields the optimal solution given by

$$\tilde{\mathbf{w}}_{\text{opt}} = \frac{\gamma \tilde{\mathbf{R}}^{-1} \tilde{\mathbf{a}}(\theta_1)}{\tilde{\mathbf{a}}^H(\theta_1) \tilde{\mathbf{R}}^{-1} \tilde{\mathbf{a}}(\theta_1)}. \quad (3.15)$$

The performance of a widely-linear adaptive beamformer is evaluated through the WL SINR, which is expressed similarly to (3.7) as

$$\widetilde{\text{SINR}}(i) = \frac{\sigma_1^2 |\tilde{\mathbf{w}}^H(i) \tilde{\mathbf{a}}(\theta_1)|^2}{\tilde{\mathbf{w}}^H(i) \tilde{\mathbf{R}}_u \tilde{\mathbf{w}}(i)}, \quad (3.16)$$

where $\tilde{\mathbf{R}}_u$ is the augmented covariance matrices of the interference plus noise. The maximum output SINR in the WL case is given by

$$\text{SINR}_{\text{max}}^{\text{WL-CMV}} = \frac{\sigma_1^2 \tilde{\mathbf{a}}^H(\theta_1) \tilde{\mathbf{R}}^{-1} \tilde{\mathbf{a}}(\theta_1)}{1 - \sigma_1^2 \tilde{\mathbf{a}}^H(\theta_1) \tilde{\mathbf{R}}^{-1} \tilde{\mathbf{a}}(\theta_1)}. \quad (3.17)$$

3.4 Widely-linear beamforming based on the AVF algorithm

In this part, the widely-linear adaptive beamforming algorithm adopting the AVF technique, termed WL-AVF algorithm, is developed. It utilizes the auxiliary vectors provided by the AVF algorithm to iteratively update the widely-linear weight vector $\tilde{\mathbf{w}}$. After introducing the general structure of the WL-AVF-based beamforming design, the algorithm is derived in detail according to the previous work in [9].

Structure of the WL-AVF algorithm for beamforming

The general framework of the proposed beamformer based on the WL-AVF algorithm is depicted in Figure 3.2. First, the augmented received vector $\tilde{\mathbf{r}}(i)$ is obtained by applying a bijective transformation \mathcal{T} to the received input vector $\mathbf{r}(i)$. The augmented vector is then processed by the filter, whose complex weights are adjusted via the WL-

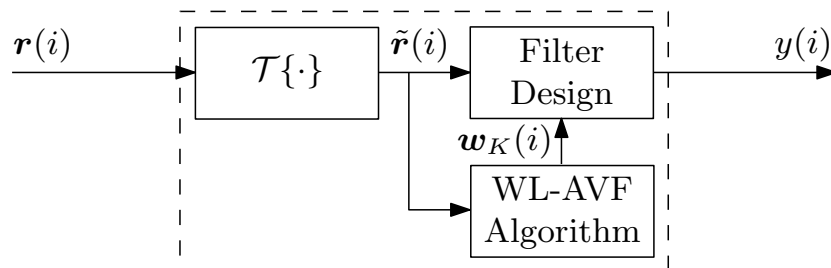


Fig. 3.2: Structure of the WL-AVF algorithm.

AVF algorithm to generate the beamformer output $y(i)$. The final weight $\mathbf{w}_K(i)$ per data update is computed after K iterations of the WL-AVF algorithm. In the following derivation, we drop the time instant i to increase the readability.

Proposed WL-AVF algorithm

The development of the WL-AVF algorithm starts with the initialization of the augmented weight vector $\tilde{\mathbf{w}}$, which is chosen to be equal to the conventional matched filter solution for a desired response γ in the direction θ_1 , given by

$$\tilde{\mathbf{w}}_0 = \gamma^* \frac{\tilde{\mathbf{a}}(\theta_1)}{\|\tilde{\mathbf{a}}(\theta_1)\|^2}. \quad (3.18)$$

Then, the weight vectors are iteratively updated in a stochastic gradient manner by subtracting scaled auxiliary vectors $\tilde{\mathbf{g}}$ that are constructed to be orthogonal to $\tilde{\mathbf{a}}(\theta_1)$. The successively computed augmented weight vectors are obtained by

$$\tilde{\mathbf{w}}_k = \tilde{\mathbf{w}}_{k-1} - \mu_k \tilde{\mathbf{g}}_k, \quad k = 1, \dots, K, \quad (3.19)$$

where μ_k is the step size for the k th iteration. The augmented auxiliary vectors $\tilde{\mathbf{g}}_k$ are designed to maximize the magnitude of the cross-correlation between $\tilde{\mathbf{g}}_k^H \tilde{\mathbf{r}}$ and $\tilde{\mathbf{w}}_{k-1}^H \tilde{\mathbf{r}}$, subject to the orthonormality constraint with respect to $\tilde{\mathbf{a}}(\theta_1)$ [9], which is formulated by the optimization problem

$$\begin{aligned} \tilde{\mathbf{g}}_k &= \underset{\tilde{\mathbf{g}}_k}{\operatorname{argmax}} \quad \left| \mathbb{E} \left\{ \tilde{\mathbf{w}}_{k-1}^H \tilde{\mathbf{r}} [\tilde{\mathbf{g}}_k^H \tilde{\mathbf{r}}]^H \right\} \right| \\ &= \underset{\tilde{\mathbf{g}}_k}{\operatorname{argmax}} \quad \left| \mathbb{E} \left\{ \tilde{\mathbf{w}}_{k-1}^H \tilde{\mathbf{R}} \tilde{\mathbf{g}}_k \right\} \right| \\ &\text{s.t. } \tilde{\mathbf{g}}_k^H \tilde{\mathbf{a}}(\theta_1) = 0, \quad \|\tilde{\mathbf{g}}_k\| = 1. \end{aligned} \quad (3.20)$$

According to [9], the solution to this problem is expressed by

$$\tilde{\mathbf{g}}_k = \frac{\left(\mathbf{I} - \frac{\tilde{\mathbf{a}}(\theta_1) \tilde{\mathbf{a}}^H(\theta_1)}{\|\tilde{\mathbf{a}}(\theta_1)\|^2} \right) \tilde{\mathbf{R}} \tilde{\mathbf{w}}_{k-1}}{\left\| \left(\mathbf{I} - \frac{\tilde{\mathbf{a}}(\theta_1) \tilde{\mathbf{a}}^H(\theta_1)}{\|\tilde{\mathbf{a}}(\theta_1)\|^2} \right) \tilde{\mathbf{R}} \tilde{\mathbf{w}}_{k-1} \right\|} \quad (3.21)$$

Eventually, the value for the step size μ_k is determined by minimizing the variance at the output, i.e.,

$$\mu_k = \min_{\mu_k} \mathbb{E} \left\{ |\tilde{\mathbf{w}}_k^H \tilde{\mathbf{r}}|^2 \right\} \quad (3.22)$$

with the solution

$$\mu_k = \frac{\tilde{\mathbf{g}}_k^H \tilde{\mathbf{R}} \tilde{\mathbf{w}}_{k-1}}{\tilde{\mathbf{g}}_k^H \tilde{\mathbf{R}} \tilde{\mathbf{g}}_k}. \quad (3.23)$$

Tab. 3.1: The proposed WL-AVF algorithm

<p>Initialization: $\tilde{\mathbf{w}}_0 = \gamma^* \frac{\tilde{\mathbf{a}}(\theta_1)}{\ \tilde{\mathbf{a}}(\theta_1)\ ^2}$</p> <p>for each snapshot $i = 1, \dots, N$</p> <p style="padding-left: 20px;">$\tilde{\mathbf{R}}_{\text{dl}}(i) = \lambda \tilde{\mathbf{R}}_{\text{dl}}(i-1) + \tilde{\mathbf{r}}(i)\tilde{\mathbf{r}}^H(i) + \xi \mathbf{I}_{2M}$</p> <p>for iteration $k = 1, \dots, K$</p> <p style="padding-left: 40px;">$\tilde{\mathbf{g}}_k = \frac{\left(\mathbf{I}_{2M} - \frac{\tilde{\mathbf{a}}(\theta_1)\tilde{\mathbf{a}}^H(\theta_1)}{\ \tilde{\mathbf{a}}(\theta_1)\ ^2} \right) \tilde{\mathbf{R}}_{\text{dl}}\tilde{\mathbf{w}}_{k-1}}{\left\ \left(\mathbf{I}_{2M} - \frac{\tilde{\mathbf{a}}(\theta_1)\tilde{\mathbf{a}}^H(\theta_1)}{\ \tilde{\mathbf{a}}(\theta_1)\ ^2} \right) \tilde{\mathbf{R}}_{\text{dl}}\tilde{\mathbf{w}}_{k-1} \right\ }$</p> <p style="padding-left: 40px;">If $\ \tilde{\mathbf{g}}_k - \tilde{\mathbf{g}}_{k-1}\ \rightarrow 0$, EXIT.</p> <p style="padding-left: 40px;">$\mu_k = \frac{\tilde{\mathbf{g}}_k^H \tilde{\mathbf{R}}_{\text{dl}}\tilde{\mathbf{w}}_{k-1}}{\tilde{\mathbf{g}}_k^H \tilde{\mathbf{R}}\tilde{\mathbf{g}}_k}$</p> <p style="padding-left: 40px;">$\tilde{\mathbf{w}}_k = \tilde{\mathbf{w}}_{k-1} - \mu_k \tilde{\mathbf{g}}_k$</p> <p>end</p> <p>end</p>
--

For the proof of (3.23), the reader is referred to Appendix A.3.

The proposed beamforming technique based on the WL-AVF algorithm is summarized in Table 3.1, where the time instant i is included again to emphasize the adaptive approach of obtaining the augmented weight vector for each snapshot. As the auxiliary vectors approach zero when k increases, the iterative procedure is terminated if $\|\tilde{\mathbf{g}}_k - \tilde{\mathbf{g}}_{k-1}\| \rightarrow 0$.

Applying the developed WL-AVF beamforming algorithm to non-stationary systems, the covariance matrix $\tilde{\mathbf{R}}$ is estimated by its recursive form using the exponentially weighted estimate:

$$\tilde{\mathbf{R}}(i) = \lambda \tilde{\mathbf{R}}(i-1) + \tilde{\mathbf{r}}(i)\tilde{\mathbf{r}}^H(i), \quad (3.24)$$

where λ is the forgetting factor, which is close to but less than 1. The first initialization of $\tilde{\mathbf{R}}(0) = \delta \mathbf{I}_{2M}$, where a common value for $\delta = \sigma_n^2$. Furthermore, the diagonal loading technique [26] is adopted to achieve more accurate estimates of $\tilde{\mathbf{R}}$ for a small number of available snapshots, i.e.,

$$\tilde{\mathbf{R}}_{\text{dl}}(i) = \tilde{\mathbf{R}}(i) + \xi \mathbf{I}_{2M}, \quad (3.25)$$

where the diagonal loading factor ξ is typically chosen to be $\xi = 10 \cdot \sigma_n^2$ according to [27]. Other approaches to improve the estimates in short data records include reduced-rank algorithms as in [28].

3.5 Widely-linear beamforming based on the CG algorithm

This part of the chapter deals with the derivation of the WL-CG algorithm for adaptive beamforming in the case of strictly non-circular signals. The WL-CG algorithm forms

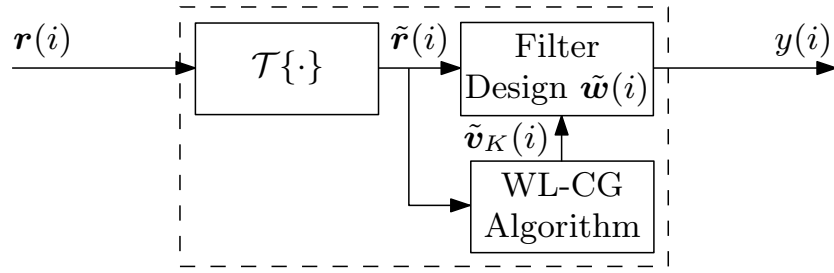


Fig. 3.3: Structure of the WL-CG algorithm.

orthogonal residual vectors, which are employed to iteratively update the widely-linear weight vector $\tilde{\mathbf{w}}(i)$. Whereas the general structure is described first, the second part is concerned with the development of the WL-CG method as an extension of the previous work in [8, 23].

Structure of the WL-CG algorithm for beamforming

The block diagram of the WL-CG-based beamforming procedure depicted in Figure 3.3 exhibits a similar structure as for the WL-AVF algorithm. The bijective transformation \mathcal{T} applied to the original received vector $\mathbf{r}(i)$ yields the augmented received vector $\tilde{\mathbf{r}}(i)$, which is processed by the filter to provide the output $y(i)$. However, contrary to the WL-AVF procedure, the WL-CG method iteratively updates a new defined augmented vector $\tilde{\mathbf{v}}(i)$ to avoid the computation of $\tilde{\mathbf{R}}^{-1}$ that is passed onto the filter after performing K iterations of the WL-CG algorithm. Thus, the final beamforming weight vector $\tilde{\mathbf{w}}(i)$ is computed in the filter design. Again, we drop the time instant i in the following development.

The proposed WL-CG algorithm

In order to derive the WL-CG beamforming algorithm for non-circular sources, the WL-CG method is applied to minimize the cost function [29]

$$\min J(\tilde{\mathbf{v}}) = \tilde{\mathbf{v}}^H \tilde{\mathbf{R}} \tilde{\mathbf{v}} - 2\text{Re} \left\{ \tilde{\mathbf{a}}^H(\theta_1) \tilde{\mathbf{v}} \right\}, \quad (3.26)$$

where $\tilde{\mathbf{v}} \in \mathbb{C}^{2M \times 1}$ is a newly defined augmented CG weight vector, which is different from the beamforming weight vector $\tilde{\mathbf{w}}$ to be designed. The CG method was originally developed to solve the optimization problem in (3.26) [6]. However, by taking the gradient of (3.26) with respect to the CG weight vector $\tilde{\mathbf{v}}$ and equating it to zero, it can be shown that minimizing the optimization problem in (3.26) is equivalent to

solving the system of linear equations [23]

$$\tilde{\mathbf{R}}\tilde{\mathbf{v}} = \tilde{\mathbf{a}}(\theta_1) \in \mathbb{C}^{2M \times 1}. \quad (3.27)$$

The WL-CG algorithm solves (3.27) by approaching the optimal weight solution step by step via a line search along successive directions, which are sequentially determined at each iteration [6]. The solution for the WL-CG optimization problem (3.26) is obtained as

$$\tilde{\mathbf{v}} = \tilde{\mathbf{R}}^{-1}\tilde{\mathbf{a}}(\theta_1). \quad (3.28)$$

As the expression $\tilde{\mathbf{R}}^{-1}\tilde{\mathbf{a}}(\theta_1)$ also occurs in the optimal WL-CMV solution in (3.15), the WL-CMV beamformer can thus be iteratively computed without the calculation of $\tilde{\mathbf{R}}^{-1}$ by updating the new augmented CG weight vector $\tilde{\mathbf{v}}$ as

$$\tilde{\mathbf{v}}_k = \tilde{\mathbf{v}}_{k-1} + \alpha_k \tilde{\mathbf{p}}_k, \quad k = 1, \dots, K, \quad (3.29)$$

where $\tilde{\mathbf{p}}_k$ is the direction vector, α_k is the step size value to control its weight and k is the iteration number. The directions $\tilde{\mathbf{p}}_k$ are orthogonal with respect to $\tilde{\mathbf{R}}$, termed $\tilde{\mathbf{R}}$ -orthogonality, i.e.,

$$\tilde{\mathbf{p}}_k^H \tilde{\mathbf{R}} \tilde{\mathbf{p}}_l = 0 \quad (3.30)$$

for all $k \neq l$. The following direction was determined in the previous iteration and is obtained by

$$\tilde{\mathbf{p}}_{k+1} = \tilde{\mathbf{g}}_k + \beta_k \tilde{\mathbf{p}}_k, \quad (3.31)$$

where $\tilde{\mathbf{g}}_k$ is the residual vector defined in [6] that is given by

$$\tilde{\mathbf{g}}_k = \tilde{\mathbf{a}}(\theta_1) - \tilde{\mathbf{R}}\tilde{\mathbf{v}}_k. \quad (3.32)$$

The step size α_k is chosen to minimize the cost function in the determined direction and β_k ensures the $\tilde{\mathbf{R}}$ -orthogonality of the direction vectors $\tilde{\mathbf{p}}_k$ in (3.30). According to [6], both parameters are calculated by

$$\alpha_k = \frac{\tilde{\mathbf{g}}_{k-1}^H \tilde{\mathbf{p}}_k}{\tilde{\mathbf{p}}_k^H \tilde{\mathbf{R}} \tilde{\mathbf{p}}_k} \quad \text{and} \quad \beta_k = \frac{\tilde{\mathbf{g}}_k^H \tilde{\mathbf{g}}_k}{\tilde{\mathbf{g}}_{k-1}^H \tilde{\mathbf{g}}_{k-1}}. \quad (3.33)$$

After K iterations of the WL-CG algorithm the augmented complex weight vector $\tilde{\mathbf{w}}$ is formed as

$$\tilde{\mathbf{w}} = \frac{\gamma \tilde{\mathbf{v}}_K}{\tilde{\mathbf{a}}^H(\theta_1) \tilde{\mathbf{v}}_K}. \quad (3.34)$$

A summary of the proposed WL-CG-based beamforming technique is given in Table

Tab. 3.2: The proposed WL-CG algorithm

<p>Initialization: $\tilde{\mathbf{v}}_0(1) = \mathbf{0}$, $\tilde{\mathbf{R}}_{\text{dl}}(0) = \delta \mathbf{I}_{2M}$ for each snapshot $i = 1, \dots, N$ $\tilde{\mathbf{R}}_{\text{dl}}(i) = \lambda \tilde{\mathbf{R}}_{\text{dl}}(i-1) + \tilde{\mathbf{x}}(i) \tilde{\mathbf{x}}^H(i) + \xi \mathbf{I}_{2M}$, $\tilde{\mathbf{p}}_1(i) = \tilde{\mathbf{g}}_0(i) = \tilde{\mathbf{a}}(\theta_1) - \tilde{\mathbf{R}}_{\text{dl}}(i) \tilde{\mathbf{v}}_0(i)$ for iteration $k = 1, \dots, K$ $\tilde{\mathbf{d}}_k(i) = \tilde{\mathbf{R}}_{\text{dl}}(i) \tilde{\mathbf{p}}_k(i)$ $\alpha_k(i) = [\tilde{\mathbf{p}}_k^H(i) \tilde{\mathbf{d}}_k(i)]^{-1} \tilde{\mathbf{g}}_{k-1}^H(i) \tilde{\mathbf{p}}_k(i)$ $\tilde{\mathbf{v}}_k(i) = \tilde{\mathbf{v}}_{k-1}(i) + \alpha_k(i) \tilde{\mathbf{p}}_k(i)$ $\tilde{\mathbf{g}}_k(i) = \tilde{\mathbf{g}}_{k-1}(i) - \alpha_k(i) \tilde{\mathbf{d}}_k(i)$ $\beta_k(i) = [\tilde{\mathbf{g}}_{k-1}^H(i) \tilde{\mathbf{g}}_{k-1}(i)]^{-1} \tilde{\mathbf{g}}_k^H(i) \tilde{\mathbf{g}}_k(i)$ $\tilde{\mathbf{p}}_{k+1}(i) = \tilde{\mathbf{g}}_k(i) + \beta_k(i) \tilde{\mathbf{p}}_k(i)$ end $\tilde{\mathbf{v}}_0(i+1) = \tilde{\mathbf{v}}_K(i)$ $\tilde{\mathbf{w}}(i) = [\tilde{\mathbf{a}}^H(\theta_1) \tilde{\mathbf{v}}_K(i)]^{-1} \gamma \tilde{\mathbf{v}}_K(i)$ end</p>

3.2, where again the included time instant i indicates the adaptive way to obtain the weight solution for each data snapshot.

As already outlined in the previous section, the covariance matrix $\tilde{\mathbf{R}}$ is estimated by its recursive form using the exponentially weighted estimate and incorporating diagonal loading:

$$\tilde{\mathbf{R}}_{\text{dl}}(i) = \lambda \tilde{\mathbf{R}}_{\text{dl}}(i-1) + \tilde{\mathbf{r}}(i) \tilde{\mathbf{r}}^H(i) + \xi \mathbf{I}_{2M}, \quad (3.35)$$

where the diagonal loading factor ξ is again chosen to be $\xi = 10 \cdot \sigma_n^2$ [27].

3.6 Widely-linear beamforming based on the MCG algorithm

In this section, a modified version of the WL-CG method, termed WL-MCG algorithm, is developed for widely-linear adaptive beamforming. Similarly to the WL-CG algorithm, it applies residual vectors to update the beamforming weight vector in an iterative fashion. However, it only requires one iteration of the CG algorithm per sample update. Again, the first part deals with the structure of the MCG method and in the second part, the detailed algorithm is derived according to [8].

Structure of the WL-MCG algorithm for beamforming

The general structure of the WL-MCG algorithm for adaptive beamforming is shown as a block diagram in Figure 3.4. The augmented received vector $\tilde{\mathbf{r}}(i)$ obtained after the bijective transformation is processed by the WL-MCG algorithm to provide the weight

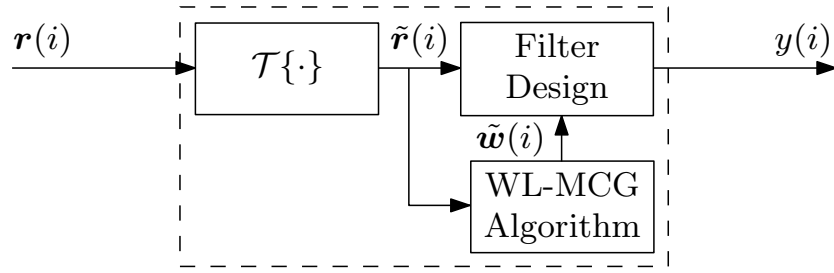


Fig. 3.4: Structure of the WL-MCG algorithm.

vector $\tilde{\mathbf{w}}(i)$ for the filter. The key advantage is the property that, unlike the WL-CG developed in the previous section, the MCG method requires only one iteration per data snapshot, saving computational resources. Furthermore it also adopts the new defined augmented vector $\tilde{\mathbf{v}}(i)$ to avoid the costly computation of $\tilde{\mathbf{R}}^{-1}$.

The proposed WL-MCG algorithm

Corresponding to the WL-CG beamforming method, the WL-MCG algorithm is another way of solving the system of equations stated in (3.27) in the previous section. The covariance matrix is estimated by using the diagonal-loading enhanced exponentially weighted data window

$$\hat{\tilde{\mathbf{R}}}_{\text{dl}}(i) = \lambda \hat{\tilde{\mathbf{R}}}_{\text{dl}}(i-1) + \tilde{\mathbf{r}}(i)\tilde{\mathbf{r}}^H(i) + \xi \mathbf{I}_{2M}, \quad (3.36)$$

where λ is the forgetting factor and ξ the diagonal loading factor. According to [1], the estimated covariance matrix can be approximated for a large sample size as

$$\hat{\tilde{\mathbf{R}}}_{\text{dl}}(i) \approx \frac{1}{1-\lambda}(\tilde{\mathbf{R}} + \xi \mathbf{I}_{2M}). \quad (3.37)$$

Now, we define the new augmented weight vector $\tilde{\mathbf{v}}(i)$ to avoid the computationally expensive computation of $\hat{\tilde{\mathbf{R}}}_{\text{dl}}^{-1}(i)$ at each snapshot as

$$\tilde{\mathbf{v}}(i) = \hat{\tilde{\mathbf{R}}}_{\text{dl}}^{-1}(i)\tilde{\mathbf{a}}(\theta_1). \quad (3.38)$$

Inserting equation (3.37) into (3.38), we obtain

$$\tilde{\mathbf{v}}(i) = \left(\frac{1}{1-\lambda}(\tilde{\mathbf{R}} + \xi \mathbf{I}_{2M}) \right)^{-1} \tilde{\mathbf{a}}(\theta_1) \quad (3.39)$$

for a sufficiently large number of snapshots.

Similarly to the WL-CG algorithm, the WL-MCG method iteratively computes the

solution of (3.38) by updating the new defined augmented vector $\tilde{\mathbf{v}}(i)$ as

$$\tilde{\mathbf{v}}(i) = \tilde{\mathbf{v}}(i-1) + \alpha(i)\tilde{\mathbf{p}}(i), \quad (3.40)$$

where the direction vector $\tilde{\mathbf{p}}(i)$ was determined at the previous snapshot by

$$\tilde{\mathbf{p}}(i+1) = \tilde{\mathbf{g}}(i) + \beta(i)\tilde{\mathbf{p}}(i) \quad (3.41)$$

and the residual vector $\tilde{\mathbf{g}}(i)$ is given by

$$\tilde{\mathbf{g}}(i) = \tilde{\mathbf{a}}(\theta_1) - \hat{\mathbf{R}}(i)\tilde{\mathbf{v}}(i). \quad (3.42)$$

In order to realize sample-by-sample processing, a recursive expression for the residual vector $\tilde{\mathbf{g}}(i)$ can be derived by taking into account the equations (3.42), (3.36), and (3.40), leading to

$$\tilde{\mathbf{g}}(i) = (1-\lambda)\tilde{\mathbf{a}}(\theta_1) + \lambda\tilde{\mathbf{g}}(i-1) - (\tilde{\mathbf{r}}(i)\tilde{\mathbf{r}}^H(i) + \xi\mathbf{I}_{2M})\tilde{\mathbf{v}}(i-1) - \alpha(i)\hat{\mathbf{R}}(i)\tilde{\mathbf{p}}(i). \quad (3.43)$$

The proof of (3.43) is shown in Appendix A.4.

The basic idea of the WL-MCG is to employ a degenerated scheme [8], meaning that the obtained residual vector $\tilde{\mathbf{g}}(i)$ is not required to be orthogonal to the subspace spanned by the previously determined direction vectors $\mathcal{S} = \text{span}\{\tilde{\mathbf{p}}(1), \tilde{\mathbf{p}}(2), \dots, \tilde{\mathbf{p}}(i)\}$, i.e., $\tilde{\mathbf{p}}^H(i)\tilde{\mathbf{g}}(l) \neq 0$ for $l < i$. Under this condition the step size $\alpha(i)$ has to satisfy the convergence bound defined according to [8, 23] as

$$0 \leq \mathbb{E}\{\tilde{\mathbf{p}}^H(i)\tilde{\mathbf{g}}(i)\} \leq 0.5 \mathbb{E}\{\tilde{\mathbf{p}}^H(i)\tilde{\mathbf{g}}(i-1)\}. \quad (3.44)$$

To this end, premultiplying equation (3.43) by $\tilde{\mathbf{p}}^H(i)$, taking the expectation of both sides and considering (3.39) yields

$$\mathbb{E}\{\tilde{\mathbf{p}}^H(i)\tilde{\mathbf{g}}(i)\} \approx \lambda\mathbb{E}\{\tilde{\mathbf{p}}^H(i)\tilde{\mathbf{g}}(i-1)\} - \mathbb{E}\{\alpha(i)\}\mathbb{E}\{\tilde{\mathbf{p}}^H(i)\hat{\mathbf{R}}(i)\tilde{\mathbf{p}}(i)\}, \quad (3.45)$$

where the convergence of the adaptive algorithm is assumed, such that the approximation in (3.39) holds, and therefore

$$(1-\lambda)\tilde{\mathbf{a}}(\theta_1) - [\mathbb{E}\{\tilde{\mathbf{r}}(i)\tilde{\mathbf{r}}^H(i)\} + \xi\mathbf{I}_{2M}]\tilde{\mathbf{v}}(i-1) = \mathbf{0}. \quad (3.46)$$

Inserting the obtained expression (3.45) into the convergence bound in (3.44) and

Tab. 3.3: The proposed WL-MCG algorithm

<p>Initialization: $\tilde{\mathbf{v}}(0) = \mathbf{0}$, $\tilde{\mathbf{R}}_{\text{dl}}(0) = \delta \mathbf{I}_{2M}$, $\tilde{\mathbf{p}}(1) = \tilde{\mathbf{g}}(0) = \tilde{\mathbf{a}}(\theta_1)$</p> <p>for each snapshot $i = 1, \dots, N$</p> <p style="padding-left: 20px;">$\tilde{\mathbf{R}}_{\text{dl}}(i) = \lambda \tilde{\mathbf{R}}_{\text{dl}}(i-1) + \tilde{\mathbf{x}}(i) \tilde{\mathbf{x}}^H(i) + \xi \mathbf{I}_{2M}$,</p> <p style="padding-left: 20px;">$\tilde{\mathbf{d}}(i) = \tilde{\mathbf{R}}_{\text{dl}}(i) \tilde{\mathbf{p}}(i)$</p> <p style="padding-left: 20px;">$\alpha(i) = [\tilde{\mathbf{p}}^H(i) \tilde{\mathbf{d}}(i)]^{-1} (\lambda - \eta) \tilde{\mathbf{p}}^H(i) \tilde{\mathbf{g}}(i-1)$ ($0 \leq \eta \leq 0.5$)</p> <p style="padding-left: 20px;">$\tilde{\mathbf{v}}(i) = \tilde{\mathbf{v}}(i-1) + \alpha(i) \tilde{\mathbf{p}}(i)$</p> <p style="padding-left: 20px;">$\tilde{\mathbf{g}}(i) = (1 - \lambda) \tilde{\mathbf{a}}(\theta_1) + \lambda \tilde{\mathbf{g}}(i-1) - [\tilde{\mathbf{r}}(i) \tilde{\mathbf{r}}^H(i) + \xi \mathbf{I}_{2M}] \tilde{\mathbf{v}}(i-1) - \alpha(i) \tilde{\mathbf{d}}(i)$</p> <p style="padding-left: 20px;">$\beta(i) = [\tilde{\mathbf{g}}^H(i-1) \tilde{\mathbf{g}}(i-1)]^{-1} [\tilde{\mathbf{g}}(i) - \tilde{\mathbf{g}}(i-1)]^H \tilde{\mathbf{g}}(i)$</p> <p style="padding-left: 20px;">$\tilde{\mathbf{p}}(i+1) = \tilde{\mathbf{g}}(i) + \beta(i) \tilde{\mathbf{p}}(i)$</p> <p style="padding-left: 20px;">$\tilde{\mathbf{w}}(i) = [\tilde{\mathbf{a}}^H(\theta_1) \tilde{\mathbf{v}}(i)]^{-1} \gamma \tilde{\mathbf{v}}(i)$</p> <p>end</p>
--

rearranging the terms, we have that

$$(\lambda - 0.5) \frac{\mathbb{E} \left\{ \tilde{\mathbf{p}}^H(i) \tilde{\mathbf{g}}(i-1) \right\}}{\mathbb{E} \left\{ \tilde{\mathbf{p}}^H(i) \hat{\tilde{\mathbf{R}}}(i) \tilde{\mathbf{p}}(i) \right\}} \leq \mathbb{E} \{ \alpha(i) \} \leq \lambda \frac{\mathbb{E} \left\{ \tilde{\mathbf{p}}^H(i) \tilde{\mathbf{g}}(i-1) \right\}}{\mathbb{E} \left\{ \tilde{\mathbf{p}}^H(i) \hat{\tilde{\mathbf{R}}}(i) \tilde{\mathbf{p}}(i) \right\}}. \quad (3.47)$$

From (3.47), the inequality is satisfied if $\alpha(i)$ is computed by

$$\alpha(i) = (\lambda - \eta) \frac{\tilde{\mathbf{p}}^H(i) \tilde{\mathbf{g}}(i-1)}{\tilde{\mathbf{p}}^H(i) \hat{\tilde{\mathbf{R}}}(i) \tilde{\mathbf{p}}(i)}, \quad (3.48)$$

where $0 \leq \eta \leq 0.5$ to fulfill the convergence criterion. The step size $\beta(i)$ is computed according to the Polak-Ribiere approach [30] to avoid the reset procedure [8] and is stated as

$$\beta(i) = \frac{[\tilde{\mathbf{g}}(i) - \tilde{\mathbf{g}}(i-1)]^H \tilde{\mathbf{g}}(i)}{\tilde{\mathbf{g}}(i-1)^H \tilde{\mathbf{g}}(i-1)}. \quad (3.49)$$

The proposed WL-MCG algorithm for widely-linear adaptive beamforming is summarized in Table 3.3. It only performs one iteration of the CG algorithm per snapshot, saving significant computational efforts. The diagonal loading factor ξ in the algorithm is again chosen to be $\xi = 10 \cdot \sigma_n^2$ [27].

3.7 Computational complexity

The computational effort of the WL processing is one of the most important aspects to take into account when developing novel WL adaptive beamforming algorithms. To this end, we evaluate the computational complexity of the proposed WL Krylov-based beamforming algorithms and compare them to their linear counterparts. For

comparison purposes, we first focus on the complexity of the linear algorithms, and then consider the complexity of the WL algorithms.

3.7.1 Complexity of LCMV algorithms

The computational cost, shown in Table 3.4, is measured in terms of the arithmetical operations, where M is the number of sensor elements and K is the number of iterations. The expressions in Table 3.4 are obtained from the work in [23]. It is evident that the complexity of the AVF and the CG algorithm depends on the iteration number K . Figure 3.5 illustrates the computational cost as a function of the number of sensors M . The iteration numbers for the AVF and the CG method are chosen to be $K = 4$ and $K = 5$ respectively, as these numbers are used in the following performance evaluation. Comparing the cost of the linear Krylov-based algorithms to the RLS method, the AVF technique clearly exceeds the computational requirements of the RLS method, whereas the CG algorithm demands a slightly higher cost. The aforementioned trade-off of the CG method only becomes apparent for a smaller number of iterations. However, the MCG algorithm provides a lower computational burden than the RLS technique, especially for a large number of sensors M , but still requires a higher cost than the LMS algorithm.

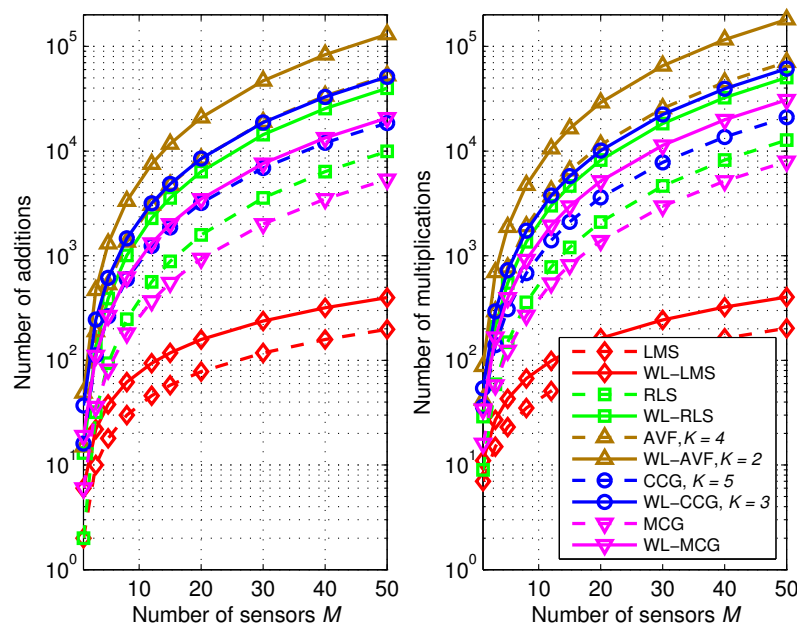


Fig. 3.5: Complexity in terms of arithmetic operations versus the sensors M .

Tab. 3.4: Computational complexity of LCMV beamforming algorithms

Algorithm	Additions	Multiplications
LMS [5]	$4M - 2$	$4M + 3$
RLS [5]	$4M^2 - M - 1$	$5M^2 + 5M - 1$
AVF [9]	$K(4M^2 + M - 2) + 5M^2 - M - 1$	$K(5M^2 + 3M) + 8M^2 + 2M$
CG [8]	$K(M^2 + 4M - 2) + 2M^2 - 1$	$K(M^2 + 4M + 1) + 3M^2 + 3$
MCG [8]	$2M^2 + 7M - 3$	$3M^2 + 9M + 4$

Tab. 3.5: Computational complexity of WL-CMV beamforming algorithms

Algorithm	Additions	Multiplications
WL-LMS [21]	$8M - 2$	$8M + 3$
WL-RLS [22]	$16M^2 - 2M - 1$	$20M^2 + 10M - 1$
WL-AVF	$K(16M^2 + 2M - 2) + 20M^2 - 2 * M - 1$	$K(20M^2 + 6M) + 32M^2 + 4M$
WL-CG	$K(4M^2 + 8M - 2) + 8M^2 - 1$	$K(4M^2 + 8M + 1) + 12M^2 + 3$
WL-MCG	$8M^2 + 14M - 3$	$12M^2 + 18M + 4$

3.7.2 Complexity of WL-CMV algorithms

The computational complexity for the WL beamforming algorithms is depicted in Table 3.5. Due to the WL processing, the analyzed algorithms developed for non-circular sources consider the additional information contained in the augmented steering vector, which can be interpreted as an array composed of twice as many sensor elements M . Thus, the computational cost of all the WL beamforming methods increases by nearly the same amount, complying with the structure of the augmented covariance matrix $\tilde{\mathbf{R}}$. As a result, the same observations for the linear methods also apply to the WL case. According to Figure 3.5, where the number of iterations for the WL-AVF and the WL-CG techniques is now $K = 2$ and $K = 3$ respectively, the gap between the cost of the WL-RLS and the WL-CG is substantially decreased. The complexity of some of the considered algorithms might be further reduced by using symmetries and individual properties. However, these complexity reductions are beyond the scope of this work and are left for future investigations.

3.8 Simulation results

In this section, the output SINR performance of the proposed WL Krylov-based algorithms in stationary and non-stationary scenarios is evaluated and compared to the WL-RLS, the WL-LMS algorithm, and their linear counterparts. For the simulations, we employ a ULA consisting of $M = 24$ sensor elements whose interelement spacing equals half a signal wavelength. Among d sources in the system, the DOA of the desired user with signal power $\sigma_1^2 = 1$ is $\theta_1 = 0^\circ$, which is known beforehand by the receiver. All the signals are assumed to be binary phase-shift keying (BPSK)-modulated, and $\gamma = 1$ is set to satisfy the condition for the MVDR leading to a maximum achievable SINR performance. The diagonal loading factor is $\xi = 10 \cdot \sigma_n^2$ and each curve is obtained by averaging a total of 1000 runs. Notice that in the simulations the number of iterations K for the WL-AVF and the WL-CG algorithm is fixed for all the realizations. The first part of the computer simulations deals with the performance in stationary scenarios and the second part is concerned with the performance assessment in non-stationary scenarios.

3.8.1 Performance in stationary scenarios

In the first experiment, we examine the SINR performance of the proposed WL adaptive beamforming algorithms in a stationary system. Assuming that there are $d = 15$ users in the scenario, the $d - 1 = 14$ interfering signals impinge on the sensor array from the directions $(\pm 10^\circ \cdot [1, \dots, (d - 1)/2])$ with an input SNR = 10 dB and a signal-to-interference ratio (SIR) of -20 dB. Due to the stationarity of the system, the forgetting factor is set to be $\lambda = 1$.

Figure 3.6 shows the output SINR performance as a function of the number of snapshots N . The number of iterations K for the AVF algorithm and for the WL-AVF algorithm were found to be $K = 4$ and $K = 2$ and the iteration number for the CG algorithm and the WL-CG algorithm is $K = 3$ and $K = 5$, respectively. The amount of iterations was optimized to yield the best output performance in terms of the convergence speed. The lower number of iterations for the WL version of the AVF and the CG algorithm can be explained by the fact that the augmented weight vector provides additional information and reaches the optimum solution with fewer iterations. It is apparent from Figure 3.6 that all the WL beamforming algorithms provide substantial improvements over the linear techniques in general. Specifically, the proposed WL-AVF algorithm outperforms the adaptive WL-LMS and the WL-RLS in terms of both the convergence and the steady state. The WL-CG method and the

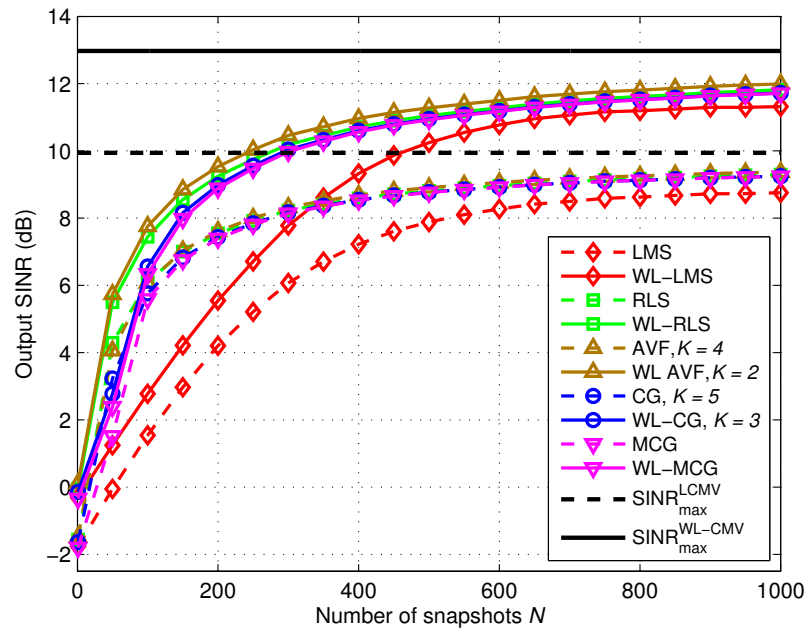


Fig. 3.6: Output SINR versus the number of snapshots N in a stationary scenario with $M = 24$, $d = 15$, $\text{SNR} = 10$ dB, $\text{SIR} = -20$ dB, $\lambda = 1$.

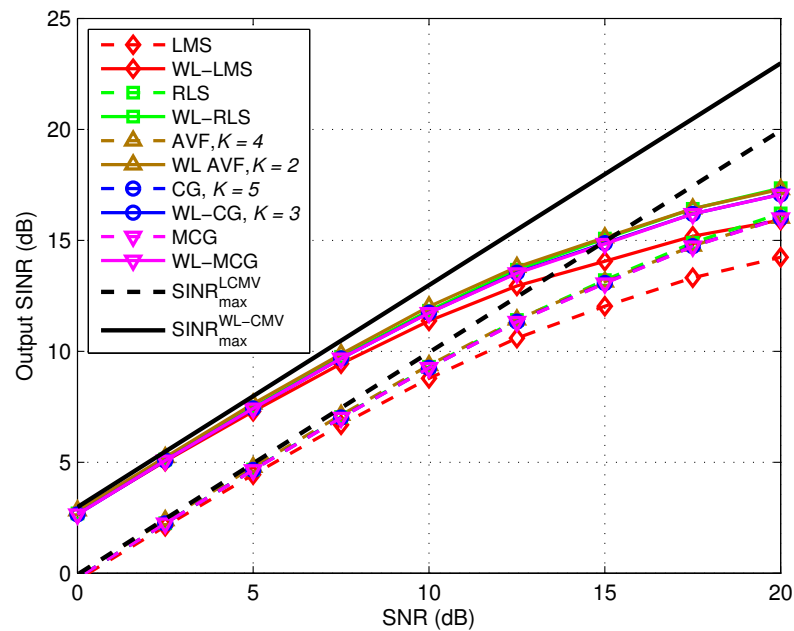


Fig. 3.7: Output SINR versus the input SNR in a stationary scenario with $M = 24$, $d = 15$, $N = 1000$, $\text{SIR} = -20$ dB, $\lambda = 1$.

WL-MCG algorithm perform close to the level of the WL-RLS algorithm and outclass the WL-LMS technique. However, as discussed in the previous section, the WL-MCG algorithm significantly reduces the complexity of the WL-CG method. As seen for the $\text{SINR}_{\max}^{\text{WL-CMV}}$ compared to the $\text{SINR}_{\max}^{\text{LCMV}}$, by exploiting the additional information in the presence of non-circular sources, a higher gain can be achieved. This is due to the WL processing, where the augmented steering vector can be interpreted as a virtual array with twice as many sensors.

The SINR performance as a function of the SNR is illustrated in Figure 3.7, where the number of snapshots is fixed to $N = 1000$. As expected, the SINR increases with the SNR, and for the $\text{SINR}_{\max}^{\text{WL-CMV}}$ the additional gain is expressed by shifting the curve for the $\text{SINR}_{\max}^{\text{LCMV}}$ to a higher SINR. The proposed WL algorithms performs similarly to the results in Figure 3.6. The WL-AVF method outperforms the WL-LMS and the WL-RLS algorithm, whereas the WL-CG and the WL-MCG techniques almost reach the level of the WL-RLS algorithm.

3.8.2 Performance in non-stationary scenarios

In the second experiment, the SINR performance in a non-stationary scenario is analyzed and compared to the WL-LMS and the WL-RLS. The system starts with the same scenario as in Figure 3.6, but with different power levels of the interfering signals,

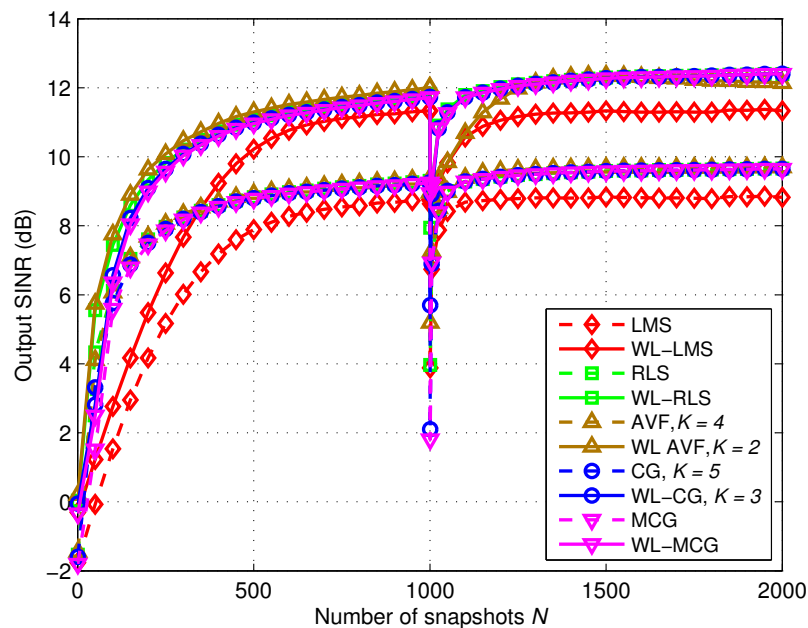


Fig. 3.8: Output SINR versus the number of snapshots N in a non-stationary scenario with $M = 24$, $d_1 = 15$, $d_2 = 12$, $\text{SNR} = 10$ dB, $\lambda = 0.998$.

namely 8 interferers with a power of 20 dB, 4 with 10 dB and 2 with 5 dB above the level of the SOI. At the 1000th snapshot, 4 users with a signal power of 20 dB and one user with 10 dB above the SOI leave the system, and 2 users with a power of 20 dB and 5 dB above the SOI enter the system. As can be seen in Figure 3.8, the proposed WL-CG and the WL-MCG quickly adapt to the changed system and exhibit the convergence speed and the steady-state level of the WL-RLS method. Thus, the WL-CG and the WL-MCG approaches provide a better performance after a change in the environment. Nevertheless, the same conclusion can not be drawn for the proposed WL-AVF algorithm. After the changing event, it barely exceeds the convergence speed of the WL-LMS method and only attains the level of the other algorithms after requiring a significant number of data samples. This behavior is due to the relatively low number of iterations of the AVF algorithm per data update. However, a larger iteration number would decrease the performance in a stationary system. In consequence of the fixed number of iterations K for the experiments, it is evident that the performance can be improved by applying an automatic scheme to adaptively adjust K .

3.9 Conclusions

In this chapter, an extension of the Krylov subspace-based algorithms employing the AVF, the CG and the MCG methods for adaptive beamforming to the WL processing is developed, resulting in the WL-AVF, the WL-CG and the WL-MCG algorithm. After exploring the performance advantages associated with the WL processing in the face of implying a loss of the computational efficiency, the WL-CMV optimization criterion is introduced to update the augmented beamforming weight vector. Then by assuming strictly non-circular signals in the system, the general framework of the three proposed adaptive algorithms is discussed and their detailed derivation presented. The developed algorithms fully exploit the second-order statistics of the strictly non-circular signals and avoid the computation of the inverse of the augmented covariance matrix. Whereas the WL-AVF algorithm applies augmented auxiliary vectors within a number of iterations to adapt the augmented weight vector at each data sample, the WL-CG resorts to augmented residual vectors. The key benefit of the WL-MCG is the fact that it only performs one iteration per data snapshot. To assess the computational requirements, an analysis of the complexity is conducted, which demonstrates that the same computational behavior in the linear case also holds for the WL processing. Specifically, the WL-AVF algorithm requires the highest complexity and the WL-MCG the lowest cost. Furthermore, the SINR performance of these algorithms is evaluated by computer simulations for stationary and non-stationary scenarios, where

the number of iterations for the WL-AVF and the WL-CG method is optimized. It is illustrated that the WL processing provides significant performance improvements over the linear processing. In stationary scenarios, the WL-AVF algorithm outperforms the WL-RLS method, and the WL-CG and the WL-MCG algorithm perform close to the WL-RLS technique. Considering non-stationary scenarios, the WL-CG and the WL-MCG method attain the performance of the WL-RLS approach after a change in the system; however, the WL-AVF achieves a slower adaptation due to the lower number of iterations. This motivates an automatic scheme for adaptively switching the iteration number.

4. BEAMSPACE DIRECTION FINDING USING KRYLOV SUBSPACE-BASED ALGORITHMS

In this chapter, we develop a new class of beamspace direction finding algorithms based on the recently proposed Krylov subspace-based algorithms, which utilize a non-eigenvector basis for the signal subspace. Combining their superior estimation performance under severe conditions and the benefits of operation in beamspace, the estimation accuracy is further improved while simultaneously reducing the computational complexity.

4.1 Introduction

The need for the DOA estimation of impinging signal wavefronts using sensor arrays is encountered in a broad range of important engineering applications, including radar, sonar, wireless communications, radio astronomy, etc. As a result of this extensively studied problem, numerous high-resolution methods for estimating the signal directions of multiple emitter sources have been proposed in the last few decades [1, 10]. Among the most profitable signal localization techniques are the subspace-based methods, such as MUSIC [12], Root-MUSIC [13] and ESPRIT [14], which are proven to yield excellent capabilities. These algorithms are based on a subspace approach, where the measured covariance matrix

$$\hat{\mathbf{R}} = \frac{1}{N} \sum_{i=1}^N \mathbf{x}(i) \mathbf{x}^H(i) \in \mathbb{C}^{M \times M} \quad (4.1)$$

from M sensor elements is decomposed into two orthogonal subspaces, named the signal and the noise subspace (cf. Section 2.2.1). The most effectively used factorization to obtain estimates of orthonormal bases for these subspaces is the eigenvalue decomposition of the covariance matrix $\hat{\mathbf{R}}$ in (4.1). Nevertheless, this theoretical approach is subject to a major problem as its practical calculation is computationally intensive, requiring $\mathcal{O}(M^3)$ operations. Due to the cubic increase of the computational burden with

the number of sensor elements, considerable research interest has emerged to address this problem.

A new class of subspace-based methods for the DOA estimation, referred to as Krylov subspace-based methods, adopting the auxiliary vector filtering (AVF) algorithm [16] or the conjugate gradient (CG) algorithm [17], was recently proposed. These techniques avoid the computation of an eigenvalue decomposition of the measured covariance matrix, but iteratively generate an extended signal subspace basis of rank $d+1$, the so-called extended Krylov subspace. The successively created basis comprises the estimated signal subspace of rank d and the dimension of the scanning vector itself. While the AVF-based algorithm [16] forms the signal subspace from auxiliary vectors, the CG-based method [17] applies the orthogonal residual vectors to span the extended Krylov signal subspace. Then, the unknown signal directions are determined by searching over the spatial spectrum for the rank-collapse of the extended signal subspace from $d+1$ to d , as the scanning vector belongs to it. This novel approach results into a superior resolution performance for closely-spaced sources under severe conditions, i.e., at a low signal-to-noise ratio (SNR) and a small data record N . However, despite utilizing a non-eigenvector basis for the signal subspace, these methods suffer from a similar computational complexity to the eigenvector-based methods, as the extended Krylov signal subspace is constructed for each search angle.

To overcome the challenging issue of the increased computational complexity for large sensor arrays, the inclusion of a beamforming preprocessor was firstly proposed in [31]. This approach, termed beamspace (BS) processing, significantly reduces the computational cost by linearly transforming the original data into a lower-dimensional subspace, the beamspace. Afterwards, the conventional direction finding methods are applied to the reduced beamspace data to obtain the DOAs. In addition to the computational savings, operation in beamspace can provide further benefits over the element space, such as an improved estimation accuracy and increased resolution capabilities. The transformation into the beamspace of lower dimension can be physically interpreted as the utilization of less beams B than the number of sensors initially involved in the DOA estimation. Nevertheless, this requires the search for signal sources is only conducted in a limited subband of the entire spatial spectrum. Thus, *a priori* knowledge about the approximate positions of the transmitting signal sources is necessary to effectively reduce the complexity while simultaneously increasing the degree of resolution associated with the operation in the element space. If no prior information is available, a two-step DOA estimation can be used. This implies a rough estimation of the signal directions in the first step, and a fine estimation to exploit this information in the second step. Another approach in the unknown case is parallel processing of

overlapping sectors of the angle spectrum to cover the whole space.

These observations motivate the development of a beamspace implementation of the Krylov subspace-based direction finding methods. As a consequence, computationally efficient versions of the AVF-based and the CG-based algorithm with improved performance are presented in this chapter. In conjunction with these two proposed algorithms, termed beamspace auxiliary vector filtering (BS AVF) algorithm and beamspace conjugate gradient (BS CG) algorithm, their ability to reduce the complexity and their achievable localization accuracy is studied. To this end, we compare the proposed beamspace algorithms to BS MUSIC [32], BS Root-MUSIC [33], BS ESPRIT [34]. In our development, we assume that there are only signal sources in the sector of interest.

4.2 Beamspace processing

The strategy of beamspace DOA estimation can be divided into two stages as depicted in Figure 4.1. The first processing step is concerned with the beamforming methodology, where the M -dimensional output data associated with the incident signals at each of the M sensor elements is passed through the beamforming preprocessor. If properly designed on the basis of the prior knowledge, it provides the transformed data in the B -dimensional beamspace, where B is the number of beams and $d < B < M$. In the second stage, the DOA estimation scheme, the signal directions are estimated with increased accuracy by processing the obtained beamspace data.

Employing the system model introduced in Section 2.1 the linear transformation of the original data from \mathbb{C}^M into \mathbb{C}^B performed by the preprocessor is achieved by

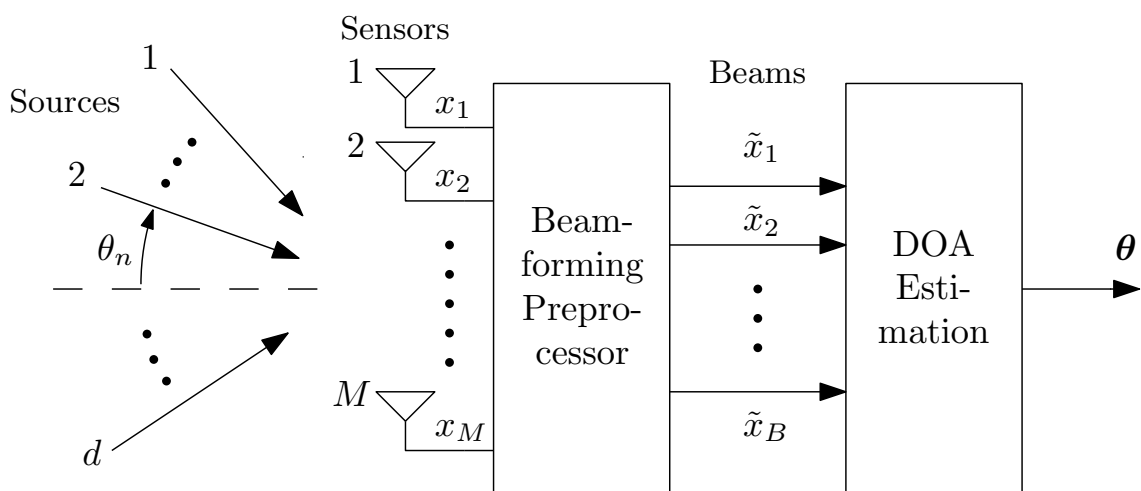


Fig. 4.1: Diagram of the beamspace environment.

premultiplying the array output vector $\mathbf{x}(i)$ by the transformation matrix \mathbf{W} . Thus, the new beamspace snapshot vector is given by

$$\tilde{\mathbf{x}}(i) = \mathbf{W}^H \mathbf{x}(i) \in \mathbb{C}^{B \times 1}, \quad (4.2)$$

where \mathbf{W} is the $M \times B$ beamforming matrix consisting of the steering vectors that generate beams pointing into the *a priori* information-based directions. In what follows, all the quantities in beamspace are denoted by an over tilde. Taking into account the available data record N , equation (4.2) can be compactly rewritten in matrix form as

$$\tilde{\mathbf{X}} = \mathbf{W}^H \mathbf{X} \in \mathbb{C}^{B \times N}. \quad (4.3)$$

Furthermore, we can expand the transformed output in the beamspace by using the signal model stated in Section 2.1, which yields

$$\tilde{\mathbf{X}} = \mathbf{W}^H \mathbf{A}(\boldsymbol{\theta}) \mathbf{S} + \mathbf{W}^H \mathbf{N}. \quad (4.4)$$

The $B \times B$ beamspace covariance matrix for a zero-mean $\tilde{\mathbf{x}}(i)$ is then computed by

$$\tilde{\mathbf{R}} = \mathbb{E} \left\{ \tilde{\mathbf{x}}(i) \tilde{\mathbf{x}}^H(i) \right\} = \mathbf{W}^H \mathbf{R} \mathbf{W}, \quad (4.5)$$

where \mathbf{R} is the covariance matrix of dimension $M \times M$ in the element space. Inserting the expression for \mathbf{R} into (4.5), we get

$$\tilde{\mathbf{R}} = \mathbf{W}^H \mathbf{A}(\boldsymbol{\theta}) \mathbf{R}_{ss} \mathbf{A}^H(\boldsymbol{\theta}) \mathbf{W} + \sigma_n^2 \mathbf{W}^H \mathbf{W}, \quad (4.6)$$

where $\mathbf{R}_{ss} = \mathbb{E} \{ \mathbf{s}(i) \mathbf{s}^H(i) \}$ is the signal covariance matrix that is diagonal if the incident signals are uncorrelated. Assuming that the columns of \mathbf{W} are orthonormal gives

$$\mathbf{W}^H \mathbf{W} = \mathbf{I}. \quad (4.7)$$

Now, according to (4.2), we apply the same transformation to the steering vectors to obtain their lower-dimensional beamspace versions, which are calculated by

$$\tilde{\mathbf{a}}(\theta_n) = \mathbf{W}^H \mathbf{a}(\theta_n), \quad n = 1, \dots, d. \quad (4.8)$$

Employing the matrix version of (4.8) and using (4.7), we can rewrite equation (4.6) as

$$\tilde{\mathbf{R}} = \tilde{\mathbf{A}}(\boldsymbol{\theta}) \mathbf{R}_{ss} \tilde{\mathbf{A}}^H(\boldsymbol{\theta}) + \sigma_n^2 \mathbf{I} \in \mathbb{C}^{B \times B}. \quad (4.9)$$

An eigenvalue decomposition enables us to express $\tilde{\mathbf{R}}$ in terms of its eigenvalues and corresponding eigenvectors, leading to

$$\tilde{\mathbf{R}} = \tilde{\mathbf{U}}_s \tilde{\mathbf{\Lambda}}_s \tilde{\mathbf{U}}_s^H + \tilde{\mathbf{U}}_n \tilde{\mathbf{\Lambda}}_n \tilde{\mathbf{U}}_n^H, \quad (4.10)$$

where the diagonal matrices $\tilde{\mathbf{\Lambda}}_s$ and $\tilde{\mathbf{\Lambda}}_n$ in the beamspace domain contain the d largest eigenvalues and the $B - d$ smallest eigenvalues, respectively, and $\tilde{\mathbf{U}}_s$ and $\tilde{\mathbf{U}}_n$ represent their corresponding orthonormal eigenvectors.

4.3 Beamspace transformation matrix

In order to maintain or even improve the degree of resolution compared to the element space, the beamspace transformation matrix needs to be chosen properly. Otherwise we may lose information, which can degrade the estimation performance. The design of the transformation matrix is determined by the beam pattern, which is constructed to suit for different characteristics in the system. More specifically, the columns of the transformation matrix \mathbf{B} can be physically interpreted as beams that point to different angles. Thus, the performance of the operation in beamspace simply depends on the properties of those beams. It was shown in [31] that an adequately designed beamforming preprocessor leads to a more robust estimator regarding array calibration perturbations and increases the ability to resolve two closely-spaced signals. The only restriction as seen from (4.7) is the orthonormality of the beam vectors that form the transformation matrix. Also, for the sake of convenience, we assume that a uniform linear array (ULA) is employed. In this section, we discuss the properties of two various beamspace matrices, namely the discrete Fourier transform (DFT) matrix and the discrete prolate spheroidal sequences (DPSS) matrix.

4.3.1 Discrete Fourier transform (DFT) beamspace

The most common preprocessing scheme is the $M \times B$ DFT matrix beamformer composed of B consecutive columns of the M -point DFT matrix with $d < B < M$. The output in the DFT beamspace is formed as

$$\tilde{\mathbf{x}}_{B,m}(i) = \mathbf{W}_{B,m}^H \mathbf{x}(i) \in \mathbb{C}^{B \times 1}, \quad (4.11)$$

where m denotes the first column of the DFT manifold $0 \leq m \leq (M - 1)$, which is determined from the prior knowledge and thus selects the sector of interest. The subscripts B and m in $\mathbf{W}_{B,m}$ are intended to clarify the dependency on the number of

beams B and the subband m under consideration, respectively. The resulting orthogonal beam pointing angles are equispaced by the distance $\Delta u = \frac{2}{M}$, so that $\mathbf{W}_{B,m}$ is given by

$$\mathbf{W}_{B,m} = \left[\mathbf{w} \left(m \frac{2}{M} \right), \mathbf{w} \left((m+1) \frac{2}{M} \right), \dots, \mathbf{w} \left((m+B-1) \frac{2}{M} \right) \right], \quad (4.12)$$

where the DFT beamforming vector $\mathbf{w}(u)$ exhibits the Vandermonde structure

$$\mathbf{w}(u) = [1, e^{j\pi u}, \dots, e^{j(M-1)\pi u}]^T \in \mathbb{C}^{M \times 1} \quad (4.13)$$

with $u \in \left\{ m \frac{2}{M}, (m+1) \frac{2}{M}, \dots, (m+B-1) \frac{2}{M} \right\}$ defining the range of the sector of interest.

4.3.2 Discrete prolate spheroidal sequences (DPSS) beamspace

Discrete prolate spheroidal sequences, also referred to as Slepian sequences, were firstly introduced in the work of [35] and later on applied to beamspace processing in [36]. The basic idea is to maximize the ratio of the energy of the b th beam in the sector defined by $[-\theta_0, \theta_0]$ to the total energy of the b th beam in the entire spatial spectrum described by $[-\theta_0, \theta_0]$, which can be formulated according to [1] as

$$\alpha_b = \frac{\int_{-\theta_0}^{\theta_0} |\mathbf{w}_b^H \mathbf{a}(\theta)|^2 d\theta}{\int_{-\pi}^{\pi} |\mathbf{w}_b^H \mathbf{a}(\theta)|^2 d\theta} \quad b = 1, \dots, B, \quad (4.14)$$

where \mathbf{w}_b is the b th columns of the transformation matrix \mathbf{W}_{B,θ_0} . Similar to the previous section, the subscripts B and θ_0 denote the number of beams B and the width $2\theta_0$ of the subband. Equation (4.14) can be more compactly expressed in matrix form as

$$\alpha_b = \frac{\mathbf{w}_b^H \mathbf{K} \mathbf{w}_b}{2\pi \mathbf{w}_b^H \mathbf{w}_b}, \quad (4.15)$$

where the (m, n) of \mathbf{K} is defined by

$$\mathbf{K}_{(m,n)} = \frac{2 \sin[(m-n)\theta_0]}{(m-n)} \quad \text{for } m \neq n \quad (4.16)$$

and

$$\mathbf{K}_{(m,n)} = 2\theta_0 \quad \text{for } m = n. \quad (4.17)$$

As shown in [1], maximizing the expression (4.15) corresponds to finding the B eigenvectors of the matrix \mathbf{K} associated with the B largest eigenvectors. These eigenvectors are termed DPSSs and construct the columns of \mathbf{W}_{B,θ_0} .

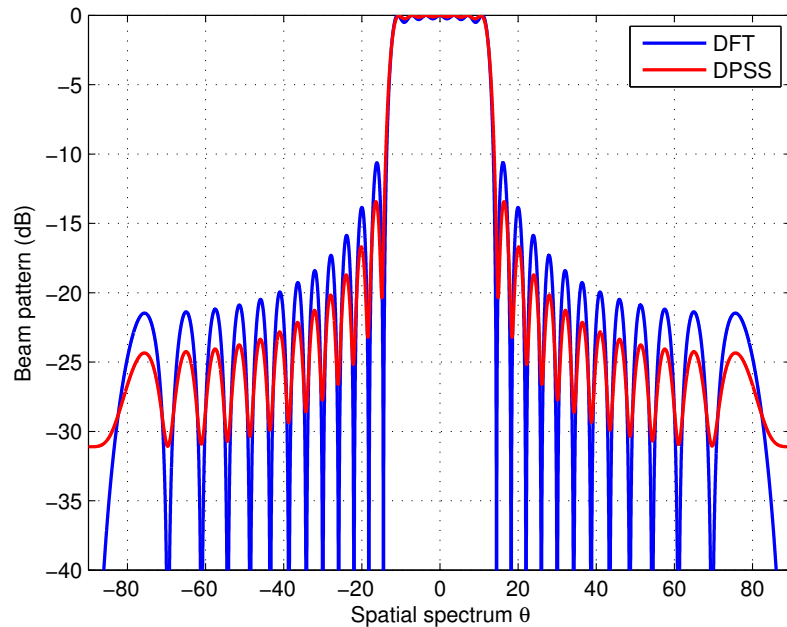


Fig. 4.2: Comparison of the DFT and DPSS spatial filters with $M = 32$ and $B = 7$.

4.3.3 Comparison of the DFT and DPSS spatial filters

In this section, we compare the characteristics of the DFT and the DPSS spatial filters in terms of their passband transmission and their stopband attenuation. Figure 4.2 shows the response of a sensor array composed of $M = 32$ elements, where both spatial filters are formed by $B = 7$ beams and offer a bandwidth of 24° . It is evident from Figure 4.2 that the DFT and the DPSS filters perform similarly, but the passband of the DPSS window exhibits a smaller ripple, and provides a better rejection performance in the stopband as the peaks are significantly lower. According to these observations, we expect a slightly better estimation performance of direction finding algorithms in the DPSS beamspace than in the DFT beamspace.

4.4 Beamspace direction finding based on the CG algorithm

In this section, we apply the beamspace strategy to the direction finding technique based on the conjugate gradient (CG) algorithm in order to reduce the dimensionality of the data resulting in a lower computational complexity, and to further increase its ability to resolve two closely-spaced signal sources under severe conditions. The novel BS CG algorithm is developed according to the previous work in [16, 17].

The originally proposed CG method [6] is used to minimize a cost function or,

equivalently, to solve a linear system of equations. It approaches the optimal solution step by step via a line search along successive directions, which are sequentially determined at each iteration [6]. Applying the CG algorithm to beamspace direction finding, the system of equations, also known as the Wiener-Hopf equations, which is iteratively solved for \mathbf{w} at each scanning angle, is given by

$$\tilde{\mathbf{R}}\tilde{\mathbf{w}} = \tilde{\mathbf{b}}(\theta), \quad (4.18)$$

where $\tilde{\mathbf{R}}$ is the covariance matrix of the transformed data (4.2) and $\tilde{\mathbf{b}}(\theta)$ is the initial vector depending on the search angle. The initialization for $\tilde{\mathbf{b}}(\theta)$ is defined, according to [17], as

$$\tilde{\mathbf{b}}(\theta) = \frac{\tilde{\mathbf{R}}\tilde{\mathbf{a}}(\theta)}{\|\tilde{\mathbf{R}}\tilde{\mathbf{a}}(\theta)\|}, \quad (4.19)$$

where $\tilde{\mathbf{a}}(\theta)$ is the scanning vector in the beamspace, which is linearly transformed by the beamspace covariance matrix $\tilde{\mathbf{R}}$ and normalized. The scanning vector is expressed corresponding to (4.8) as

$$\tilde{\mathbf{a}}(\theta) = \mathbf{W}^H \mathbf{a}(\theta). \quad (4.20)$$

The extended Krylov-based signal subspace of rank $d+1$ is generated by performing d iterations of the BS CG algorithm summarized in Table 4.1. The set of orthogonal residual vectors

$$\tilde{\mathbf{G}}_{d+1}(\theta) = [\tilde{\mathbf{b}}(\theta), \tilde{\mathbf{g}}_1(\theta), \dots, \tilde{\mathbf{g}}_d(\theta)], \quad (4.21)$$

where $\tilde{\mathbf{b}}(\theta) = \tilde{\mathbf{g}}_0(\theta)$, spans the extended Krylov subspace composed of the true signal subspace of dimension d and the scanning vector itself. All the residual vectors are normalized apart from the last one. If $\theta \in \{\theta_1, \dots, \theta_d\}$, the initial vector $\tilde{\mathbf{b}}(\theta)$ lies in the true signal subspace $\mathbf{A}(\theta)$ (cf. Section 2.2.1) and thus, the set of vectors $\tilde{\mathbf{G}}_{d+1}(\theta)$ are also contained in the column space of $\mathbf{A}(\theta)$ [17]. However, $\tilde{\mathbf{G}}_{d+1}$ is not a basis for the true signal subspace so that the rank of the generated Krylov signal subspace drops from $d+1$ to d . This implies that since $\tilde{\mathbf{g}}_d(\theta)$ is not a linear combination of the other residual vectors because it is orthogonal to all of them, the following equation holds:

$$\tilde{\mathbf{g}}_d(\theta) = \mathbf{0}, \quad (4.22)$$

where $\tilde{\mathbf{g}}_d(\theta)$ is the last unnormalized residual vector.

In order to exploit this observation, the spectral function of the proposed BS CG direction finding algorithm as defined in [16] is given by

$$\tilde{P}(\theta_n) = \frac{1}{\|\tilde{\mathbf{g}}_d^H(\theta_n)\tilde{\mathbf{G}}_{d+1}(\theta_{n-1})\|^2}, \quad (4.23)$$

Tab. 4.1: The proposed DFT BS CG algorithm

<p>Beamspace transformation: $\tilde{\mathbf{x}}_{B,m}(i) = \mathbf{W}_{B,m}^H \mathbf{x}(i)$, $\tilde{\mathbf{a}}_{B,m}(\theta) = \mathbf{W}_{B,m}^H \mathbf{a}(\theta)$ for each angle θ $\tilde{\mathbf{d}}_1(\theta) = \tilde{\mathbf{g}}_0(\theta) = \tilde{\mathbf{b}}(\theta)$, $\tilde{\rho}_0(\theta) = \tilde{\mathbf{g}}_0^H(\theta) \tilde{\mathbf{g}}_0(\theta)$ for $k = 1, \dots, d$ $\tilde{\mathbf{v}}_k(\theta) = \tilde{\mathbf{R}} \tilde{\mathbf{d}}_k(\theta)$ $\tilde{\alpha}_k(\theta) = [\tilde{\mathbf{d}}_k^H(\theta) \tilde{\mathbf{v}}_k(\theta)]^{-1} \tilde{\rho}_{k-1}(\theta)$ $\tilde{\mathbf{g}}_k(\theta) = \tilde{\mathbf{g}}_{k-1}(\theta) - \tilde{\alpha}_k(\theta) \tilde{\mathbf{v}}_k(\theta)$ $\tilde{\rho}_k(\theta) = \tilde{\mathbf{g}}_k^H(\theta) \tilde{\mathbf{g}}_k(\theta)$ $\tilde{\beta}_k(\theta) = [\tilde{\rho}_{k-1}(\theta)]^{-1} \tilde{\rho}_k(\theta)$ $\tilde{\mathbf{d}}_{k+1}(\theta) = \tilde{\mathbf{g}}_k(\theta) + \tilde{\beta}_k(\theta) \tilde{\mathbf{d}}_k(\theta)$ end end</p>
--

where θ_n denotes the search angle in the entire angle range $\{-90^\circ, \dots, 90^\circ\}$ with $\theta_n = n\Delta^\circ - 90^\circ$, where Δ° is the search step and $n = 0, 1, \dots, 180^\circ/\Delta^\circ$. The matrix $\tilde{\mathbf{G}}_{d+1}(\theta_{n-1})$ contains all the residual vectors at the $(n-1)$ th angle and $\tilde{\mathbf{g}}_d(\theta_n)$ is the last residual vector calculated at the current search step n . If $\theta_n \in \{\theta_1, \dots, \theta_d\}$, then $\tilde{\mathbf{g}}_d(\theta_n) = \mathbf{0}$ and we expect to see a peak in the pseudo spectrum.

In practical applications, the true covariance matrix in the beamspace domain $\tilde{\mathbf{R}}$ is unknown and needs to be estimated. Thus, the terms $\tilde{\mathbf{g}}_d(\theta_n)$ and $\tilde{\mathbf{G}}_{d+1}(\theta_{n-1})$ in the denominator become approximations and as a result, the spectral function defined in (4.23) will merely provide a very large value but not approach infinity as for the genuine covariance matrix. Eventually, a peak search algorithm is applied to obtain the signal directions $\boldsymbol{\theta}$ from the d largest peaks of the pseudo spectrum.

4.5 Beamspace direction finding based on the AVF algorithm

This section is concerned with the development of the DOA estimation algorithm in the beamspace based on the auxiliary vector filtering (AVF) algorithm, which we refer to as the BS AVF algorithm. The concept of iteratively generating a non-eigenvector basis for the signal subspace and the search for the rank collapse of the extended Krylov signal subspace is the same as for the CG-based version. This approach employs the AVF algorithm to solve the system of equations in (4.18) for each search angle step by step by utilizing auxiliary vectors. The AVF algorithm was firstly applied to sensor signal processing by the adaptive filtering work in [9] and was then exploited for direction finding in [16]. In this work, the latter algorithm is extended to the operation

in beamspace to reduce the computational burden while enhancing the estimation performance.

According to [16] and to Section 4.4, we start our development with the initial vector $\tilde{\mathbf{b}}(\theta)$ after performing the beamspace transformations stated in (4.2) and (4.20). Again, the initialization for $\tilde{\mathbf{b}}(\theta)$ is a normalized linear transformation of the transformed scanning vector $\tilde{\mathbf{a}}(\theta)$ depending on the angle, i.e.,

$$\tilde{\mathbf{b}}(\theta) = \frac{\tilde{\mathbf{R}}\tilde{\mathbf{a}}(\theta)}{\|\tilde{\mathbf{R}}\tilde{\mathbf{a}}(\theta)\|}. \quad (4.24)$$

Then, we aim to find an arbitrary fixed auxiliary vector $\tilde{\mathbf{g}}_1(\theta)$ that is orthonormal with respect to $\tilde{\mathbf{b}}(\theta)$ in the beamspace and maximizes the magnitude of the cross correlation between $\tilde{\mathbf{b}}^H(\theta)\tilde{\mathbf{x}}$ and $\tilde{\mathbf{g}}_1^H(\theta)\tilde{\mathbf{x}}$. Formulating this concept as an optimization problem with respect to the orthonormality constraint yields

$$\begin{aligned} \tilde{\mathbf{g}}_1(\theta) &= \underset{\tilde{\mathbf{g}}_1(\theta)}{\operatorname{argmax}} \quad \left| \mathbb{E} \left\{ \tilde{\mathbf{b}}^H(\theta)\tilde{\mathbf{x}}[\tilde{\mathbf{g}}_1^H(\theta)\tilde{\mathbf{x}}]^H \right\} \right| \\ &= \underset{\tilde{\mathbf{g}}_1(\theta)}{\operatorname{argmax}} \quad \left| \mathbb{E} \left\{ \tilde{\mathbf{b}}^H(\theta)\tilde{\mathbf{R}}\tilde{\mathbf{g}}_1(\theta) \right\} \right| \\ &\text{s.t. } \tilde{\mathbf{g}}_1^H(\theta)\tilde{\mathbf{b}}(\theta) = 0, \quad \|\tilde{\mathbf{g}}_1(\theta)\| = 1. \end{aligned} \quad (4.25)$$

The solution to this constraint problem is given in [16] as

$$\tilde{\mathbf{g}}_1(\theta) = \frac{(\mathbf{I} - \tilde{\mathbf{b}}(\theta)\tilde{\mathbf{b}}^H(\theta))\tilde{\mathbf{R}}\tilde{\mathbf{b}}(\theta)}{\|(\mathbf{I} - \tilde{\mathbf{b}}(\theta)\tilde{\mathbf{b}}^H(\theta))\tilde{\mathbf{R}}\tilde{\mathbf{b}}(\theta)\|}. \quad (4.26)$$

Now, in order to compute the first step to solve the beamspace-transformed system of equations in (4.18), we define the iteration

$$\tilde{\mathbf{w}}_1(\theta) = \tilde{\mathbf{b}}(\theta) - \mu_1(\theta)\tilde{\mathbf{g}}_1(\theta), \quad (4.27)$$

where $\mu_1(\theta)$ is the step size, which is the solution of the minimization problem dealing with the output power described as

$$\mu_1(\theta) = \min \quad \mathbb{E} \left\{ |\tilde{\mathbf{w}}_1^H(\theta)\tilde{\mathbf{x}}|^2 \right\} \quad (4.28)$$

and is computed by [16]

$$\mu_1(\theta) = \frac{\tilde{\mathbf{g}}_1^H(\theta)\tilde{\mathbf{R}}\tilde{\mathbf{b}}(\theta)}{\tilde{\mathbf{g}}_1^H(\theta)\tilde{\mathbf{R}}\tilde{\mathbf{g}}_1(\theta)}. \quad (4.29)$$

As the constructed extended Krylov signal subspace $\tilde{\mathbf{G}}_{d+1}(\theta)$ in the beamspace domain includes the initial vector, $d - 1$ further iterations of this procedure above to

Tab. 4.2: The proposed DFT BS AVF algorithm

<p>Beamspace transformation:</p> $\tilde{\mathbf{x}}_{B,m}(i) = \mathbf{W}_{B,m}^H \mathbf{x}(i), \quad \tilde{\mathbf{a}}_{B,m}(\theta) = \mathbf{W}_{B,m}^H \mathbf{a}(\theta)$ <p>for each angle θ</p> $\tilde{\mathbf{b}}(\theta) = \frac{\tilde{\mathbf{R}}\tilde{\mathbf{a}}(\theta)}{\ \tilde{\mathbf{R}}\tilde{\mathbf{a}}(\theta)\ }, \quad \tilde{\mathbf{g}}_1(\theta) = \frac{(\mathbf{I} - \tilde{\mathbf{b}}(\theta)\tilde{\mathbf{b}}^H(\theta))\tilde{\mathbf{R}}\tilde{\mathbf{b}}(\theta)}{\ (\mathbf{I} - \tilde{\mathbf{b}}(\theta)\tilde{\mathbf{b}}^H(\theta))\tilde{\mathbf{R}}\tilde{\mathbf{b}}(\theta)\ }$ <p>for $k = 2, \dots, d-1$</p> $\tilde{\mathbf{g}}_k(\theta) = \frac{\left(\mathbf{I} - \sum_{i=k-2}^{i=k-1} \tilde{\mathbf{g}}_i(\theta)\tilde{\mathbf{g}}_i^H(\theta) \right) \tilde{\mathbf{R}}\tilde{\mathbf{g}}_{k-1}(\theta)}{\left\ \left(\mathbf{I} - \sum_{i=k-2}^{i=k-1} \tilde{\mathbf{g}}_i(\theta)\tilde{\mathbf{g}}_i^H(\theta) \right) \tilde{\mathbf{R}}\tilde{\mathbf{g}}_{k-1}(\theta) \right\ }$ $\mu_n(\theta) = -\mu_{n-1}(\theta) \frac{\tilde{\mathbf{g}}_n^H(\theta)\tilde{\mathbf{R}}\tilde{\mathbf{g}}_{n-1}(\theta)}{\tilde{\mathbf{g}}_n^H(\theta)\tilde{\mathbf{R}}\tilde{\mathbf{g}}_n(\theta)}$ <p>end</p> $\tilde{\mathbf{g}}_d(\theta) = -\mu_{d-1}(\theta) \left(\mathbf{I} - \sum_{i=d-2}^{i=d-1} \tilde{\mathbf{g}}_i(\theta)\tilde{\mathbf{g}}_i^H(\theta) \right) \tilde{\mathbf{R}}\tilde{\mathbf{g}}_{d-1}(\theta)$ <p>end</p>

determine the d auxiliary vectors are performed. It is important to note that the last auxiliary vector is unnormalized. Similarly to the CG-based beamspace algorithm, the auxiliary vector basis is formed in the following way:

$$\tilde{\mathbf{G}}_{d+1}(\theta) = [\tilde{\mathbf{b}}(\theta), \tilde{\mathbf{g}}_1(\theta), \dots, \tilde{\mathbf{g}}_d(\theta)]. \quad (4.30)$$

Considering the fact that this strategy requires the computation of the vectors $\tilde{\mathbf{w}}_k(\theta)$ for each iteration $k = 2, \dots, d-1$, a direct way of obtaining the d auxiliary vectors was proposed in [37] and is summarized in Table 4.2 for the beamspace version.

Finally, by using the concept that $\tilde{\mathbf{g}}_d(\theta) = \mathbf{0}$ if $\theta \in \{\theta_1, \dots, \theta_d\}$, we define the spectral function for the pseudo spectrum in the same fashion as in (4.23) for the CG-based version, yielding

$$\tilde{P}(\theta_n) = \frac{1}{\|\tilde{\mathbf{g}}_d^H(\theta_n)\tilde{\mathbf{G}}_{d+1}(\theta_{n-1})\|^2}. \quad (4.31)$$

Once more θ_n is the search angle in the angle range $\{-90^\circ, \dots, 90^\circ\}$ with $\theta_n = n\Delta^\circ - 90^\circ$, where Δ° is the search step and $n = 0, 1, \dots, 180^\circ/\Delta^\circ$. Again, $\tilde{\mathbf{G}}_{d+1}(\theta_{n-1})$ contains all the auxiliary vectors at the $(n-1)$ th angle, and $\tilde{\mathbf{g}}_d(\theta_n)$ is the last unnormalized auxiliary vector calculated at the current search step n . If $\theta_n \in \{\theta_1, \dots, \theta_d\}$, then $\tilde{\mathbf{g}}_d(\theta_n) = \mathbf{0}$ and a peak occurs in the pseudo spectrum. The desired signal directions $\boldsymbol{\theta}$ are extracted from the location of the d largest peaks in the spatial spectrum.

4.6 Computational complexity

As mentioned in the introduction, the key advantage of the operation in the beamspace domain is to reduce the computational complexity linked with the conventional techniques in element space. Therefore, in this part, we evaluate the computational cost of the two proposed Krylov subspace-based methods, the BS AVF and the BS CG algorithms, and compare them to the complexity of the classical direction finding methods in element space as well as their beamspace versions. Considering the well-established DOA estimation algorithms, such as MUSIC [12], Root-MUSIC [13] and ESPRIT [14], the required subspace estimate for them is obtained by applying either a singular value decomposition (SVD) to the received array output matrix \mathbf{X} or an equivalent eigenvalue decomposition (EVD) of the covariance matrix \mathbf{R} . As the dimensions of both matrices are different, these two decompositions also cause different computational costs. Thus, we distinguish between them in the following analysis.

4.6.1 Subspace estimation via SVD

The computational cost, depicted in Table 4.3 and Table 4.4, is measured in terms of the number of additions and multiplications respectively, where M denotes the number of sensor elements, B is the number of the beam pointing angles, d is the number of signals, and Δ° is the search step. It is important to note that the arithmetic operations in Table 4.3 and Table 4.4 assume the application of an SVD to estimate the signal subspace for the conventional direction finding methods. Moreover, the search for peaks in the pseudo spectrum is not considered as necessary for MUSIC and the CG algorithm in order to provide a fair comparison of all the methods. It is evident from the two tables that the BS AVF and the BS CG algorithm have a cost, which is variable with $O((180/\Delta^\circ)M^2d)$ and depends on the search step Δ° as the Krylov signal subspace is generated for each search angle. However, by performing the transformation into the lower dimensional beamspace, the number of sensor elements M can be replaced by the number of beams B although the transformation itself also needs to be taken into account.

Figure 4.3 shows the complexity in terms of arithmetic operations of the analyzed algorithms as a function of the number of sensor elements M . The number of beams B is optimized for each direction finding algorithm in beamspace to provide the best estimation performance. The proposed BS CG method requires $B = 5$ beams to achieve its optimal performance, whereas the proposed BS AVF, the BS MUSIC, BS Root-MUSIC, and the BS ESPRIT algorithms only demand $B = 3$ beams. This is due

Tab. 4.3: Number of additions applying the SVD

Algorithm	Additions
MUSIC [12]	$180/\Delta^\circ(M^2 - M(d-1) - 2) + 8MN^2$
BS MUSIC [32]	$180/\Delta^\circ(B^2 - B(d-1) - 2) + B(8N^2 + N(M-1) + M-1)$
Root-MUSIC [13]	$2M^3 - dM^2 + M(8N^2 - 2) + 1$
BS Root-MUSIC [33]	$B^4 + 3B^3 - B^2(d+1) + B(8N^2 + N(M-1) + d-2) + 1$
ESPRIT [14]	$2dM^2 + M(d^2 - 4d + 8N^2) + 8d^3 - d^2 + 2d$
BS ESPRIT [34]	$B^2(M + 3d - 1) + B(2M^2 + M(N-4) + d^2 - d) + B(8N^2 - N + 2) + 8d^3$
AVF [16]	$180/\Delta^\circ(4dM^2 + M(2d-3) - 3d+2) + M^2(N-1)$
Proposed BS AVF	$180/\Delta^\circ(4dB^2 + B(2d-3) - 3d+2) + B^2(N-1) + B(N(M-1) + M-1)$
CG [17]	$180/\Delta^\circ(M^2(d+1) + M(5d+1) - 3d-2) + M^2(N-1)$
Proposed BS CG	$180/\Delta^\circ(B^2(d+1) + B(5d+1) - 3d-2) + B^2(N-1) + B(N(M-1) + M-1)$

Tab. 4.4: Number of multiplications applying the SVD

Algorithm	Multiplications
MUSIC [12]	$180/\Delta^\circ(M^2 + M(2-d) - d) + 8MN^2$
BS MUSIC [32]	$180/\Delta^\circ(B^2 + B(2-d) - d) + B(M(N+1) + 8N^2)$
Root-MUSIC [13]	$2M^3 - dM^2 + 8MN^2$
BS Root-MUSIC [33]	$B^4 + 3B^3 - B^2(d-4) + B(MN + 8N^2 - 4)$
ESPRIT [14]	$2dM^2 + M(d^2 - 2d + 8N^2) + 8d^3 - d^2$
BS ESPRIT [34]	$B^2(M + 3d - 1) + B(2M^2 + M(N-4) + 8N^2 - N + d^2) - B(d-2) + 8d^3$
AVF [16]	$180/\Delta^\circ(M^2(3d+1) + M(4d-2) + d+2) + M^2N$
Proposed BS AVF	$180/\Delta^\circ(B^2(3d+1) + B(4d-2) + d+2) + B^2N + BM(N+1)$
CG [17]	$180/\Delta^\circ(M^2(d+1) + M(6d+2) + d+1) + M^2N$
Proposed BS CG	$180/\Delta^\circ(B^2(d+1) + B(6d+2) + d+1) + B^2N + BM(N+1)$

to the iterative way of constructing the signal subspace by the residual vectors in the BS CG method, which requires more input data. The curves in Figure 4.3 indicate that the beamspace algorithms provide a significantly lower complexity than their counterparts in element space as M increases. Specifically, the conventional AVF- and CG-based algorithms in element space constitute a higher computational burden than the other approach for a large array size. However, in the beamspace, the complexity of the BS AVF and the BS CG method is significantly lower than the one of the beamspace

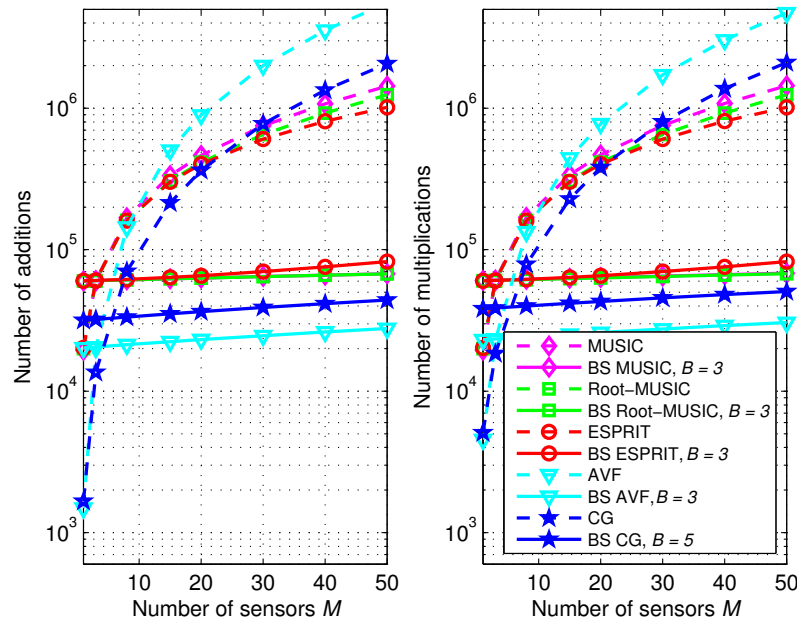


Fig. 4.3: Complexity in terms of arithmetic operations versus the number of sensors M applying the SVD with $d = 3$, $N = 50$, and $\Delta^\circ = 1^\circ$.

versions of MUSIC, Root-MUSIC and ESPRIT, where the BS AVF algorithm requires the lowest complexity. The reason for the higher complexity of the beamspace methods for small M is the applied transformation into the lower dimensional subspace, which increases the number of operations.

4.6.2 Subspace estimation via EVD

Similarly to the previous part, in this section, we assess the computational complexity of the proposed BS AVF and the BS CG algorithm when the EVD is applied to the $M \times M$ covariance matrix \mathbf{R} of the received array output data to estimate the signal subspace. As the dimensions are smaller than for the processing of the entire $(M \times N)$ -dimensional data block \mathbf{X} , a lower computational burden can be expected. Again, the required cost for the analyzed methods is measured in terms of the number of arithmetic operations and depicted in Table 4.5 and Table 4.6. Once more, the peak search is not considered and the EVD is applied to the data covariance matrix.

A visual comparison of the expressions in the tables is depicted in Figure 4.4. The computational savings with regard to the dimensions when applying the EVD translates into a lower complexity of the conventional beamspace techniques. Thus, the two proposed algorithms demand a higher computational burden. However, as the complexity depends on the number of beams, it can be further reduced for large sen-

Tab. 4.5: Number of additions applying the EVD

Algorithm	Additions
MUSIC [12]	$180/\Delta^\circ(M^2 + M(1 - d) - 2) + 8M^3$
BS MUSIC [32]	$180/\Delta^\circ(B^2 + B(1 - d) - 2) + 8B^3 + B(N(M - 1) + M - 1)$
Root-MUSIC [13]	$10M^3 - dM^2 - 2M + 1$
BS Root-MUSIC [33]	$B^4 + 11B^3 - B^2(d + 1) + B(N(M - 1) + d - 2) + 1$
ESPRIT [14]	$8M^3 + 2dM^2 + M(d^2 - 4d) + 8d^3 - d^2 + 2d$
BS ESPRIT [34]	$8B^3 + B^2(M + 3d - 1) + B(2M^2 + M(N - 4) + d^2 - d) - B(N - 2) + 8d^3$
AVF [16]	$180/\Delta^\circ(4dM^2 + M(2d - 3) - 3d + 2) + M^2(N - 1)$
Proposed BS AVF	$180/\Delta^\circ(4dB^2 + B(2d - 3) - 3d + 2) + B^2(N - 1) + B(N(M - 1) + M - 1)$
CG [17]	$180/\Delta^\circ(M^2(d + 1) + M(5d + 1) - 3d - 2) + M^2(N - 1)$
Proposed BS CG	$180/\Delta^\circ(B^2(d + 1) + B(5d + 1) - 3d - 2) + B^2(N - 1) + B(N(M - 1) + M - 1)$

Tab. 4.6: Number of multiplications applying the EVD

Algorithm	Multiplications
MUSIC [12]	$180/\Delta^\circ(M^2 + M(2 - d) - d) + 8M^3$
BS MUSIC [32]	$180/\Delta^\circ(B^2 + B(2 - d) - d) + 8B^3 + BM(N + 1)$
Root-MUSIC [13]	$10M^3 - dM^2$
BS Root-MUSIC [33]	$B^4 + 11B^3 - B^2(d - 4) + B(MN - 4)$
ESPRIT [14]	$8M^3 + 2dM^2 + M(d^2 - 2d) + 8d^3 - d^2$
BS ESPRIT [34]	$8B^3 + B^2(M + 3d - 1) + B(2M^2 + M(N - 4) - N + d^2) - B(d - 2) + 8d^3$
AVF [16]	$180/\Delta^\circ(M^2(3d + 1) + M(4d - 2) + d + 2) + M^2N$
Proposed BS AVF	$180/\Delta^\circ(B^2(3d + 1) + B(4d - 2) + d + 2) + B^2N + BM(N + 1)$
CG [17]	$180/\Delta^\circ(M^2(d + 1) + M(6d + 2) + d + 1) + M^2N$
Proposed BS CG	$180/\Delta^\circ(B^2(d + 1) + B(6d + 2) + d + 1) + B^2N + BM(N + 1)$

sor arrays by decreasing the parameter B and taking a slight loss of the estimation performance. The computational benefit of the two proposed Krylov subspace-based algorithms in beamspace mainly becomes apparent when the entire block of data snapshots is processed via the SVD. However, if each data snapshot is considered separately by applying the EVD, the beamspace versions of MUSIC, Root-MUSIC and ESPRIT still require a lower complexity than the proposed methods.

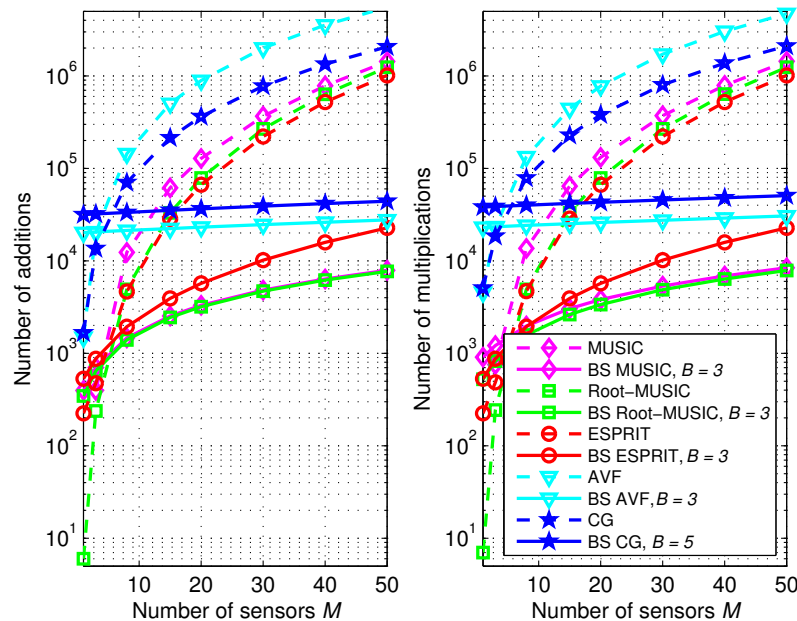


Fig. 4.4: Complexity in terms of arithmetic operations versus the number of sensors M applying the EVD with $d = 3$, $N = 50$, and $\Delta^\circ = 1^\circ$.

4.7 Simulation results

In this section, we extensively examine the efficacy of the two proposed Krylov subspace-based algorithms in beam-space in terms of the estimation accuracy and the resolution capability and compare them to the BS MUSIC, BS Root-MUSIC, BS ESPRIT and their counterparts in element space. The first part of the simulations is concerned with the comparison of all the algorithms in the DFT beam-space, and in the last part we compare the DFT and the DPSS beam-space and analyze the behavior of the considered methods for large sensor arrays to emphasize the link to practical implementations.

4.7.1 Comparison of the proposed algorithms in the DFT beam-space

In order to ascertain the estimation performance of the proposed algorithms for closely-spaced sources in the DFT beam-space, we employ a uniform linear array (ULA) consisting of $M = 10$ omnidirectional sensors with interelement spacing $\Delta = \lambda_c/2$. We assume that there are two uncorrelated complex Gaussian signals with equal power impinging on the array, which are located at 35° and 40° , where the angles of arrival are measured with respect to the broadside of the array. Furthermore, we assume *a priori* knowledge about the approximate positions of the DOAs to select the sector of

interest as $m = 2$. The number of available snapshots at the array output is $N = 50$ and each curve is obtained by averaging a total of $T = 2000$ trials. In order to get relevant results, we set the search step to $\Delta^\circ = 0.1^\circ$.

In the first experiment, the resolution performance of the BS AVF and the BS CG algorithm in comparison to the conventional beamspace techniques is assessed. Figure 4.5 shows the probability of resolution as a function of the SNR, where the number of beams B for each direction finding algorithm in beamspace is optimized to yield the best performance. The signal sources are said to be resolved if the following criterion holds:

$$\sum_{l=1}^{d=2} |\hat{\theta}_l - \theta_l| < \frac{|\theta_1 - \theta_2|}{2}, \quad (4.32)$$

where θ_l is the true direction of arrival and $\hat{\theta}_l$ the estimated angle of the l th source.

It is evident from Figure 4.5 that the resolution capability of the algorithms in beamspace is generally higher compared to their counterparts in element space, since *a priori* knowledge about the approximate positions of the sources is exploited. However, this is not necessarily the case for the proposed BS AVF algorithm whose resolution performance is slightly worse than its counterpart in element space for an SNR between -3 and 5 dB. In our comparison, the proposed BS CG algorithm outperforms the CG algorithm and demonstrates the best ability to resolve the two sources among the existing methods in beamspace and in element space. The fact that the BS CG algorithm reaches its best performance for $B = 5$ beams, while the BS AVF method and the eigenvector-based schemes attain their maximum for only $B = 3$ beams is due to the iterative way of constructing the signal subspace by the residual vectors, which requires more data. We also note that at low SNR the CG method in element space still resolves the two sources better than the eigenvector-based algorithms in beamspace. However, the proposed BS CG method can further improve the performance of the original CG method.

In Figure 4.6, the probability of resolution as a function of the number of snapshots N is illustrated. In order to evaluate the performance under severe conditions, the SNR is fixed at -7 dB. The BS CG algorithm clearly outperforms all the analyzed direction finding techniques in beamspace and element space, and is able to resolve the two sources at such a low SNR with more than 50 percent probability using only $N = 20$ snapshots. Also, it can be seen that the BS AVF algorithm substantially improves the resolution performance of its counterpart but is outperformed by BS ESPRIT and BS Root-MUSIC. We also verify that BS MUSIC, MUSIC, Root-MUSIC, ESPRIT, and the AVF algorithm almost completely fail to separate the two sources under these severe conditions.

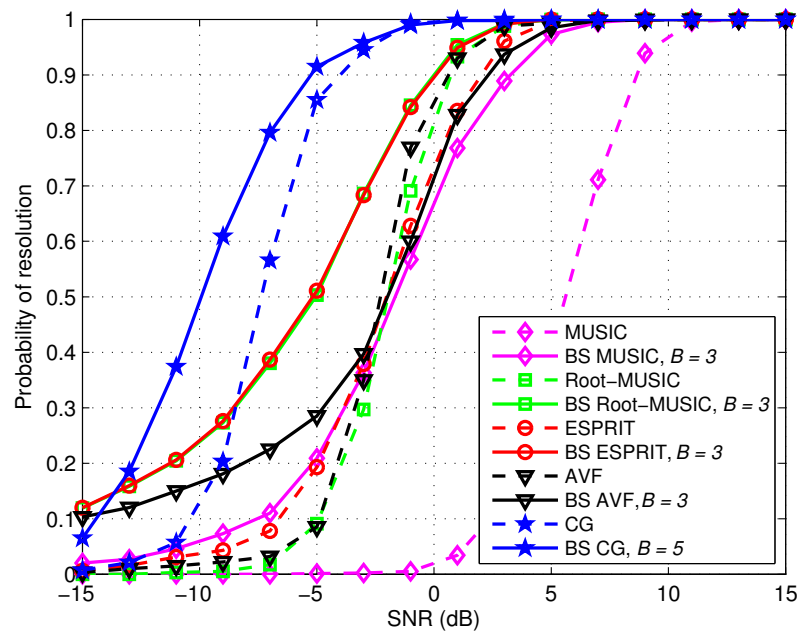


Fig. 4.5: Probability of resolution versus the SNR in the DFT beamspace with $M = 10$, $\theta_1 = 35^\circ$, $\theta_2 = 40^\circ$, $N = 50$, $m = 2$.

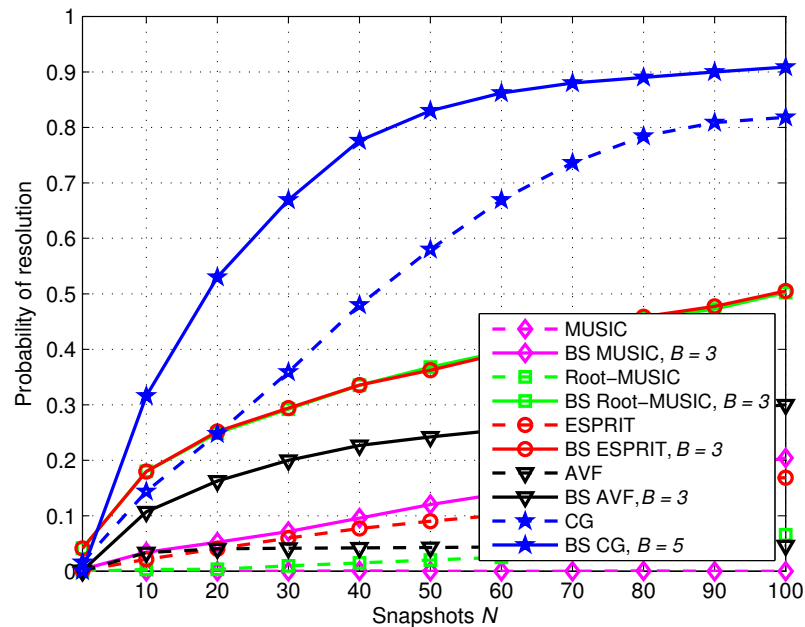


Fig. 4.6: Probability of resolution versus the number of snapshots N in the DFT beamspace with $M = 10$, $\theta_1 = 35^\circ$, $\theta_2 = 40^\circ$, SNR = -7 dB, $m = 2$.

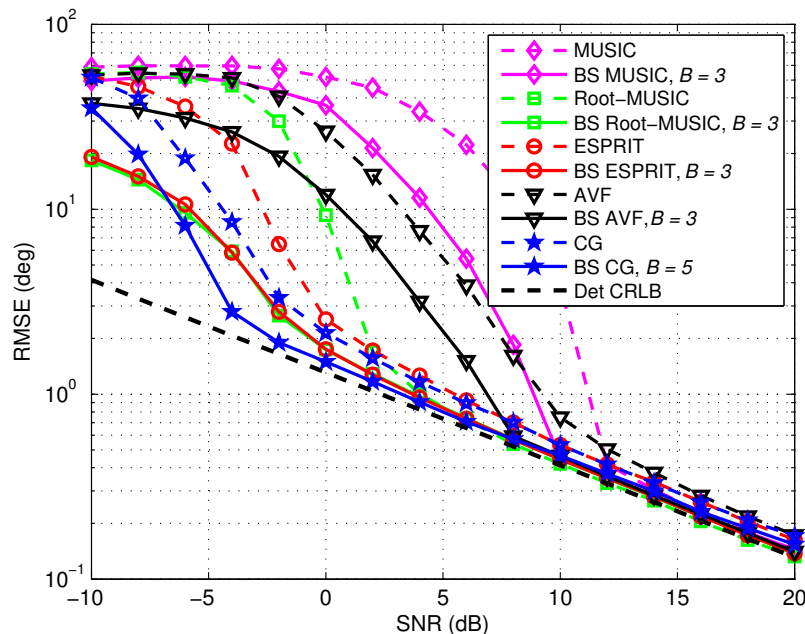


Fig. 4.7: RMSE versus the SNR in the DFT beamspace with $M = 10$, $\theta_1 = 35^\circ$, $\theta_2 = 40^\circ$, $N = 50$, $m = 2$.

In the last part, the estimation accuracy in terms of the root mean square error (RMSE) is investigated, where the RMSE is estimated using T trials by

$$\text{RMSE} = \sqrt{\frac{1}{T} \sum_{t=1}^T \sum_{l=1}^d (\theta_l - \hat{\theta}_l(t))^2}. \quad (4.33)$$

The investigated direction finding algorithms in beamspace and in element space are compared to the deterministic Cramér-Rao lower bound (CRLB) [1]. It was derived in [1] that the CRLB in beamspace is almost equal to the element-space CRLB if the sources are well inside the sector of interest. Since this is the case in our study, only the CRLB in the element space is applied as a reference for the comparison. The resulting RMSE as a function of the SNR is presented in Figure 4.7. Again, all the beamspace versions of the analyzed methods yield a higher estimation accuracy in the underlying scenario. However, whereas the proposed BS AVF method only provides a limited performance, the BS CG algorithm outperforms the beamspace versions of ESPRIT and Root-MUSIC within the range of $\text{SNR} = (-5, \dots, 5)$ dB. Thus, applying the beamspace transformation to the original CG direction finding algorithm significantly improves the estimation accuracy for each SNR value.

4.7.2 Comparison of the DFT and DPSS beamspace

The aim of this section is to examine the potential of operating in the DFT and the DPSS beamspace. It was stated in Section 4.3 that, apart from the applied direction finding method, the estimation performance mainly depends of the design of the beamspace transformation matrix. To this end, we compare the efficacy of the DFT and the DPSS beamspace for the two proposed Krylov subspace-based algorithms. For the simulations, the same scenario from the previous section is chosen to simplify the comparison and similarly to the DFT beamspace, the number of beams for the DPSS beamspace is optimized to yield the best results.

According to Figure 4.8, the resolution performance of the BS CG algorithm in the DPSS beamspace against the SNR is slightly better than that in the DFT beamspace. Furthermore, the DPSS beamspace version of the AVF algorithm compensates the deficiency of the DFT version for relatively high SNR values and thus provides an enhanced resolution capability for closely-spaced sources.

The results shown in Figure 4.9 verify the conclusions drawn from the first figure. The DPSS spatial filter yields a small improvement of the probability of resolution for both proposed beamspace techniques as the data record increases.

Figure 4.10 evaluates the RMSE performance against the SNR and once more, the

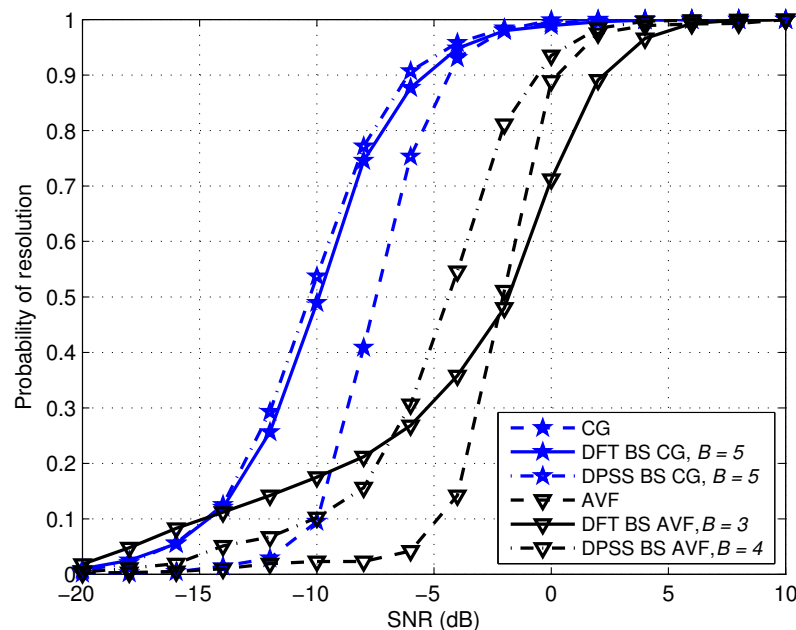


Fig. 4.8: Comparison of the DFT and DPSS beamspace regarding the probability of resolution versus the SNR with $M = 10$, $\theta_1 = 35^\circ$, $\theta_2 = 40^\circ$, $N = 50$, $m = 2$.

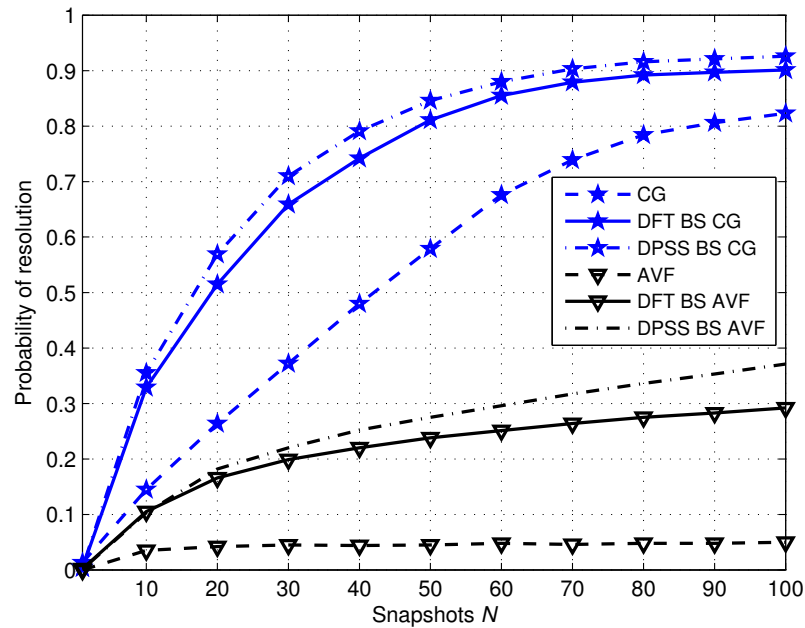


Fig. 4.9: Comparison of the DFT and DPSS beamspace regarding the probability of resolution versus the number of snapshots N with $M = 10$, $\theta_1 = 35^\circ$, $\theta_2 = 40^\circ$, $\text{SNR} = -7$ dB, $m = 2$.

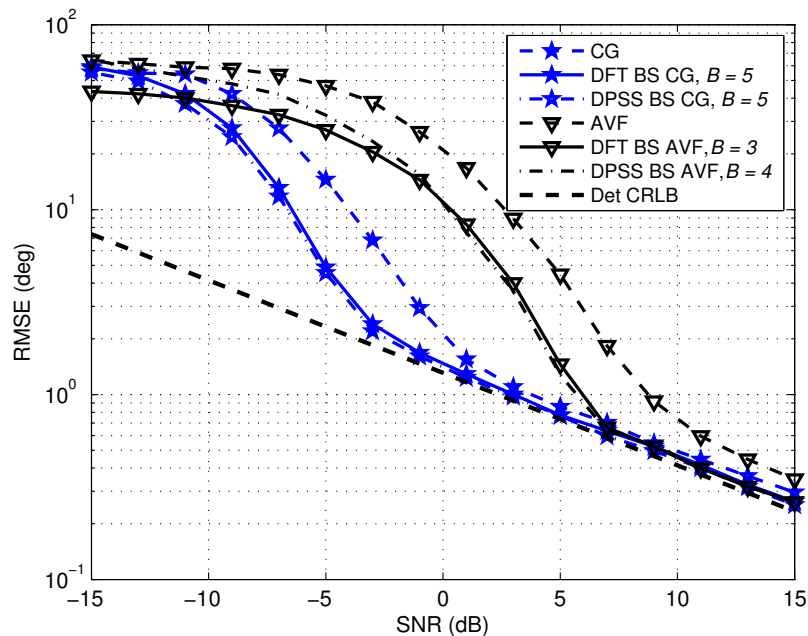


Fig. 4.10: Comparison of the DFT and DPSS beamspace regarding the RMSE versus the SNR with $M = 10$, $\theta_1 = 35^\circ$, $\theta_2 = 40^\circ$, $N = 50$, $m = 2$.

advantage of the DPSS beamspace becomes obvious. The proposed algorithms benefit from the transformation into the lower-dimensional DPSS beamspace, outperforming the versions associated with the DFT beamspace.

As evident from the simulation results, the spatial filter designed by using DPSS tapers implicates a slight performance advantage over the DFT beamspace. This behavior was already anticipated in Section 4.3 based on the fact that the DPSS filter provides a better rejection performance in the stopband and exhibits a smoother transmission in the passband.

4.8 Conclusions

In this chapter, the extension of the recently proposed Krylov subspace-based direction finding techniques based on the auxiliary vector filtering (AVF) algorithm and the conjugate gradient (CG) algorithm to the operation in the beamspace domain is developed. After introducing the promising benefits associated with a reduced complexity while enhancing the estimation performance of the beamspace approach, the general concept and its dependency on the transformation matrix is highlighted. Thus, two different ways of designing the beamspace, namely the discrete Fourier transform (DFT) and the discrete prolate spheroidal sequences (DPSS) beamspace are analyzed and compared. Eventually, the BS AVF algorithm and the BS CG algorithm are proposed, which exploit the knowledge about approximate positions of signal sources to significantly improve their estimation accuracy of closely-spaced sources at a low SNR and a small data record size. While adopting either the residual vectors of the CG algorithm or the auxiliary vectors of the AVF algorithm to iteratively generate the signal subspace in the beamspace domain, they do not resort to an eigendecomposition of the signal covariance matrix saving computational resources. To verify the reduction of the computational burden, an extensive analysis of the complexity requirements is conducted, which illustrates that the proposed beamspace algorithms unfold their reduced demands if the entire snapshot data block is processed. Moreover, the efficacy of these algorithms is assessed by conducting simulations, where the number of beams is optimized. It is shown that operation in beamspace substantially enhances the resolution capability and the estimation accuracy, where the BS CG outperforms the BS AVF algorithm. Also, it is demonstrated that the operation in the DPSS beamspace provides a higher estimation performance than that in the DFT beamspace.

5. KNOWLEDGE-AIDED DIRECTION OF ARRIVAL ESTIMATION

The goal of this chapter is to discuss a practical scenario, where prior knowledge of a subset of the signal directions to be estimated is available. We develop an adaptive procedure for processing this *a priori* knowledge to improve the estimation accuracy of unknown sources in the environment and then devise direction finding algorithms that exploit this information.

5.1 Introduction

Extracting the DOA from received signals impinging on an antenna array has long been of great research interest, given its importance in a broad variety of array signal processing related applications including radar, sonar, biomedical imaging, and wireless communications. With the steady expansion of the field of applications in recent years, the problem of high-resolution parameter estimation has attracted increased attention in the last few decades, and many techniques reported in literature [1] were the result of an extensive study. The most prominent DOA estimation schemes can be categorized into Capon-type algorithms [1, 11], maximum-likelihood (ML) techniques [1, 10] and subspace-based methods [1, 10].

Despite the numerous DOA estimation techniques developed over the years and all their specific properties, advantages and drawbacks, their estimation accuracy mainly depends on the estimate of the covariance matrix \mathbf{R} of the $M \times 1$ array output vector \mathbf{x} , which is defined for the i th of N available snapshots as

$$\mathbf{R} = \mathbb{E} \{ \mathbf{x}(i) \mathbf{x}^H(i) \} \in \mathbb{C}^{M \times M}. \quad (5.1)$$

In practical implementation, the true covariance matrix in (5.1) is unknown, but can

be estimated via the commonly used sample-average formula given by

$$\hat{\mathbf{R}} = \frac{1}{N} \sum_{i=1}^N \mathbf{x}(i)\mathbf{x}^H(i). \quad (5.2)$$

Applying the estimation procedure in (5.2), the estimation accuracy of the covariance matrix is essentially determined by the data record size N . Thus, in applications, where the number of available snapshots approaches the number of sensor elements M or is even smaller ($N < M$), the sample covariance matrix $\hat{\mathbf{R}}$ is a poor estimate of the true covariance matrix \mathbf{R} , which consequently degrades the performance of the subsequent DOA estimation technique.

Considering a practical scenario, e.g., a radar application, with a low signal-to-noise ratio (SNR) and stationary and non-stationary signal sources whose DOAs are to be estimated, the knowledge of the signal directions of certain users can be effectively exploited in order to increase the estimation accuracy of non-stationary unknown sources. Examples of stationary sources are signals coming from base stations or from static users in the system. The knowledge of these DOAs that were previously estimated can be efficiently processed in the form of a known *a priori* covariance matrix \mathbf{C} .

Knowledge-aided (KA) signal processing techniques, which make use of *a priori* knowledge of key parameters of interest such as the existence of jamming signals and the clutter in radar and sonar systems, have recently gained significant attention [38–44]. In KA techniques, the main issues are how to obtain the *a priori* knowledge of the parameters of interest and how to process and exploit them. Prior work on KA algorithms has considered the design of space-time adaptive processing (STAP) techniques [38–41, 43, 44] and beamforming algorithms [42]. These methods have shown superior performance to conventional approaches that do not rely on KA schemes when the limited sample support is used in highly non-stationary clutter environments.

Several applications of KA techniques to the problem of DOA estimation have been developed in the past. One of the most well-known approaches to incorporate prior knowledge of specific signal directions to obtain improved DOA estimates is the so-called constrained MUSIC algorithm [45]. It is based on an orthogonal projection of the array output matrix onto the complement of the true signal subspace spanned by the known steering vectors. While this concept estimates all the DOAs in the system, its extension applying oblique projectors [46] is reduced to only estimating the unknown DOAs. These methods provide substantial performance gains in terms of the estimation accuracy if a large data record size N is available. However, under severe conditions in the environment, such as a low SNR, and especially when $N < M$ as described above, they completely break down and fail to estimate the desired DOAs.

To overcome this problem, the concept of effectively exploiting prior knowledge for STAP and beamforming is applied to DOA estimation.

In this work, we derive a general preprocessing KA technique for high-resolution parameter estimation, which can be applied to any DOA estimation scheme depending on the estimate of the true covariance matrix \mathbf{R} . The novel strategy is shown to substantially improve the estimates of the covariance matrix by incorporating *a priori* knowledge of the signal directions under severe conditions. The proposed technique estimates the DOAs of all the present signals in the scenario and considers the general case, where the known matrix \mathbf{C} is rank deficient and the noise power is assumed to be unknown. In order to evaluate the performance and the gain over the conventional estimation schemes we apply the KA technique for DOA estimation to ESPRIT-type methods, i.e., the standard ESPRIT algorithm [14] and the Unitary ESPRIT algorithm [15] and to MUSIC-type methods, i.e., the classical MUSIC algorithm [12] and the Root-MUSIC algorithm [13].

5.2 Enhanced covariance matrix estimation

In this section, we derive a strategy for computing an enhanced covariance matrix, denoted as $\tilde{\mathbf{R}}$, by linearly combining the *a priori* covariance matrix \mathbf{C} and the sample covariance matrix $\hat{\mathbf{R}}$ whose weights are automatically chosen based on the data and the conditions in the scenario.

5.2.1 Computation of the *a priori* covariance matrix

Supposing the knowledge of the DOAs of k uncorrelated signals that are impinging on the sensor array, the subset is defined as

$$\bar{\boldsymbol{\theta}} = [\theta_1, \dots, \theta_k]^T. \quad (5.3)$$

These signal directions $\bar{\boldsymbol{\theta}}$ have been previously estimated by applying an arbitrary direction finding scheme. Having $\bar{\boldsymbol{\theta}}$ available, this information is processed to form an $(M \times M)$ -dimensional *a priori* covariance matrix \mathbf{C} , which is rank deficient with rank k and is computed by

$$\mathbf{C} = \sum_{l=1}^k \sigma_l^2 \mathbf{a}(\theta_l) \mathbf{a}^H(\theta_l), \quad l = 1, \dots, k, \quad (5.4)$$

where $\mathbf{a}(\theta_l)$ is the array steering vector of the l th known DOA and σ_l^2 is the power of the l th signal. Here, the signal powers σ_l^2 are also assumed to be previously estimated via the prior applied estimation technique. The *a priori* covariance matrix \mathbf{C} is then further processed to provide an improved estimate of the true covariance matrix after changed positions of unknown users. Rewriting equation (5.4) in matrix form, yields

$$\mathbf{C} = \mathbf{A}(\bar{\boldsymbol{\theta}})\mathbf{P}\mathbf{A}^H(\bar{\boldsymbol{\theta}}), \quad (5.5)$$

where the diagonal matrix $\mathbf{P} = \text{diag}\{\sigma_1^2, \dots, \sigma_k^2\}$ contains the powers of the k sources.

The computation of \mathbf{C} in (5.4) implies accurate knowledge about the true directions $\bar{\boldsymbol{\theta}}$, which leads to a perfectly known *a priori* covariance matrix. However, in practical applications, the DOAs $\bar{\boldsymbol{\theta}}$ and the signal powers σ_l^2 are usually erroneous, so that \mathbf{C} becomes an approximation $\hat{\mathbf{C}}$, calculated as

$$\hat{\mathbf{C}} = \mathbf{A}(\hat{\boldsymbol{\theta}})\hat{\mathbf{P}}\mathbf{A}^H(\hat{\boldsymbol{\theta}}). \quad (5.6)$$

For convenience, we first proceed on the assumption that accurate knowledge of the true signal directions is available and consider the inaccurate case later on.

5.2.2 Problem statement

In order to obtain the enhanced covariance matrix estimate $\tilde{\mathbf{R}}$, we process the *a priori* known matrix \mathbf{C} according to [41] as a linear combination of the weighted \mathbf{C} and the weighted sample covariance matrix $\hat{\mathbf{R}}$. Applying the real-valued combination factors α and β , the improved estimate $\tilde{\mathbf{R}}$ is formulated as

$$\tilde{\mathbf{R}} = \alpha\mathbf{C} + \beta\hat{\mathbf{R}}, \quad (5.7)$$

where the combination factors are constrained to $\alpha > 0$ and $\beta > 0$, and \mathbf{C} is restricted to be positive semi-definite to ensure that $\tilde{\mathbf{R}}$ is also positive semi-definite.

Now, the aim is to find optimal estimates of the weight factors α and β , which efficiently combine \mathbf{C} and $\hat{\mathbf{R}}$ depending on the data in the scenario. One of the most commonly used criteria is the optimization of the parameters to minimize the difference between the enhanced covariance matrix $\tilde{\mathbf{R}}$ and the true covariance matrix \mathbf{R} in a mean square error (MSE) sense, i.e.,

$$\begin{aligned} \min_{\alpha, \beta} \text{MSE} &= \mathbb{E} \left\{ \|\tilde{\mathbf{R}} - \mathbf{R}\|_F^2 \right\} \\ \text{s.t. } \tilde{\mathbf{R}} &= \alpha\mathbf{C} + \beta\hat{\mathbf{R}}, \end{aligned} \quad (5.8)$$

where $\|\cdot\|_F$ denotes the Frobenius matrix norm. Note that the optimization problem is solved by minimizing the MSE with respect to the two parameters α and β , which depend on each other and the unknown true covariance matrix \mathbf{R} . The formulation in (5.8) aims to support the poor sample covariance matrix estimate $\hat{\mathbf{R}}$ in the case of a small data record size N and at a low SNR by simply adding the weighted *a priori* covariance matrix \mathbf{C} . The weight factors are automatically adjusted depending on the data and properties of the system. Under severe conditions as mentioned above, we expect α to be a large value and β to be small.

Another widely used constraint, which reduces the complexity of the optimization problem is the function

$$\tilde{\mathbf{R}} = \alpha\mathbf{C} + (1 - \alpha)\hat{\mathbf{R}} \quad (5.9)$$

with α being restricted to $\alpha \in (0, 1)$ to ensure the positive semi-definiteness of $\tilde{\mathbf{R}}$. This combination, in literature referred to as convex combination [41], provides the benefit of minimizing the MSE subject to only one parameter and can be considered as a special case of (5.8). However, since we aim for a more general description to obtain an improved estimate of the covariance matrix, we focus on (5.7) in the following development.

5.2.3 Computation of the optimal weight factors

The parameters α and β are determined by solving the minimization problem stated in (5.8) in the following way [41]. Inserting the constraint (5.7) into the equation for the MSE and expanding the expression by an algebraic manipulation, gives

$$\begin{aligned} \text{MSE} &= \mathbb{E} \left\{ \|\tilde{\mathbf{R}} - \mathbf{R}\|_F^2 \right\} = \mathbb{E} \left\{ \|\alpha\mathbf{C} + \beta\hat{\mathbf{R}} - \mathbf{R}\|_F^2 \right\} \\ &= \mathbb{E} \left\{ \|\alpha\mathbf{C} + \beta\hat{\mathbf{R}} + \beta\mathbf{R} - \beta\mathbf{R} - \mathbf{R}\|_F^2 \right\} \\ &= \mathbb{E} \left\{ \|\alpha\mathbf{C} - (1 - \beta)\mathbf{R} + \beta(\hat{\mathbf{R}} - \mathbf{R})\|_F^2 \right\}. \end{aligned} \quad (5.10)$$

In order to further compute the result in (5.10) we make use of the following Lemmas:

Lemma 5.2.1. *For any two matrices $\mathbf{A} \in \mathbb{C}^{p \times q}$ and $\mathbf{B} \in \mathbb{C}^{p \times q}$ the binomial formula for the Frobenius matrix norm is given by*

$$\|\mathbf{A} + \mathbf{B}\|_F^2 = \|\mathbf{A}\|_F^2 + \|\mathbf{B}\|_F^2 + 2\langle \mathbf{A}, \mathbf{B} \rangle_F, \quad (5.11)$$

where $\langle \cdot, \cdot \rangle_F$ is the Frobenius norm inner product, which is defined as

$$\langle \mathbf{A}, \mathbf{B} \rangle_F = \sum_{i=1}^p \sum_{j=1}^p a_{ij} b_{ij}. \quad (5.12)$$

Lemma 5.2.2. For two Hermitian matrices $\mathbf{A} \in \mathbb{C}^{p \times p}$ and $\mathbf{B} \in \mathbb{C}^{p \times p}$ the following identity for Frobenius norm inner products holds:

$$\langle \mathbf{A}, \mathbf{B} \rangle_F = \text{Tr}\{\mathbf{A}^H \mathbf{B}\} = \text{Tr}\{\mathbf{A} \mathbf{B}^H\}, \quad (5.13)$$

where the Trace-operator of the matrix product $\mathbf{A} \mathbf{B}$ is defined as in (5.12).

Using Lemma 5.2.1, equation (5.10) is computed as

$$\begin{aligned} \text{MSE} = \mathbb{E} \left\{ \|\tilde{\mathbf{R}} - \mathbf{R}\|_F^2 \right\} &= \|\alpha \mathbf{C} - (1 - \beta) \mathbf{R}\|_F^2 + \beta^2 \mathbb{E} \left\{ \|\hat{\mathbf{R}} - \mathbf{R}\|_F^2 \right\} \\ &+ 2\beta \mathbb{E} \left\{ \langle \hat{\mathbf{R}} - \mathbf{R}, \alpha \mathbf{C} - (1 - \beta) \mathbf{R} \rangle_F \right\}, \end{aligned} \quad (5.14)$$

where the last term can be rewritten as

$$2\beta \mathbb{E} \left\{ \langle \hat{\mathbf{R}} - \mathbf{R}, \alpha \mathbf{C} - (1 - \beta) \mathbf{R} \rangle_F \right\} = 2\beta \langle \mathbb{E} \{ \hat{\mathbf{R}} \} - \mathbf{R}, \alpha \mathbf{C} - (1 - \beta) \mathbf{R} \rangle_F. \quad (5.15)$$

Now we adopt the property that the expected value $\mathbb{E}\{\hat{\mathbf{R}}\} = \mathbf{R}$ as $\hat{\mathbf{R}}$ is an unbiased estimate of \mathbf{R} .

As easily seen, the first factor of the Frobenius norm inner product is zero and therefore the whole term becomes

$$2\beta \mathbb{E} \left\{ \langle \hat{\mathbf{R}} - \mathbf{R}, \alpha \mathbf{C} - (1 - \beta) \mathbf{R} \rangle_F \right\} = \underbrace{\langle \underbrace{\mathbb{E} \{ \hat{\mathbf{R}} \}}_0 - \mathbf{R}, \alpha \mathbf{C} - (1 - \beta) \mathbf{R} \rangle_F}_0. \quad (5.16)$$

This leaves for the MSE the expression

$$\text{MSE} = \mathbb{E} \left\{ \|\tilde{\mathbf{R}} - \mathbf{R}\|_F^2 \right\} = \|\alpha \mathbf{C} - (1 - \beta) \mathbf{R}\|_F^2 + \beta^2 \mathbb{E} \left\{ \|\hat{\mathbf{R}} - \mathbf{R}\|_F^2 \right\}. \quad (5.17)$$

In order to simplify the first term of (5.17) we require the following Corollary:

Corollary 5.2.3. For any two matrices $\mathbf{A} \in \mathbb{C}^{p \times p}$ and $\mathbf{B} \in \mathbb{C}^{p \times p}$ the following property holds

$$\text{Tr}\{\mathbf{A}^H \mathbf{B}\} > 0, \quad (5.18)$$

if \mathbf{A} and \mathbf{B} are positive semi-definite, i.e.,

$$\mathbf{x}^H \mathbf{A} \mathbf{x} \geq 0 \quad \text{and} \quad \mathbf{x}^H \mathbf{B} \mathbf{x} \geq 0, \quad (5.19)$$

which also implies that \mathbf{A} and \mathbf{B} are Hermitian matrices whose eigenvalues are non-negative.

Eventually, by using Lemma 5.2.1, Lemma 5.2.2 and Corollary 5.2.3 we have that

$$\begin{aligned} \text{MSE} &= \alpha^2 \|\mathbf{C}\|_F^2 - 2\alpha(1-\beta) \text{Tr}\{\mathbf{C}^H \mathbf{R}\} \\ &+ (1-\beta)^2 \|\mathbf{R}\|_F^2 + \beta^2 \mathbb{E} \left\{ \|\hat{\mathbf{R}} - \mathbf{R}\|_F^2 \right\}, \end{aligned} \quad (5.20)$$

Our objective is now to determine the optimal parameters α_{opt} and β_{opt} , which minimize the obtained unconstrained optimization problem in (5.20). These are obviously dependent on each other, such that we fix β to β_{opt} while solving equation (5.20) for the parameter α . Taking the gradient of (5.20) with respect to α and equating it to zero gives

$$\frac{\partial \text{MSE}(\alpha, \beta_{\text{opt}})}{\partial \alpha} = 2\alpha \|\mathbf{C}\|_F^2 - 2(1-\beta_{\text{opt}}) \text{Tr}\{\mathbf{C}^H \mathbf{R}\} \stackrel{!}{=} 0. \quad (5.21)$$

Then, in order to find the optimal solution α_{opt} we rearrange the terms and get the final equation

$$\alpha_{\text{opt}} = \frac{(1-\beta_{\text{opt}}) \text{Tr}\{\mathbf{C}^H \mathbf{R}\}}{\|\mathbf{C}\|_F^2}. \quad (5.22)$$

As we also need to determine the expression for the parameter β_{opt} , inserting (5.22) into equation (5.20) and substituting β for β_{opt} , equation (5.20) becomes

$$\begin{aligned} \text{MSE}(\beta) &= \frac{(1-\beta)^2 \text{Tr}^2\{\mathbf{C}^H \mathbf{R}\} \|\mathbf{C}\|_F^2}{\|\mathbf{C}\|_F^4} - 2 \frac{(1-\beta)^2 \text{Tr}^2\{\mathbf{C}^H \mathbf{R}\}}{\|\mathbf{C}\|_F^2} \\ &+ (1-\beta)^2 \|\mathbf{R}\|_F^2 + \beta^2 \mathbb{E} \left\{ \|\hat{\mathbf{R}} - \mathbf{R}\|_F^2 \right\}. \end{aligned} \quad (5.23)$$

After some elementary computations we can simplify (5.23) as

$$\text{MSE}(\beta) = \frac{(1-\beta)^2 (\|\mathbf{R}\|_F^2 \|\mathbf{C}\|_F^2 - \text{Tr}^2\{\mathbf{C}^H \mathbf{R}\})}{\|\mathbf{C}\|_F^2} + \beta^2 \mathbb{E} \left\{ \|\hat{\mathbf{R}} - \mathbf{R}\|_F^2 \right\}. \quad (5.24)$$

To find the equation for the optimal parameter β_{opt} , we equate the gradient of (5.24) with respect to β to zero, which yields

$$\frac{\partial \text{MSE}(\beta)}{\partial \beta} = 2\beta \mathbb{E} \left\{ \|\hat{\mathbf{R}} - \mathbf{R}\|_F^2 \right\} + 2(\beta-1) \frac{\|\mathbf{R}\|_F^2 \|\mathbf{C}\|_F^2 - \text{Tr}^2\{\mathbf{C}^H \mathbf{R}\}}{\|\mathbf{C}\|_F^2} \stackrel{!}{=} 0. \quad (5.25)$$

Solving for β , the computation of the optimal parameter β_{opt} can be compactly ex-

pressed by

$$\beta_{\text{opt}} = \frac{\gamma}{\rho + \gamma}, \quad (5.26)$$

where γ is defined as

$$\gamma = \frac{\|\mathbf{R}\|_F^2 \|\mathbf{C}\|_F^2 - \text{Tr}^2\{\mathbf{C}^H \mathbf{R}\}}{\|\mathbf{C}\|_F^2} \quad (5.27)$$

and ρ is given by

$$\rho = \mathbb{E} \left\{ \|\hat{\mathbf{R}} - \mathbf{R}\|_F^2 \right\}. \quad (5.28)$$

Note that during the derivation, the earlier stated constraint on the two combination factors, namely $\alpha_{\text{opt}} > 0$ and $\beta_{\text{opt}} > 0$ needs to be guaranteed. In order to prove this property, we apply the Cauchy-Schwarz inequality and require the following Lemma about its extension to matrices:

Lemma 5.2.4. *For any two arbitrary matrices $\mathbf{A} \in \mathbb{C}^{p \times p}$ and $\mathbf{B} \in \mathbb{C}^{p \times p}$ the Cauchy-Schwarz inequality for the Frobenius norm of these matrices is given by*

$$|\langle \mathbf{A}, \mathbf{B} \rangle_F| \leq \|\mathbf{A}\|_F \cdot \|\mathbf{B}\|_F, \quad (5.29)$$

which can be obtained from the Cauchy-Schwarz inequality for vectors.

From the Cauchy-Schwarz inequality in Lemma 5.2.4 it can be deduced for equation (5.27) that γ is restricted to

$$\gamma > 0. \quad (5.30)$$

The proof of equation (5.30) was moved to Appendix A.5 to enhance the readability of the derivation. This restriction implies that α_{opt} and β_{opt} also have to be greater than zero and therefore minimize the MSE.

For a derivation later on we can further simplify the expression for γ in (5.27) as

$$\gamma = \frac{\|\mathbf{R}\|_F^2 \|\mathbf{C}\|_F^2 - \text{Tr}^2\{\mathbf{C}^H \mathbf{R}\}}{\|\mathbf{C}\|_F^2} = \|\mathbf{R}\|_F^2 - \frac{\text{Tr}^2\{\mathbf{C}^H \mathbf{R}\}}{\|\mathbf{C}\|_F^2} \quad (5.31)$$

and by applying an algebraic manipulation, we have that

$$\begin{aligned} \gamma &= \frac{\text{Tr}^2\{\mathbf{C}^H \mathbf{R}\}}{\|\mathbf{C}\|_F^2} - 2 \frac{\text{Tr}^2\{\mathbf{C}^H \mathbf{R}\}}{\|\mathbf{C}\|_F^2} + \|\mathbf{R}\|_F^2 \\ &= \left\| \frac{\text{Tr}\{\mathbf{C}^H \mathbf{R}\}}{\|\mathbf{C}\|_F^2} \mathbf{C} - \mathbf{R} \right\|_F^2, \end{aligned} \quad (5.32)$$

where we applied Lemma 5.2.1 to obtain an equivalent equation (5.32) for γ .

5.2.4 Estimation of the optimal weight factors

As the weight factors α_{opt} and β_{opt} depend on the true covariance matrix \mathbf{R} , in practical applications, \mathbf{R} is unknown. Therefore, the combination weights α_{opt} and β_{opt} have to be estimated by approximating \mathbf{R} , that is for β_{opt}

$$\hat{\beta}_{\text{opt}} = \frac{\hat{\gamma}}{\hat{\rho} + \hat{\gamma}} \quad (5.33)$$

and for α_{opt} we get

$$\hat{\alpha}_{\text{opt}} = \frac{\text{Tr}\{\mathbf{C}^H \hat{\mathbf{R}}\}}{\|\mathbf{C}\|_F^2} (1 - \hat{\beta}_{\text{opt}}), \quad (5.34)$$

with $\hat{\alpha}_{\text{opt}}$ and $\hat{\beta}_{\text{opt}}$ being the estimates of α_{opt} and β_{opt} respectively, and where $\text{Tr}\{\mathbf{C}^H \mathbf{R}\}$ in (5.22) is replaced by $\text{Tr}\{\mathbf{C}^H \hat{\mathbf{R}}\}$. Using expression (5.32) to compute γ , the estimate $\hat{\gamma}$ in (5.33) is given by

$$\hat{\gamma} = \left\| \frac{\text{Tr}\{\mathbf{C}^H \hat{\mathbf{R}}\}}{\|\mathbf{C}\|_F^2} \mathbf{C} - \hat{\mathbf{R}} \right\|_F^2, \quad (5.35)$$

where we also replaced \mathbf{R} by $\hat{\mathbf{R}}$ in the expression for the Frobenius norm. The estimate $\hat{\rho}$ of the parameter ρ is obtained according to the derivations in [41] as

$$\hat{\rho} = \frac{1}{N^2} \sum_{i=1}^N \|\mathbf{x}(i)\|_F^4 - \frac{1}{N} \|\hat{\mathbf{R}}\|_F. \quad (5.36)$$

For further details about the deduction and assumptions to find this formulation for $\hat{\rho}$, we refer to the work in [41].

5.2.5 Improved estimation of the optimal weight factors

The previously derived estimates of the combination factors $\hat{\alpha}_{\text{opt}}$ and $\hat{\beta}_{\text{opt}}$ are simply obtained by replacing the unknown covariance matrix \mathbf{R} by its sample-average version $\hat{\mathbf{R}}$. However, the established estimate $\hat{\gamma} + \hat{\rho}$ of the optimal $\gamma + \rho$ in the denominator of (5.26) is suboptimal as $\hat{\gamma} + \hat{\rho}$ is a biased estimate. Therefore, in this section, we aim to develop an unbiased and in this context an enhanced estimate of the parameters α_{opt} and β_{opt} .

Rewriting the optimal estimate $\gamma + \rho$ in denominator of (5.26) yields

$$\begin{aligned}\gamma + \rho &= \left\| \frac{\text{Tr}\{\mathbf{C}^H \mathbf{R}\}}{\|\mathbf{C}\|_F^2} \mathbf{C} - \mathbf{R} \right\|_F^2 + \mathbb{E} \left\{ \|\hat{\mathbf{R}} - \mathbf{R}\|_F^2 \right\} \\ &= \mathbb{E} \left\{ \left\| \hat{\mathbf{R}} - \frac{\text{Tr}\{\mathbf{C}^H \mathbf{R}\}}{\|\mathbf{C}\|_F^2} \mathbf{C} \right\|_F^2 \right\}\end{aligned}\quad (5.37)$$

Proof:

First of all we define a new factor ν containing the $\text{Tr}\{\cdot\}$ as

$$\nu = \frac{\text{Tr}\{\mathbf{C}^H \mathbf{R}\}}{\|\mathbf{C}\|_F^2} \quad (5.38)$$

to simplify this expression for convenience in the following derivation. Now, starting with the result of (5.37), we expand the terms in the Frobenius norm by using an algebraic manipulation, i.e.,

$$\mathbb{E} \left\{ \|\hat{\mathbf{R}} - \nu \mathbf{C}\|_F^2 \right\} = \mathbb{E} \left\{ \|\hat{\mathbf{R}} - \mathbf{R} + \mathbf{R} - \nu \mathbf{C}\|_F^2 \right\}. \quad (5.39)$$

This equation can be transformed by applying Lemma 5.2.2, yielding the form

$$\begin{aligned}\mathbb{E} \left\{ \|\hat{\mathbf{R}} - \nu \mathbf{C}\|_F^2 \right\} &= \mathbb{E} \left\{ \|(\hat{\mathbf{R}} - \mathbf{R}) + (\mathbf{R} - \nu \mathbf{C})\|_F^2 \right\} \\ &= \mathbb{E} \left\{ \|\hat{\mathbf{R}} - \mathbf{R}\|_F^2 \right\} + \mathbb{E} \left\{ \|\mathbf{R} - \nu \mathbf{C}\|_F^2 \right\} \\ &\quad + 2\mathbb{E} \left\{ \langle \hat{\mathbf{R}} - \mathbf{R}, \mathbf{R} - \nu \mathbf{C} \rangle_F \right\}\end{aligned}\quad (5.40)$$

The last part in (5.40) is then simplified as

$$2\mathbb{E} \left\{ \langle \hat{\mathbf{R}} - \mathbf{R}, \mathbf{R} - \nu \mathbf{C} \rangle_F \right\} = 2\langle \mathbb{E} \left\{ \hat{\mathbf{R}} \right\} - \mathbf{R}, \mathbf{R} - \nu \mathbf{C} \rangle_F. \quad (5.41)$$

Again, using the fact that $\hat{\mathbf{R}}$ is an unbiased estimate, i.e., $\mathbb{E} \left\{ \hat{\mathbf{R}} \right\} = \mathbf{R}$, the Frobenius inner product in equation (5.41) is zero. Hence, combining (5.39) and (5.40) leaves the expression

$$\begin{aligned}\mathbb{E} \left\{ \|\hat{\mathbf{R}} - \nu \mathbf{C}\|_F^2 \right\} &= \mathbb{E} \left\{ \|\hat{\mathbf{R}} - \mathbf{R}\|_F^2 \right\} + \mathbb{E} \left\{ \|\mathbf{R} - \nu \mathbf{C}\|_F^2 \right\} \\ &= \mathbb{E} \left\{ \|\hat{\mathbf{R}} - \mathbf{R}\|_F^2 \right\} + \|\nu \mathbf{C} - \mathbf{R}\|_F^2,\end{aligned}\quad (5.42)$$

which is the desired result.

The identity in (5.37) enables us to also estimate the optimal $\gamma + \rho$ as $\|\hat{\mathbf{R}} - \hat{\nu} \mathbf{C}\|_F^2$, which is an unbiased estimate that is smaller than $\hat{\rho} + \|\hat{\mathbf{R}} - \hat{\nu} \mathbf{C}\|_F^2$ developed in the

previous section. Applying this result to the expression for $\hat{\beta}_{\text{opt}}$ and keeping $\hat{\gamma}$ in the numerator of (5.33), gives

$$\hat{\beta}_{\text{opt}} = \frac{\|\hat{\mathbf{R}} - \hat{\nu}\mathbf{C}\|_F^2}{\|\hat{\mathbf{R}} - \hat{\nu}\mathbf{C}\|_F^2} = 1, \quad (5.43)$$

which needs to be avoided. Thus, after a simple rearrangement of the equations for α_{opt} and β_{opt} we obtain

$$\alpha_{\text{opt}} = \nu \left(\frac{\rho}{\gamma + \rho} \right) \quad (5.44)$$

and

$$\beta_{\text{opt}} = 1 - \frac{\alpha_{\text{opt}}}{\nu}. \quad (5.45)$$

The corresponding improved estimates of α_{opt} and β_{opt} can now be estimated as

$$\hat{\alpha}_{\text{opt}} = \hat{\nu} \left(\frac{\hat{\rho}}{\|\hat{\mathbf{R}} - \hat{\nu}\mathbf{C}\|_F^2} \right) \quad (5.46)$$

and

$$\hat{\beta}_{\text{opt}} = 1 - \frac{\hat{\alpha}_{\text{opt}}}{\hat{\nu}}. \quad (5.47)$$

Since the estimate $\hat{\beta}_{\text{opt}}$ is not restricted to be positive as it was postulated for the computation of the optimal combination factors, we enforce this property by using the expression

$$\hat{\beta}_{\text{opt}} = \max \left(\left(1 - \frac{\hat{\alpha}_{\text{opt}}}{\hat{\nu}} \right), 0 \right) \quad (5.48)$$

instead of equation (5.47).

As we have derived two different ways of estimating the optimal combination factors α_{opt} and β_{opt} , we refer to the first one obtained in the previous section as linear combination 1 (LC₁) with the factors $\alpha_{\text{opt}1}$ and $\beta_{\text{opt}1}$ and term the second one, derived above, linear combination 2 (LC₂) with the factors $\alpha_{\text{opt}2}$ and $\beta_{\text{opt}2}$.

5.3 General knowledge-aided direction of arrival estimation scheme

In this section, we introduce the general structure of the proposed KA DOA estimation scheme. As the knowledge of static signal sources is sometimes available in practical applications, the proposed strategy to incorporate this information is of fundamental importance. As mentioned in Section 5.1, several KA techniques for DOA estimation have been developed in the past [45, 46]. However, they require a large data record to effectively exploit the prior knowledge of static signal directions and break down under

severe conditions, such as at a low SNR and a small number of available snapshots ($N < M$). The proposed method in this work performs best under exactly those severe conditions. It is a general approach and can be applied to any direction finding technique, which depends on the estimate of the covariance matrix of the array output vector \mathbf{x} . As the weighted *a priori* covariance matrix \mathbf{C} is simply added to the sample covariance matrix $\hat{\mathbf{R}}$ to obtain the enhanced covariance matrix estimate $\tilde{\mathbf{R}}$ (cf. Section 5.2), only the signal subspace is improved and not necessarily the noise subspace.

In addition, it is important to note that, as opposed to the previously developed KA DOA estimation method in [46], the proposed KA direction finding scheme estimates the DOAs of all the signals $\boldsymbol{\theta}$ in the system, including the known directions $\bar{\boldsymbol{\theta}}$. However, these DOAs can be distinguished from the unknown signal directions, so that their estimation errors are neglected for the purpose of assessing the performance against other methods.

5.3.1 Structure of KA DOA estimation

The structure of the KA direction finding scheme is depicted as a block diagram in Figure 5.1, where the time index i denotes the estimation step in the scheme. Before the actual KA method can be applied, a separate DOA estimation algorithm is required to obtain the knowledge of the static DOAs in the system. This procedure is illustrated in the upper path of Fig. 5.1. After the computation of the sample covariance matrix $\hat{\mathbf{R}}$ at the step $i - 1$ the DOAs $\bar{\boldsymbol{\theta}}(i - 1)$ are extracted by an arbitrary direction finding algorithm and the source powers on the diagonal of $\mathbf{P}(i - 1)$ are estimated. These quantities are then passed onto the block to determine the *a priori* covariance matrix \mathbf{C} . At the next estimation step the KA scheme in the lower path comes into play. It estimates the sample covariance matrix at the current step i and takes into account the

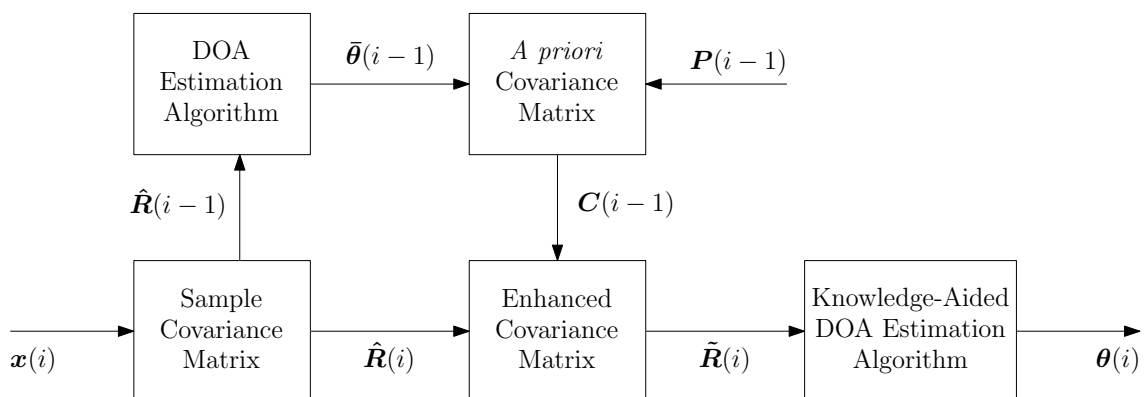


Fig. 5.1: Block diagram of the KA DOA estimation scheme.

$\mathbf{C}(i-1)$ from the previous step to provide the enhanced covariance matrix estimate $\tilde{\mathbf{R}}$. Eventually, the KA DOA estimation algorithm based on any technique that relies on the covariance matrix estimate is employed to extract the signal direction estimates with improved accuracy.

It is evident from Figure 5.1 that the operations in the upper path only need to be carried out once and \mathbf{C} can be processed as long as the static sources are present. Hence, a rerun of the upper path is only necessary after a change of their positions. Furthermore, it should be emphasized that the performance of the KA DOA algorithm in practice depends on the accuracy of the known DOA provided by the first direction finding method. Thus, in order to achieve a maximum gain, an appropriate technique to get precise estimates needs to be chosen.

5.3.2 Computational complexity

Having discussed the general structure of the proposed KA direction finding scheme, the computational complexity of this technique is analyzed. The computational cost of incorporating the known information of the DOAs $\bar{\boldsymbol{\theta}}$ to obtain the enhanced covariance matrix estimate $\tilde{\mathbf{R}}$ is measured in terms of the number of additions and multiplications. Table 5.1 shows the analytical expressions depending on the number of sensors M , the data record size N , and the number of the known signal directions k . To avoid the computationally expensive matrix multiplication of the *a priori* covariance matrix \mathbf{C} and the sample covariance matrix $\hat{\mathbf{R}}$, which causes a cost of $\mathcal{O}(M^3)$, we used the fact that \mathbf{C} can be expressed as the sum of rank-1 matrices and k is typically much less than M . Therefore, it requires only $\mathcal{O}(M^2)$ operations.

Apart from the computation of $\tilde{\mathbf{R}}$, the complexity of the general KA DOA estimation scheme depends on the cost of the two applied direction finding algorithms. If these two DOA estimation algorithms use the same method, the overall computational complexity is slightly higher than twice the cost of the conventional approach without prior knowledge. However, once the matrix \mathbf{C} of the static signal directions is determined it can be used for the improved estimation of further changes in the

Tab. 5.1: Computational complexity of the proposed versions of the KA scheme

KA version	Additions	Multiplications
LC ₁	$2M^2(5k+3) + 2M(N-k+1) - 3$	$4M^2(3k+2) + 6MN + 2$
LC ₂	$2M^2(5k+3) + 2M(N-k+1) - 4$	$4M^2(3k+2) + 6MN + 3$

environment. Thus, even a costly DOA estimation algorithm to obtain highly accurate DOAs is affordable as the KA scheme compensates a possibly moderate performance of a low-complexity second direction finding technique. In order to reduce the complexity of the proposed scheme, an adaptive strategy to combine the two covariance matrices to yield the enhanced estimate can be adopted, which will be considered in future work.

5.4 Knowledge-aided ESPRIT-type direction of arrival estimation

Among the direction finding techniques that have been developed so far, ESPRIT-type algorithms [1] are one of the most popular schemes. They belong to the class of subspace-based methods, as the signal subspace, estimated via an eigenvalue decomposition (EVD) of the covariance matrix \mathbf{R} (cf. Section 2.2.3) or a singular value decomposition (SVD) of the array output matrix \mathbf{X} (cf. Section 2.2.2), is processed to obtain the DOAs. The conventional ESPRIT-type direction finding methods are applicable to any antenna array structure, which can be decomposed in two identical subarrays displaced by a uniform distance. As this constraint holds for a large variety of sensor arrays that are used in practice, these powerful DOA estimation algorithms are of significant interest. In addition, ESPRIT-type algorithms are more computationally efficient than other methods such as ML-type techniques and MUSIC-type algorithms. In this section, we propose two KA-ESPRIT-type direction finding schemes based on the standard ESPRIT algorithm [14] termed KA-ESPRIT algorithm and based on the Unitary ESPRIT method [15], which we refer to as Unitary KA-ESPRIT. We note again that the developed algorithms estimate the DOAs of all the signals in the system.

5.4.1 KA-ESPRIT

The key idea of the proposed KA-ESPRIT algorithm is to exploit *a priori* knowledge about the DOAs $\bar{\boldsymbol{\theta}}$. This known information is incorporated by applying the method developed in Section 5.2 to obtain an enhanced covariance matrix $\tilde{\mathbf{R}}$. Then, an improved signal subspace estimate is processed via the standard ESPRIT algorithm.

Similarly to ESPRIT, we form a twofold subarray configuration, as each row of the array steering matrix $\mathbf{A}(\boldsymbol{\theta})$ corresponds to one particular sensor element of the antenna array. The subarrays are specified by two $(m \times M)$ -dimensional selection matrices \mathbf{J}_1 and \mathbf{J}_2 , which choose m elements of the M existing sensors respectively, where m is in the range $d \leq m < M$. For maximum overlap, the matrix \mathbf{J}_1 selects the first $m = M - 1$ elements and \mathbf{J}_2 selects the last $m = M - 1$ rows of $\mathbf{A}(\boldsymbol{\theta})$. Since two identical subarrays are obtained and the displacement vector is uniform, a steering

vector of the second subarray is only a scaled version of the corresponding steering vector of the first subarray. This property is termed shift invariance property and can be expressed in compact form as

$$\mathbf{J}_1 \mathbf{A}(\boldsymbol{\theta}) \boldsymbol{\Phi} = \mathbf{J}_2 \mathbf{A}(\boldsymbol{\theta}), \quad (5.49)$$

where

$$\boldsymbol{\Phi} = \text{diag}\{e^{j\mu_n}\}_{n=1}^d, \quad (5.50)$$

which is the unitary $(d \times d)$ -dimensional diagonal matrix containing the spatial frequencies μ_n given by

$$\mu_n = 2\pi \frac{\Delta}{\lambda_c} \sin \theta_n. \quad (5.51)$$

The array steering matrix $\mathbf{A}(\boldsymbol{\theta})$ in (5.49) is unknown, however, it can be shown that the columns of $\mathbf{A}(\boldsymbol{\theta})$ and the columns of \mathbf{U}_s obtained from the true covariance matrix \mathbf{R} are two equivalent bases that span the same signal subspace \mathcal{S} of dimension d (cf. Section 2.2.1), i.e.,

$$\mathcal{S} = \text{span}\{\mathbf{A}(\boldsymbol{\theta})\} = \text{span}\{\mathbf{U}_s\}. \quad (5.52)$$

Thus, $\mathbf{A}(\boldsymbol{\theta})$ can be expressed as a linear transformation of \mathbf{U}_s , i.e.,

$$\mathbf{A}(\boldsymbol{\theta}) = \mathbf{U}_s \mathbf{T}, \quad (5.53)$$

where $\mathbf{T} \in \mathbb{C}^{d \times d}$ is a unitary matrix, which linearly combines the columns of \mathbf{U}_s to form the basis columns vectors contained in $\mathbf{A}(\boldsymbol{\theta})$. Now, the shift invariance equation (5.49) can be rewritten as

$$\mathbf{J}_1 \mathbf{U}_s \boldsymbol{\Psi} = \mathbf{J}_2 \mathbf{U}_s \quad (5.54)$$

with the transformation

$$\boldsymbol{\Psi} = \mathbf{T} \boldsymbol{\Phi} \mathbf{T}^{-1} \in \mathbb{C}^{d \times d}, \quad (5.55)$$

which is eigenvalue-preserving, so that the eigenvalues of $\boldsymbol{\Psi}$ are equal to the diagonal elements in $\boldsymbol{\Phi}$.

In practical applications \mathbf{R} and \mathbf{U}_s are unknown and need to be estimated. Consequently, we apply a rank- d approximation based on the EVD of the enhanced covariance matrix $\tilde{\mathbf{R}}$ (cf. Section 2.2.3) to determine the estimated signal subspace $\hat{\mathbf{U}}_s \in \mathbb{C}^{M \times d}$. Note that we assume that the number of signals d is known beforehand. In the noisy case, equation (5.54) becomes an approximation described as

$$\mathbf{J}_1 \hat{\mathbf{U}}_s \boldsymbol{\Psi} \approx \mathbf{J}_2 \hat{\mathbf{U}}_s, \quad (5.56)$$

which represents an overdetermined set of equations that needs to be solved for Ψ by using a suitable least squares method, such as least squares (LS), total least squares (TLS) or structured least squares (SLS) [47].

Finally, the eigenvalues λ_n of Ψ contain the estimates of the spatial frequencies μ_n computed as

$$\mu_n = \arg(\lambda_n), \quad (5.57)$$

so that the DOAs θ_n can be calculated as

$$\theta_n = \arcsin\left(\frac{\mu_n \lambda_c}{2\pi\Delta}\right). \quad (5.58)$$

A brief summary of the proposed KA-ESPRIT direction finding algorithm is given in Table 5.2.

Tab. 5.2: The proposed KA-ESPRIT algorithm

<p>1. Knowledge-Aided Processing:</p> <ul style="list-style-type: none"> • Compute the <i>a priori</i> covariance matrix $\mathbf{C} \in \mathbb{C}^{M \times M}$ by (5.4). • Calculate the weight factors $\hat{\alpha}_{\text{opt}}$ and $\hat{\beta}_{\text{opt}}$ to obtain the enhanced covariance matrix estimate $\tilde{\mathbf{R}} \in \mathbb{C}^{M \times M}$. <p>2. Signal Subspace Estimation:</p> <ul style="list-style-type: none"> • Compute the matrix $\hat{\mathbf{U}}_s \in \mathbb{C}^{M \times d}$ as the d principal eigenvectors of the enhanced covariance matrix $\tilde{\mathbf{R}}$ <p>3. Invariance Equation:</p> <ul style="list-style-type: none"> • Solve the shift invariance equation $\mathbf{J}_1 \hat{\mathbf{U}}_s \Psi \approx \mathbf{J}_2 \hat{\mathbf{U}}_s$ by using the LS, TLS or SLS algorithm <p>4. DOA Estimation:</p> <ul style="list-style-type: none"> • Calculate the d eigenvalues of the solution $\Psi = \mathbf{T}\Phi\mathbf{T}^{-1}$ with $\Phi = \text{diag}\{e^{j\mu_n}\}_{n=1}^d$. • Solve $\theta_n = \arcsin\left(\frac{\mu_n \lambda_c}{2\pi\Delta}\right)$ to obtain the DOAs.

5.4.2 Unitary KA-ESPRIT

An extension to the standard ESPRIT-Algorithm is the popular Unitary ESPRIT algorithm [15], which provides significant performance improvements and computational benefits. By exploiting the fact that the displacement matrix Φ is unitary, the concept of forward-backward averaging [48] is automatically included. It also transforms the shift invariance equations into the real-valued domain reducing the computational complexity dramatically. Forward-backward averaging itself is a preprocessing scheme that uses symmetries of the array and virtually doubles the number of available data samples without decreasing the array aperture. This technique substantially improves the estimation accuracy and enables the decorrelation of coherent signals. Motivated by these advantages, we apply the derived procedure of incorporating *a priori* knowledge about the DOAs $\bar{\theta}$ to the Unitary ESPRIT algorithm, which is termed Unitary KA-ESPRIT.

Preliminaries

Following the work in [49,50], we first review the definition of centro-Hermitian matrices and introduce the feature of centro-symmetric sensor arrays.

Definition 5.4.1. A matrix $M \in \mathbb{C}^{p \times p}$ is centro-Hermitian iff

$$M = \Pi_p M^* \Pi_p, \quad (5.59)$$

where Π_p is the exchange matrix defined as

$$\Pi_p = \begin{bmatrix} & & 1 \\ & 1 & \\ & \cdot & \\ 1 & & \end{bmatrix} \in \mathbb{R}^{p \times p}. \quad (5.60)$$

Definition 5.4.2. A matrix $Q \in \mathbb{C}^{p \times p}$ is called left Π -real if it satisfies

$$\Pi_p Q_p^* = Q_p. \quad (5.61)$$

A sparse unitary left Π -real matrix for odd values of p is given by

$$Q_{2n+1} = \frac{1}{\sqrt{2}} \begin{bmatrix} \mathbf{I}_n & \mathbf{0}_{n \times 1} & \mathbf{jI}_n \\ \mathbf{0}_{n \times 1}^T & \sqrt{2} & \mathbf{0}_{n \times 1}^T \\ \Pi_n & \mathbf{0}_{n \times 1} & -\mathbf{jI}_n \end{bmatrix}, \quad (5.62)$$

where $\mathbf{0}_{n \times 1}^T$ is the zero vector. A unitary left $\mathbf{\Pi}$ -real matrix for even values of p is obtained from (5.62) by dropping its center row and center column.

Definition 5.4.3. *A sensor array is centro-symmetric if its elements are symmetric with respect to the centroid and the center of the array is chosen as the phase reference. As a ULA is centro-symmetric the array steering vector can be expressed as*

$$\mathbf{a}(\mu_n) = e^{-j(\frac{M-1}{2})\mu_n} \begin{bmatrix} 1 & e^{j\mu_n} & \dots & e^{j(M-1)\mu_n} \end{bmatrix}. \quad (5.63)$$

Derivation of Unitary KA-ESPRIT

Using the Definition 5.4.3 on the centro-symmetry of the sensor array and the fact that the displacement matrix $\mathbf{\Phi}$ is unitary, it has been shown in [15] that the array output matrix \mathbf{X} can be replaced by

$$\mathbf{Z} = \begin{bmatrix} \mathbf{X} & \mathbf{\Pi}_M \mathbf{X}^* \mathbf{\Pi}_N \end{bmatrix} \in \mathbb{C}^{M \times 2N}, \quad (5.64)$$

where \mathbf{Z} is the extended data matrix. This bijective transformation corresponds to forward-backward averaging and essentially doubles the number of available snapshots, leading to an increased estimation accuracy. It is easily proven that the array output matrix \mathbf{X} and its forward-backward averaged extension \mathbf{Z} span the same signal subspace.

As the incorporated knowledge of the signal directions $\bar{\boldsymbol{\theta}}$ provides an enhanced covariance matrix estimate, we apply the concept of forward-backward averaging to the covariance matrix yielding

$$\tilde{\mathbf{R}}_{FB} = \frac{1}{2} \left(\tilde{\mathbf{R}} + \mathbf{\Pi}_M \tilde{\mathbf{R}}^* \mathbf{\Pi}_M \right) \in \mathbb{C}^{M \times M}. \quad (5.65)$$

Besides the improved estimation accuracy Unitary KA-ESPRIT requires only real-valued computations, which leads to significant reductions in the computational complexity. In [49] it was proven that any centro-Hermitian matrix can be mapped into a real-valued matrix of the same size. In order to make use of this meaningful property, we first prove the centro-Hermitian characteristic of the forward-backward averaged enhanced covariance matrix $\tilde{\mathbf{R}}_{FB}$. Applying Definition 5.4.1 leads to

$$\begin{aligned} \mathbf{\Pi}_M \tilde{\mathbf{R}}_{FB}^* \mathbf{\Pi}_M &= \frac{1}{2} \left(\mathbf{\Pi}_M \tilde{\mathbf{R}}^* \mathbf{\Pi}_M + \mathbf{\Pi}_M \mathbf{\Pi}_M \tilde{\mathbf{R}} \mathbf{\Pi}_M \mathbf{\Pi}_M \right) \\ &= \frac{1}{2} \left(\mathbf{\Pi}_M \tilde{\mathbf{R}}^* \mathbf{\Pi}_M + \tilde{\mathbf{R}} \right), \end{aligned} \quad (5.66)$$

where we used the fact that $\mathbf{\Pi}_M \mathbf{\Pi}_M = \mathbf{I}$. Now, the mapping of (5.65) into the real-valued domain is stated in the following Theorem:

Theorem 5.4.4. *The covariance matrix $\tilde{\mathbf{R}}_{FB}$ is transformed into a real-valued matrix of the same size using the mapping*

$$\varphi(\tilde{\mathbf{R}}_{FB}) = \mathbf{Q}_M^H \tilde{\mathbf{R}}_{FB} \mathbf{Q}_M, \quad (5.67)$$

where \mathbf{Q}_M is the unitary left $\mathbf{\Pi}$ -real matrix defined in (5.62). General proof for centro-Hermitian matrices is provided in [49].

Proof:

Using Definition 5.4.2, we have that

$$\begin{aligned} \mathbf{Q}_M^H \tilde{\mathbf{R}}_{FB} \mathbf{Q}_M &= \frac{1}{2} \left(\mathbf{Q}_M^H \tilde{\mathbf{R}} \mathbf{Q}_M + \mathbf{Q}_M^H \mathbf{\Pi}_M \tilde{\mathbf{R}} \mathbf{\Pi}_M \mathbf{Q}_M \right) \\ &= \frac{1}{2} \left(\mathbf{Q}_M^H \tilde{\mathbf{R}} \mathbf{Q}_M + \mathbf{Q}_M^T \tilde{\mathbf{R}}^* \mathbf{Q}_M^* \right) \\ &= \text{Re} \left\{ \mathbf{Q}_M^H \tilde{\mathbf{R}} \mathbf{Q}_M \right\}. \end{aligned} \quad (5.68)$$

Thus, forward-backward averaging is accomplished by taking the real part of $\mathbf{Q}_M^H \tilde{\mathbf{R}} \mathbf{Q}_M$. Now, the real-valued signal subspace, denoted by $\mathbf{E}_s \in \mathbb{C}^{M \times d}$, can be estimated via a real-valued EVD (cf. Section 2.2.3).

Based on the set of shift invariance equations derived in (5.49), we reexpress this property in terms of a transformed array steering vector obtained by

$$\mathbf{d}(\mu_n) = \mathbf{Q}_M^H \mathbf{a}(\mu_n), \quad (5.69)$$

which is real-valued if the array is centro-symmetric. Then the shift invariance equation for each signal is given by

$$\mathbf{J}_1 \mathbf{Q}_M \mathbf{d}(\mu_n) e^{j\mu_n} = \mathbf{J}_2 \mathbf{Q}_M \mathbf{d}(\mu_n), \quad (5.70)$$

where we also used the unitary nature of \mathbf{Q}_M . Premultiplying both sides by \mathbf{Q}_m^H yields

$$\mathbf{Q}_m^H \mathbf{J}_1 \mathbf{Q}_M \mathbf{d}(\mu_n) e^{j\mu_n} = \mathbf{Q}_m^H \mathbf{J}_2 \mathbf{Q}_M \mathbf{d}(\mu_n). \quad (5.71)$$

Since the selection matrices \mathbf{J}_1 and \mathbf{J}_2 are real-valued and satisfy $\mathbf{J}_1 = \mathbf{\Pi}_m \mathbf{J}_2 \mathbf{\Pi}_M$, one can show that

$$\mathbf{Q}_m^H \mathbf{J}_1 \mathbf{Q}_M = \mathbf{Q}_m^H \mathbf{\Pi}_m \mathbf{\Pi}_m \mathbf{J}_1 \mathbf{\Pi}_M \mathbf{\Pi}_M \mathbf{Q}_M = \mathbf{Q}_m^T \mathbf{J}_2 \mathbf{Q}_M^*. \quad (5.72)$$

Defining two new selection matrices \mathbf{K}_1 and \mathbf{K}_2 as

$$\mathbf{K}_1 = 2 \cdot \text{Re} \left\{ \mathbf{Q}_m^H \mathbf{J}_2 \mathbf{Q}_M \right\} \quad \text{and} \quad \mathbf{K}_2 = 2 \cdot \text{Im} \left\{ \mathbf{Q}_m^H \mathbf{J}_2 \mathbf{Q}_M \right\}, \quad (5.73)$$

equation (5.71) can be rewritten as

$$(\mathbf{K}_1 - \mathbf{j}\mathbf{K}_2)\mathbf{d}(\mu_n)e^{j\mu_n} = (\mathbf{K}_1 + \mathbf{j}\mathbf{K}_2)\mathbf{d}(\mu_n). \quad (5.74)$$

After rearranging the terms we obtain

$$\mathbf{K}_1\mathbf{d}(\mu_n)(e^{j\mu_n} - 1) = \mathbf{K}_2\mathbf{d}(\mu_n) \cdot \mathbf{j}(e^{j\mu_n} + 1). \quad (5.75)$$

Now we multiply both sides by $e^{j\frac{\mu_n}{2}}$ yielding

$$\mathbf{K}_1\mathbf{d}(\mu_n)(e^{j\frac{\mu_n}{2}} - e^{-j\frac{\mu_n}{2}}) = \mathbf{K}_2\mathbf{d}(\mu_n) \cdot \mathbf{j}(e^{j\frac{\mu_n}{2}} + e^{-j\frac{\mu_n}{2}}). \quad (5.76)$$

This enables us to write the shift invariance equation in the compact way

$$\mathbf{K}_1\mathbf{d}(\mu_n) \cdot \tan\left(\frac{\mu_n}{2}\right) = \mathbf{K}_2\mathbf{d}(\mu_n). \quad (5.77)$$

Expanding this equation for all the d signals, we get

$$\mathbf{K}_1\mathbf{D}\Omega = \mathbf{K}_2\mathbf{D}, \quad (5.78)$$

where Ω contains the spatial frequencies μ_n and is given by

$$\Omega = \text{diag} \left\{ \tan\left(\frac{\mu_n}{2}\right) \right\}_{n=1}^d. \quad (5.79)$$

Note that $\mathbf{D} = \mathbf{Q}_M^H \mathbf{A}$, which is real-valued if the centroid is chosen as the phase reference.

According to the considerations in (5.52) in the previous section, we observe that in this case $\mathbf{E}_s \in \mathbb{C}^{M \times d}$ and $\mathbf{D} \in \mathbb{C}^{M \times d}$ span the same real-valued signal subspace. Thus $\mathbf{D} \in \mathbb{C}^{M \times d}$ can be expressed by a linear transformation of $\mathbf{E}_s \in \mathbb{C}^{M \times d}$, i.e.,

$$\mathbf{D} = \mathbf{E}_s \mathbf{T}, \quad (5.80)$$

where \mathbf{T} is a unitary matrix. Substituting (5.80) into (5.78) results in the real-valued shift invariance equations

$$\mathbf{K}_1 \mathbf{E}_s \Upsilon = \mathbf{K}_2 \mathbf{E}_s \quad (5.81)$$

with the transformation

$$\Upsilon = \mathbf{T}\Omega\mathbf{T}^{-1} \in \mathbb{C}^{d \times d}, \quad (5.82)$$

which is again eigenvalue-preserving and contains the desired DOA.

In practice, the signal subspace \mathbf{E}_s is estimated. For the proposed Unitary KA-ESPRIT algorithm we apply a rank- d approximation based on the EVD of the enhanced covariance matrix $\tilde{\mathbf{R}}$ to determine the estimated signal subspace $\hat{\mathbf{E}}_s \in \mathbb{C}^{M \times d}$. Taking this into account, the overdetermined set of equations (5.81) becomes

$$\mathbf{K}_1 \hat{\mathbf{E}}_s \Upsilon \approx \mathbf{K}_2 \hat{\mathbf{E}}_s, \quad (5.83)$$

which is solved for Υ via LS, TLS or SLS. Then, the eigenvalues ω_n of Υ provide the estimates of the spatial frequencies μ_n computed as

$$\mu_n = 2 \cdot \arctan(\omega_n), \quad (5.84)$$

Tab. 5.3: The proposed Unitary KA-ESPRIT algorithm

1. Knowledge-Aided Processing:

- Compute the *a priori* covariance matrix $\mathbf{C} \in \mathbb{C}^{M \times M}$ by (5.4).
- Calculate the weight factors $\hat{\alpha}_{\text{opt}}$ and $\hat{\beta}_{\text{opt}}$ to obtain the enhanced covariance matrix estimate $\tilde{\mathbf{R}} \in \mathbb{C}^{M \times M}$.

2. Signal Subspace Estimation:

- Compute the matrix $\mathbf{E}_s \in \mathbb{C}^{M \times d}$ as the d principal eigenvectors of the enhanced covariance matrix $\tilde{\mathbf{R}}$

3. Invariance Equation:

- Solve the shift invariance equation $\mathbf{K}_1 \mathbf{E}_s \Upsilon \approx \mathbf{K}_2 \mathbf{E}_s$ by using the LS, TLS or SLS algorithm

4. DOA Estimation:

- Calculate the d eigenvalues of the solution $\Upsilon = \mathbf{T}\Omega\mathbf{T}^{-1}$ with $\Omega = \text{diag}\{\omega_n\}_{n=1}^d$.
- Solve $\theta_n = \arcsin\left(\frac{\lambda_c}{\pi\Delta} \arctan(\omega_n)\right)$ to obtain the DOAs.

so that the DOAs θ_n can be calculated as

$$\theta_n = \arcsin\left(\frac{\lambda_c \mu_n}{2\pi\Delta}\right). \quad (5.85)$$

The Unitary KA-ESPRIT algorithm is summarized in Table 5.3.

5.5 Knowledge-aided MUSIC-type direction of arrival estimation

Another class of well-known direction finding methods are the MUSIC-type algorithms [1], which also belong to the subspace-based techniques as the signal subspace and the noise subspace are estimated to determine the DOAs. Contrary to the ESPRIT-type algorithms, MUSIC-type techniques are applicable to arbitrary array structures and therefore receive a considerable attention in practice. However, they require a slightly higher computational complexity than ESPRIT-type methods as a search for sources in the whole angle range is necessary. In this section, we propose two KA-MUSIC-type direction finding schemes based on the standard MUSIC algorithm [12], which we refer to as KA-MUSIC algorithm, and based on the Root MUSIC method [13], a search-free version for ULAs termed KA-Root-MUSIC. Again, we highlight the fact that the developed algorithms estimate the DOAs of all the signals in the system.

5.5.1 KA-MUSIC

In analogy to [12], the basic idea of the proposed KA-MUSIC algorithm is to search through the set of all possible steering vectors in the angle range to find those that are orthogonal to the estimated noise subspace. Its performance clearly depends on the accuracy of the noise subspace estimate. If knowledge about the DOAs of some signals in the system is available, this estimate can be improved by incorporating the known information to obtain an enhanced covariance matrix estimate as derived in Section 5.2. Thus, the KA-MUSIC algorithm is developed as follows:

The noise subspace, denoted as $\hat{\mathbf{U}}_n$, is obtained via an EVD of the enhanced covariance matrix $\tilde{\mathbf{R}}$, which was shown in Section 2.2.3 for covariance matrices in general. The improved signal subspace $\hat{\mathbf{U}}_s$ and the improved noise subspace $\hat{\mathbf{U}}_n$ are orthogonal to each other, i.e.,

$$\hat{\mathbf{U}}_s \perp \hat{\mathbf{U}}_n, \quad (5.86)$$

which is the essential property exploited by the MUSIC algorithm.

The set of all possible array steering vectors, also referred to as array manifold is given by $\mathbf{a}(\theta_i)$, where $\theta_i \in \{-90^\circ, \dots, 90^\circ\}$. Defining a search step Δ° , all the angles θ_i in the angle range can be expressed as $\theta_i = n\Delta^\circ - 90^\circ$, where $n = 0, 1, \dots, 180^\circ/\Delta^\circ$.

Now, the MUSIC algorithm consecutively correlates all the steering vectors θ_i with the noise subspace estimate $\hat{\mathbf{U}}_n$. The correlation \mathbf{c}_i can be mathematically expressed by

$$\mathbf{c}_i = \hat{\mathbf{U}}_n^H \mathbf{a}(\theta_i). \quad (5.87)$$

Is the search angle a true DOA of the set $\boldsymbol{\theta}$, then the corresponding steering vector $\mathbf{a}(\theta_i)$ belongs to the signal subspace $\hat{\mathbf{U}}_s$. Specifically, it is contained in the steering matrix $\mathbf{A}(\boldsymbol{\theta})$ and therefore orthogonal to the noise subspace $\hat{\mathbf{U}}_n$. Thus, the correlation \mathbf{c}_i becomes

$$\mathbf{c}_i = \hat{\mathbf{U}}_n^H \mathbf{a}(\theta_i) = \mathbf{0}. \quad (5.88)$$

Exploiting this property in (5.88), the spectral function $P(\theta_i)$ termed pseudo spectrum was deduced in [12] as

$$P(\theta_i) = \frac{1}{\|\hat{\mathbf{U}}_n^H \mathbf{a}(\theta_i)\|^2} = \frac{1}{\mathbf{a}^H(\theta_i) \hat{\mathbf{U}}_n \hat{\mathbf{U}}_n^H \mathbf{a}(\theta_i)}. \quad (5.89)$$

Note that the squared norm of the correlation \mathbf{c}_i is taken to obtain a real-valued scalar for each search angle. In the case of a true DOA, equation (5.88) holds and the estimated signal directions are the d largest peaks in the pseudo spectrum. As stated earlier, the proposed KA scheme only improves the signal subspace estimate. Thus, by making use of the property

$$\hat{\mathbf{U}}_s \hat{\mathbf{U}}_s^H + \hat{\mathbf{U}}_n \hat{\mathbf{U}}_n^H = \mathbf{I}_M, \quad (5.90)$$

the spectral function in equation (5.89) is rewritten as

$$P(\theta_i) = \frac{1}{\mathbf{a}^H(\theta_i) [\mathbf{I}_M - \hat{\mathbf{U}}_s \hat{\mathbf{U}}_s^H] \mathbf{a}(\theta_i)}. \quad (5.91)$$

A brief summary of the KA-MUSIC algorithm is given in Table 5.4.

Tab. 5.4: The proposed KA-MUSIC algorithm

<p>1. Knowledge-Aided Processing:</p> <ul style="list-style-type: none"> • Compute the <i>a priori</i> covariance matrix $\mathbf{C} \in \mathbb{C}^{M \times M}$ by (5.4). • Calculate the weight factors $\hat{\alpha}_{\text{opt}}$ and $\hat{\beta}_{\text{opt}}$ to obtain the enhanced covariance matrix estimate $\tilde{\mathbf{R}} \in \mathbb{C}^{M \times M}$. <p>2. Noise Subspace Estimation:</p> <ul style="list-style-type: none"> • Compute the matrix $\hat{\mathbf{U}}_n \in \mathbb{C}^{M \times M-d}$ as the $M-d$ eigenvectors corresponding to the $M-d$ smallest eigenvalues of the enhanced covariance matrix $\tilde{\mathbf{R}}$. <p>3. Pseudo Spectrum:</p> <ul style="list-style-type: none"> • Compute $P(\theta_i) = \frac{1}{\mathbf{a}^H(\theta_i)[\mathbf{I}_M - \hat{\mathbf{U}}_s \hat{\mathbf{U}}_s^H] \mathbf{a}(\theta_i)} \quad (5.92)$ for each angle θ_i in the angle range. <p>4. DOA Estimation:</p> <ul style="list-style-type: none"> • Find the d largest peaks of the pseudo spectrum to obtain the DOAs.

5.5.2 KA-Root-MUSIC

The KA-Root-MUSIC technique is an extension of the spectral KA-MUSIC algorithm, which provides a higher estimation accuracy and a lower computational complexity. However, it is only applicable for ULAs as the Vandermonde structure of the ULA is exploited. The outcome of the spectral KA-MUSIC algorithm derived in the previous section is the pseudo spectrum and in order to find the DOAs, an exhaustive search for the d largest peaks needs to be conducted. Furthermore, the accuracy of the locations of the peaks also depends on the search step Δ° , which should be very small. The proposed KA-Root-MUSIC algorithm addresses these problems by representing the spectral function as a polynomial and determining its roots. In this section, the KA-Root-MUSIC method is derived according to the work in [13].

Employing a ULA, we can define the array manifold polynomial vector

$$\mathbf{a}(z) = [1, z, \dots, z^{M-1}]^T, \quad (5.93)$$

where

$$z = e^{j\mu_n}. \quad (5.94)$$

The DOAs $\boldsymbol{\theta}$ are contained in μ_n , which is defined as (5.51). Then the spectral function (5.91) of the KA-MUSIC algorithm can be rewritten as

$$P^{-1}(\theta_i) = \mathbf{a}^H(\theta_i)[\mathbf{I}_M - \hat{\mathbf{U}}_s \hat{\mathbf{U}}_s^H] \mathbf{a}(\theta_i). \quad (5.95)$$

For convenience, we define the matrix \mathbf{C} to be

$$\hat{\mathbf{C}} = \mathbf{I}_M - \hat{\mathbf{U}}_s \hat{\mathbf{U}}_s^H, \quad (5.96)$$

such that equation (5.95) can be simplified as

$$P^{-1}(\theta_i) = \mathbf{a}^H(\theta_i) \hat{\mathbf{C}} \mathbf{a}(\theta_i). \quad (5.97)$$

As the KA-MUSIC spectrum exhibits d peaks, (5.97) will have d valleys. By representing (5.97) as a polynomial and using the identity (5.94), the spectrum is evaluated on the unit circle and the d polynomial roots correspond to the DOAs. To find the polynomial whose roots we want to determine, we replace the steering vector $\mathbf{a}(\theta_i)$ by the array manifold polynomial vector defined in (5.93), which yields

$$P^{-1}(\theta_i) = \mathbf{a}^T(z^{-1}) \hat{\mathbf{C}} \mathbf{a}(z). \quad (5.98)$$

This expression can also be written as a double summation to obtain

$$P^{-1}(\theta_i) = \sum_{p=1}^M \sum_{q=1}^M z^{-p} \hat{C}_{pq} z^q = \sum_{p=0}^{M-1} \sum_{q=0}^{M-1} z^{(q-p)} \hat{C}_{pq}, \quad (5.99)$$

where \hat{C}_{pq} are the elements in the p th row and the q th column of the matrix \mathbf{C} . The double summation can be further simplified by setting $r = q - p$ and rewriting it as a single sum, i.e.,

$$P^{-1}(\theta_i) = \sum_{r=-M+1}^{M-1} \hat{C}_r z^r, \quad (5.100)$$

where

$$\hat{C}_r = \sum_{r=p-q} \hat{C}_{pq}, \quad (5.101)$$

which is the sum of the elements along the r th diagonal. As the range of r is $(-M+1) \leq r \leq (M-1)$ equation (5.100) defines a polynomial of order $2M-2$ with $2M-2$ roots. It can be shown that the roots form reciprocal conjugate pairs, which means that if

z_0 is a root of the polynomial, $1/z_0^*$ is also a root of it as well. In the noise-free case all the roots lie exactly on the unit circle. However, this is not true in the presence of noise and although both roots still contain the same information in the phase, they have reciprocal magnitude, such that one of them lies inside the unit circle and its counterpart outside. The KA-Root-MUSIC algorithm then estimates the DOAs from the d roots that are inside and closest to the unit circle.

Finally, the phase of the roots z_n provides the information about the DOAs and is obtained by

$$\mu_n = \arg(z_n), \quad (5.102)$$

so that the DOAs θ_n can be calculated as

$$\theta_n = \arcsin\left(\frac{\lambda_c \mu_n}{2\pi\Delta}\right). \quad (5.103)$$

A brief summary of the KA-Root-MUSIC algorithm is given in Table 5.5. Note that the estimated signal subspace $\hat{\mathbf{U}}_n$ results in an error Δz_n of the location of the

Tab. 5.5: The proposed KA-Root-MUSIC algorithm

1. Knowledge-Aided Processing:

- Compute the *a priori* covariance matrix $\mathbf{C} \in \mathbb{C}^{M \times M}$ by (5.4).
- Calculate the weight factors $\hat{\alpha}_{\text{opt}}$ and $\hat{\beta}_{\text{opt}}$ to obtain the enhanced covariance matrix estimate $\tilde{\mathbf{R}} \in \mathbb{C}^{M \times M}$.

2. Noise Subspace Estimation:

- Compute the matrix $\hat{\mathbf{U}}_n \in \mathbb{C}^{M \times M-d}$ as the $M-d$ eigenvectors corresponding to the $M-d$ smallest eigenvalues of the enhanced covariance matrix $\tilde{\mathbf{R}}$
- Determine $\hat{\mathbf{C}} = \mathbf{I}_M - \hat{\mathbf{U}}_n \hat{\mathbf{U}}_n^H$.

3. Polynomial Rooting:

- Obtain the coefficients \hat{C}_r by summing the r th diagonal of $\hat{\mathbf{C}}$.
- Find the $(N-1)$ root pairs and choose the d zeros within and closest to the unit circle.

4. DOA Estimation:

- Solve $\theta_n = \arcsin\left(\frac{\lambda_c}{2\pi\Delta} \arg(z_n)\right)$ to obtain the DOAs.

root z_n , which can be expressed by

$$\Delta z_n = |\Delta z_n| e^{j \arg(\Delta z_n)}. \quad (5.104)$$

However, as the KA-Root-MUSIC technique only estimates the signal DOAs from the phase of the root, the error in the magnitude will not affect the estimation of the signal directions. Nevertheless, such radial errors do affect the pseudo spectrum of the KA-MUSIC algorithm. Thus, the KA-Root-MUSIC method may provide a better performance than the KA-MUSIC algorithm.

5.6 Simulations with accurate *a priori* knowledge

In this section, we analyze the estimation accuracy of the proposed KA methods, where we first assume accurate knowledge of the known DOAs and then abandon this assumption to investigate the case of inaccurate knowledge. For all the simulations, we consider scenarios that pose severe challenges for the estimation process to emphasize the capabilities of the developed techniques under the conditions of a low SNR and a small data record size. Furthermore, we only compute the estimation errors of the unknown signal sources and neglect the errors of the sources whose precise DOAs are already known.

5.6.1 Comparison of LC1 and LC2 using KA-ESPRIT

In this section, the estimation performance of the two KA schemes developed in Section 5.2 is evaluated by applying the proposed KA-ESPRIT algorithm. The objective is to compare the different strategies of estimating the optimal combination factors α_{opt} and β_{opt} in order to find the one that yields a higher estimation accuracy. Thus, we compare their performances in terms of the root mean square error (RMSE) to the standard ESPRIT algorithm using LS and to the deterministic CRLB associated with the number of unknown sources.

For the computer simulations, we use a ULA composed of $M = 30$ sensor elements with an interelement spacing of $\Delta = \lambda_c/2$, where the azimuth angle 0° corresponds to the broad side of the array. The number of available snapshots N is chosen to be 10, which is significantly smaller than the number of sensor elements. Now, we assume that there are $d = 5$ uncorrelated and equipowered signals with power $\sigma^2 = 1$ impinging on the sensor array. The signals are positioned at $\boldsymbol{\theta} = [-50^\circ, -10^\circ, 10^\circ, 20^\circ, 70^\circ]^T$ and the source symbols are drawn from a complex Gaussian distribution. Among these d

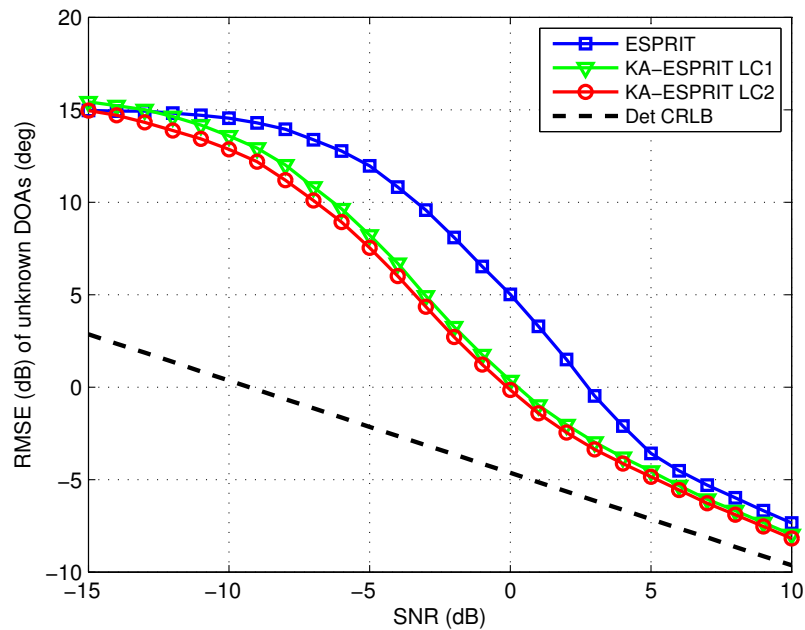


Fig. 5.2: Comparison of the LC_1 and LC_2 regarding the RMSE versus the SNR with $M = 30$, $N = 10$, $d = 5$ sources at $\boldsymbol{\theta} = [-50^\circ, -10^\circ, 10^\circ, 20^\circ, 70^\circ]^T$, $k = 2$ sources at $\theta_1 = -50^\circ$ and $\theta_5 = 70^\circ$ considered known.

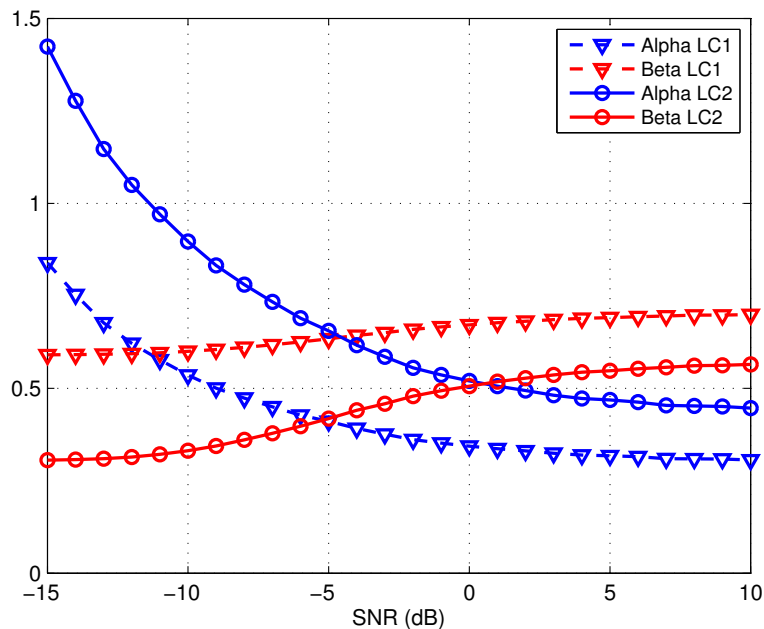


Fig. 5.3: Combination factors of the LC_1 and LC_2 versus the SNR with $M = 30$, $N = 10$, $d = 5$ sources at $\boldsymbol{\theta} = [-50^\circ, -10^\circ, 10^\circ, 20^\circ, 70^\circ]^T$, $k = 2$ sources at $\theta_1 = -50^\circ$ and $\theta_5 = 70^\circ$ considered known.

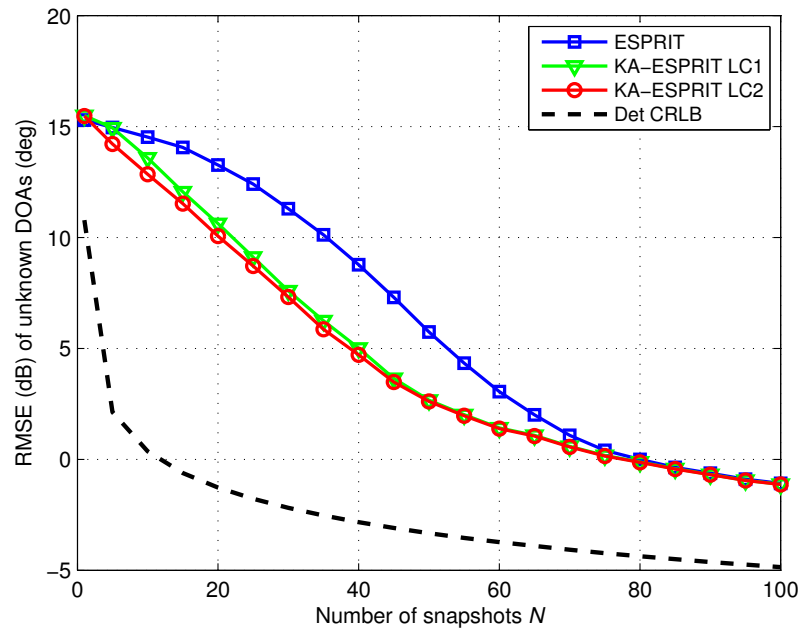


Fig. 5.4: Comparison of the LC₁ and LC₂ regarding the RMSE versus the number of snapshots N with $M = 30$, SNR = -10 dB, $d = 5$ sources at $\boldsymbol{\theta} = [-50^\circ, -10^\circ, 10^\circ, 20^\circ, 70^\circ]^T$, $k = 2$ sources at $\theta_1 = -50^\circ$ and $\theta_5 = 70^\circ$ considered known.

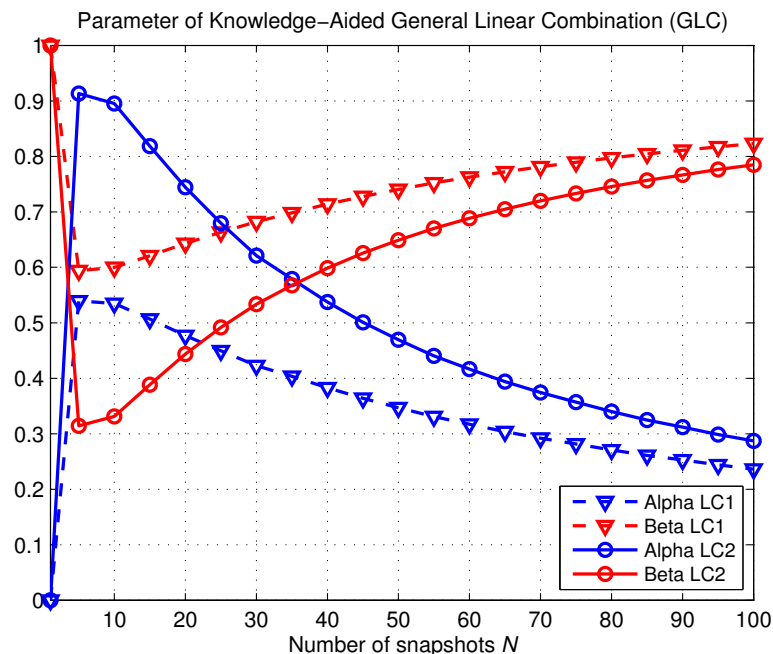


Fig. 5.5: Combination factors of the LC₁ and LC₂ versus the number of snapshots N with $M = 30$, SNR = -10 dB, $d = 5$ sources at $\boldsymbol{\theta} = [-50^\circ, -10^\circ, 10^\circ, 20^\circ, 70^\circ]^T$, $k = 2$ sources at $\theta_1 = -50^\circ$ and $\theta_5 = 70^\circ$ considered known.

sources, we assume that the $k = 2$ sources at $\theta_1 = -50^\circ$ and at $\theta_5 = 70^\circ$ have been estimated previously and are therefore known beforehand. All the simulated curves are obtained by averaging the results over 3000 independent trials.

In the first experiment, we assess the RMSE performance as a function of the SNR. The results depicted in Figure 5.2 show that the two versions of the proposed KA-ESPRIT algorithm provide a significant gain over the standard ESPRIT algorithm, especially at a moderate SNR. Thus, in this case, the performance advantage obtained from the exploitation of *a priori* knowledge is translated into a considerably better performance. Also, the gain attained by the estimate LC₂ outclasses the one for LC₁ reaching a maximum benefit of more than 5 dB over standard ESPRIT. When the SNR is increased, the conventional ESPRIT algorithm is able to approach the performance of the KA-ESPRIT method. The purpose of the simulations shown in Figure 5.3 is to study the behavior of the estimated parameters $\hat{\alpha}_{\text{opt}}$ and $\hat{\beta}_{\text{opt}}$. It is evident that the factor α which weights the *a priori* covariance matrix starts at a high value and decreases as the SNR increases, whereas the parameter β associated with the sample covariance matrix goes up. This characteristic is completely in line with the stated theory that the prior knowledge in form of the matrix \mathbf{C} is especially exploited in the low SNR regime when the sample covariance matrix is a poor estimate. We also notice that for LC₂ the knowledge is exploited in a more efficient way, which explains the better performance of this estimation strategy. Notice that the sum of α and β is not restricted to be equal to 1, which is the case for the constraint (5.9) discussed in Section 5.2 and implies a limitation.

In the second experiment, we evaluate the RMSE as a function of the number of snapshots N , where the same scenario of the first experiment is considered. The curves shown in Figure 5.4 illustrate that the gains of the proposed KA-ESPRIT algorithm over the standard ESPRIT algorithm are more pronounced for situations with a shorter data record. Again, the estimate LC₂ outperforms LC₁ and standard ESPRIT converges to the KA-ESPRIT method as the number of snapshots increases. Figure 5.5 demonstrates the characteristic of the combinations factors against the number of snapshots. The parameter α exhibits its highest values for a notably low data record size and decreases as the snapshot number grows, whereas β behaves contrarily and increases with the sample size. These properties explicitly support the achieved performance gain.

As proven in Figure 5.2 and Figure 5.4, the benefits of exploiting prior knowledge are most significant under severe conditions in the scenario. Furthermore, it is obvious that LC₂ provides slightly more accurate estimates of the two weight factors. Consequently, we will only present the results obtained by these estimates in the following simulation

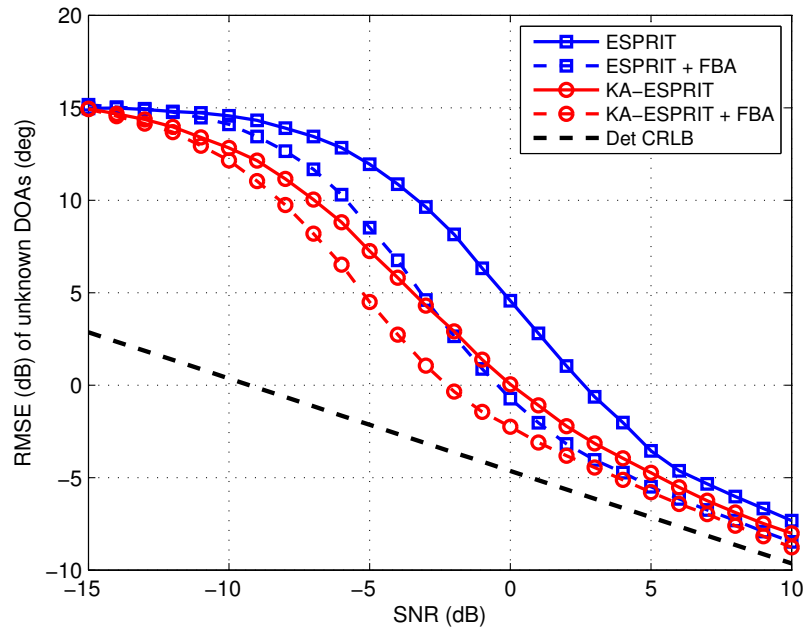


Fig. 5.6: RMSE versus the SNR of KA-ESPRIT and FBA with $M = 30$, $N = 10$, $d = 5$ sources at $\boldsymbol{\theta} = [-50^\circ, -10^\circ, 10^\circ, 20^\circ, 70^\circ]^T$, $k = 2$ sources at $\theta_1 = -50^\circ$ and $\theta_5 = 70^\circ$ considered known.

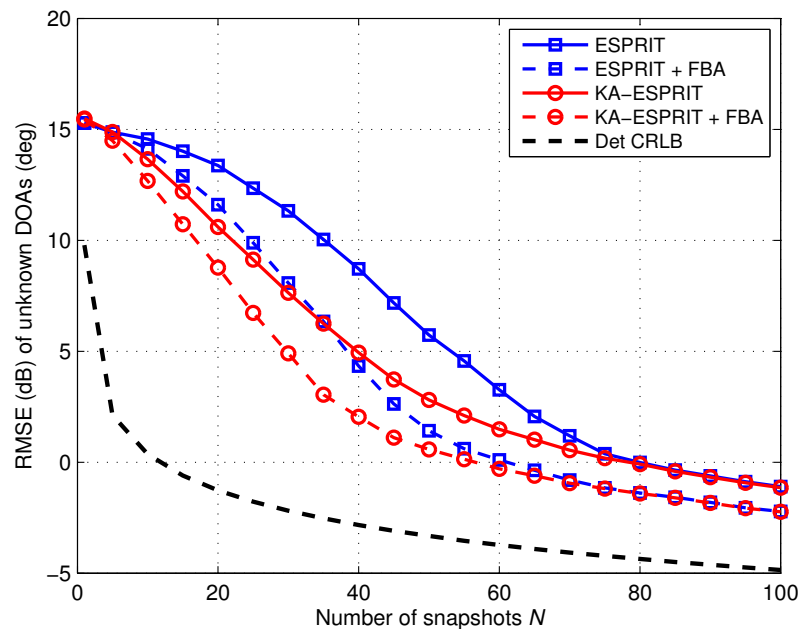


Fig. 5.7: RMSE versus the number of snapshots N of KA-ESPRIT and FBA with $M = 30$, $\text{SNR} = -10$ dB, $d = 5$ sources at $\boldsymbol{\theta} = [-50^\circ, -10^\circ, 10^\circ, 20^\circ, 70^\circ]^T$, $k = 2$ sources at $\theta_1 = -50^\circ$ and $\theta_5 = 70^\circ$ considered known.

analysis.

In addition, we also take into the account the effect of forward-backward averaging (FBA), which is known to be an efficient preprocessing method to smoothen the DOA estimates for a low data record size [48]. The results are shown in Figure 5.6 and Figure 5.7 as a function of the SNR and the number of snapshots respectively. It is evident that even if FBA is applied, the benefits of prior knowledge are almost as significant as for the non-smoothened case. Thus, the proposed KA scheme appears to be a powerful way of incorporating *a priori* knowledge to substantially improve the estimation accuracy at a low SNR and a small number of samples.

5.6.2 Comparison of the proposed KA DOA estimation algorithms

This section aims to investigate the effect of *a priori* knowledge on the proposed KA DOA estimation algorithms. As the direction finding methods exploit different properties, we also expect a different impact of prior knowledge in terms of the estimation performance.

KA-ESPRIT and Unitary KA-ESPRIT

In the first part, the RMSE performance of the KA-ESPRIT and the Unitary KA-ESPRIT algorithms is analyzed. Specifically, we focus on the various ways of solving the shift invariance equations, namely LS, TLS, and SLS [47].

In the first experiment, we assess the capabilities of LS, TLS, and SLS for KA-ESPRIT. For the sake of consistency we use the same scenario as in the previous section, where the knowledge of $\theta_1 = -50^\circ$ and $\theta_5 = 70^\circ$ from $\boldsymbol{\theta} = [-50^\circ, -10^\circ, 10^\circ, 20^\circ, 70^\circ]^T$ was assumed with $M = 30$ and $N = 10$. The results depicted in Figure 5.8 show the RMSE as a function of the SNR. It can be seen that the gain achieved by incorporating prior knowledge is almost identical for the three approaches to solve the shift invariance equation. Moreover, we notice that SLS is the only method that constitutes an efficient estimator [47], which asymptotically approaches the deterministic CRLB, whereas LS and TLS only provide a suboptimal estimation accuracy.

The same comparison as above is conducted for Unitary KA-ESPRIT in the second experiment. Again, we keep the previous scenario and show the numerical outcome in Figure 5.9. Similar to KA-ESPRIT, the SLS approach performs best and reaches the CRLB as the SNR increases. However, the impact of the prior knowledge on the estimation performance is different for all the three methods. While the gain for LS and

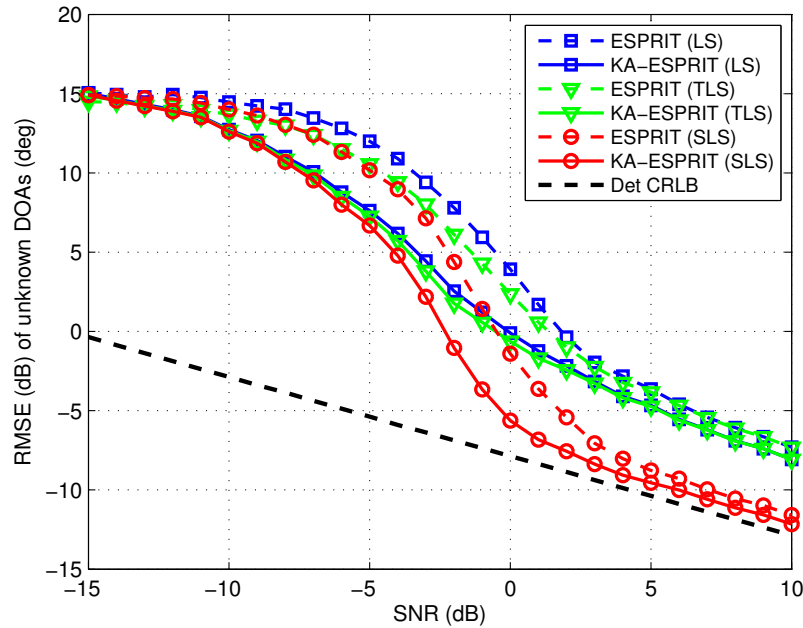


Fig. 5.8: Comparison of KA-ESPRIT-type algorithms regarding the RMSE versus the SNR with $M = 30$, $N = 10$, $d = 5$ sources at $\boldsymbol{\theta} = [-50^\circ, -10^\circ, 10^\circ, 20^\circ, 70^\circ]^T$, $k = 2$ sources at $\theta_1 = -50^\circ$ and $\theta_5 = 70^\circ$ considered known.

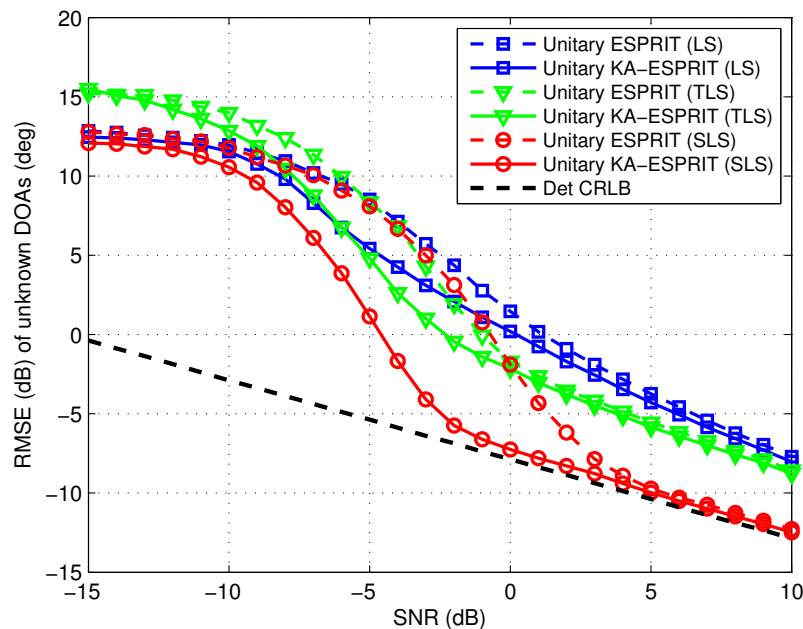


Fig. 5.9: Comparison of Unitary KA-ESPRIT-type algorithms regarding the RMSE versus the SNR with $M = 30$, $N = 10$, $d = 5$ sources at $\boldsymbol{\theta} = [-50^\circ, -10^\circ, 10^\circ, 20^\circ, 70^\circ]^T$, $k = 2$ sources at $\theta_1 = -50^\circ$ and $\theta_5 = 70^\circ$ considered known.

TLS becomes smaller than for KA-ESPRIT, SLS exhibits a more pronounced benefit if *a priori* knowledge is available. This significant gain almost attains a difference of 10 dB as evident from the scenario in Figure 5.9.

As illustrated in Figure 5.8 and in Figure 5.9, the method of SLS to solve the shift invariance equations provides the best estimator for KA-ESPRIT and Unitary KA-ESPRIT, and yields the highest gains for prior knowledge of signal directions in the system. Thus, we limit our focus to this approach in the following simulations.

Comparison of all the proposed KA algorithms

The second part is concerned with the comparison of all the proposed KA-based direction finding algorithms. Once more we use the same scenario as before and estimate the unknown signal sources. As discussed in the previous section, the method of SLS is applied to the KA-ESPRIT and Unitary KA-ESPRIT. The simulation results in Figure 5.10 illustrate that all of the presented algorithms benefit from the proposed KA scheme. However, the performance advantage is most significant for the KA-ESPRIT-type algorithms, where gains up to 10 dB can be achieved. The benefit for the proposed MUSIC-type methods is rather moderate, but still attains up to 5 dB. Furthermore,

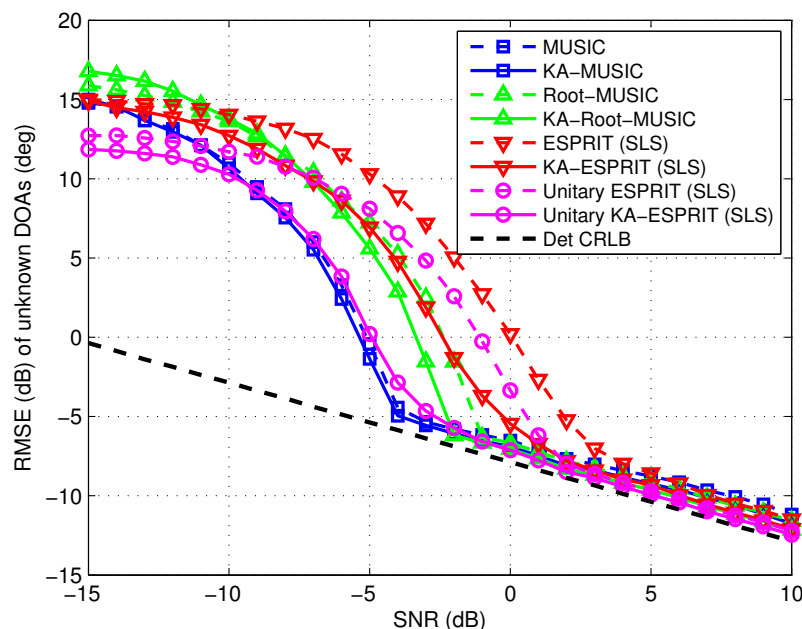


Fig. 5.10: Comparison of all the proposed KA algorithms regarding the RMSE versus the SNR with $M = 30$, $N = 10$, $d = 5$ sources at $\boldsymbol{\theta} = [-50^\circ, -10^\circ, 10^\circ, 20^\circ, 70^\circ]^T$, $k = 2$ sources at $\theta_1 = -50^\circ$ and $\theta_5 = 70^\circ$ considered known.

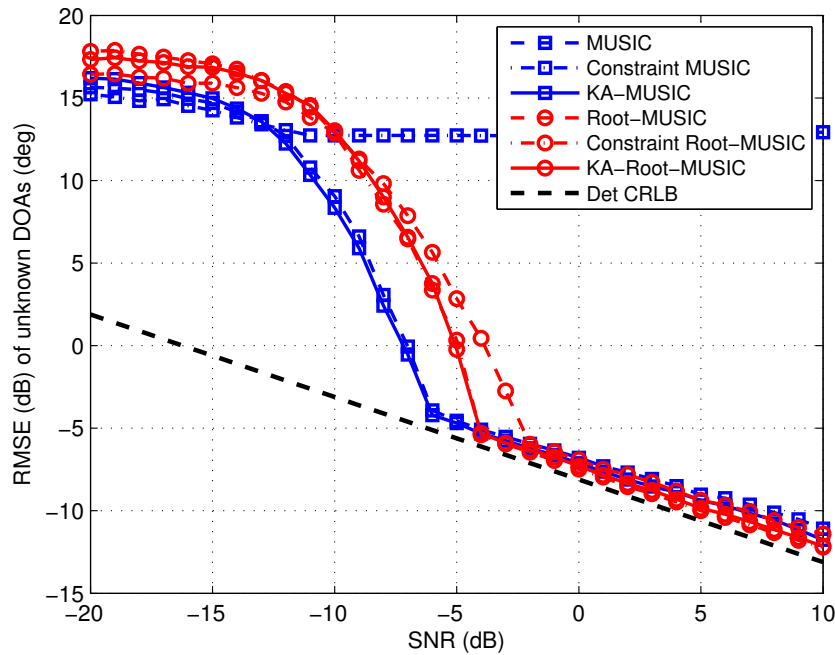


Fig. 5.11: Comparison of KA-MUSIC-type and constrained MUSIC-type algorithms regarding the RMSE versus the SNR with $M = 30$, $N = 10$, $d = 5$ sources at $\boldsymbol{\theta} = [-50^\circ, -10^\circ, 10^\circ, 20^\circ, 70^\circ]^T$, $k = 2$ sources at $\theta_1 = -50^\circ$ and $\theta_5 = 70^\circ$ considered known.

we notice that all the methods approach the deterministic CRLB, whereas KA-MUSIC and Unitary KA-ESPRIT combined with SLS provide the most precise estimates for the underlying scenario.

Comparison of KA-MUSIC-type and constrained MUSIC-type algorithms

The third part deals with the comparison of the proposed KA-MUSIC-type algorithms to the constraint MUSIC-type methods proposed in [45]. The latter approach is based on a projection onto the complement of the signal subspace spanned by the steering vectors of the known DOAs, and was applied to MUSIC and Root-MUSIC. Thus, we compare the proposed KA-MUSIC algorithm and the KA-Root-MUSIC algorithm to the constraint MUSIC and the constraint Root-MUSIC method. According to the simulations shown in Figure 5.11, the MUSIC algorithms outperform the Root-MUSIC methods for the chosen scenario. Specifically, the constraint MUSIC technique completely fails to efficiently estimate the DOAs if $N < M$, whereas the KA-MUSIC algorithm slightly improves the estimation accuracy of the classical MUSIC method. As for Root-MUSIC, the constraint approach and KA-Root-MUSIC yield an identical performance gain over the Root-MUSIC algorithm without prior knowledge.

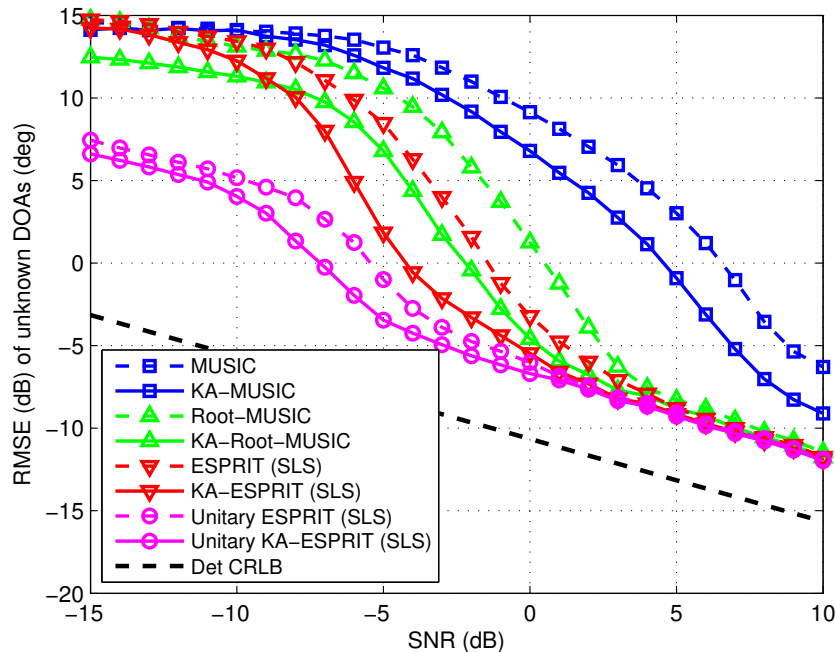


Fig. 5.12: Comparison of the proposed KA algorithms regarding RMSE versus the SNR for closely-spaced sources with $M = 30$, $N = 10$, $d = 2$ sources at $\boldsymbol{\theta} = [0^\circ, 2^\circ]^T$, $k = 1$ source at $\theta_1 = 0^\circ$ considered known.

5.6.3 Closely-spaced signal sources

In this section, we assess the performance of the proposed KA algorithms when two closely-spaced signal sources are in the system. The sources transmit uncorrelated complex Gaussian signals located at $\boldsymbol{\theta} = [0^\circ, 2^\circ]^T$, where the source $\theta_1 = 0^\circ$ is considered known. Other than that, we assume the same sensor array as before with $M = 30$ elements and an available snapshot number of $N = 10$. The results of the simulations are depicted in Figure 5.12 and demonstrate that KA-Root-MUSIC and KA-ESPRIT with SLS achieve the highest gains compared to their conventional counterparts if one of the closely-spaced DOAs is known. Also, KA-MUSIC turns out to be the worst estimator while Unitary KA-ESPRIT combined with SLS is the closest to the CRLB.

5.6.4 Widely-spaced signal sources

Contrary to the previous section, the performance gain for the widely-spaced source case is studied in this experiment. Again, we assume the same scenario as before, but two uncorrelated complex Gaussian signal sources at $\boldsymbol{\theta} = [-40^\circ, 40^\circ]^T$ with $\theta_1 = -40^\circ$ considered known. Figure 5.13 illustrates the simulation results, and it is obvious that exploiting prior knowledge of widely-spread signal sources is only beneficial for the KA-

ESPRIT-type methods. However, the performance of the KA-MUSIC-type algorithms is slightly decreased. This is due to the fact that for widely-spaced sources the noise subspace estimate required for the MUSIC algorithms is perturbed.

5.6.5 Correlated signal sources

The purpose of this section is to investigate the behavior of the proposed KA direction finding algorithms for highly correlated sources. In order to simulate this case, we use the scenario from Section 5.6.1 and describe the degree of correlation via the correlation factor $\rho \in (0, 1)$, where $\rho = 0$ if the signals are uncorrelated and $\rho = 1$ for coherent signals. In our simulations we set ρ to be 0.9 and compare all the proposed KA methods to each other. The results shown in Figure 5.14 represent the effect of correlation on the performance. In comparison to Figure 5.10, it can be seen that the efficiency of all the algorithms is decreased as they no longer approach the CRLB. It is clear that the proposed KA scheme is not able to decorrelate the signals, but it is capable of increasing the estimation accuracy for all the KA methods at a low SNR. Once more, the KA-ESPRIT-type algorithms attain the most significant performance gains and KA-MUSIC and Unitary KA-ESPRIT perform best.

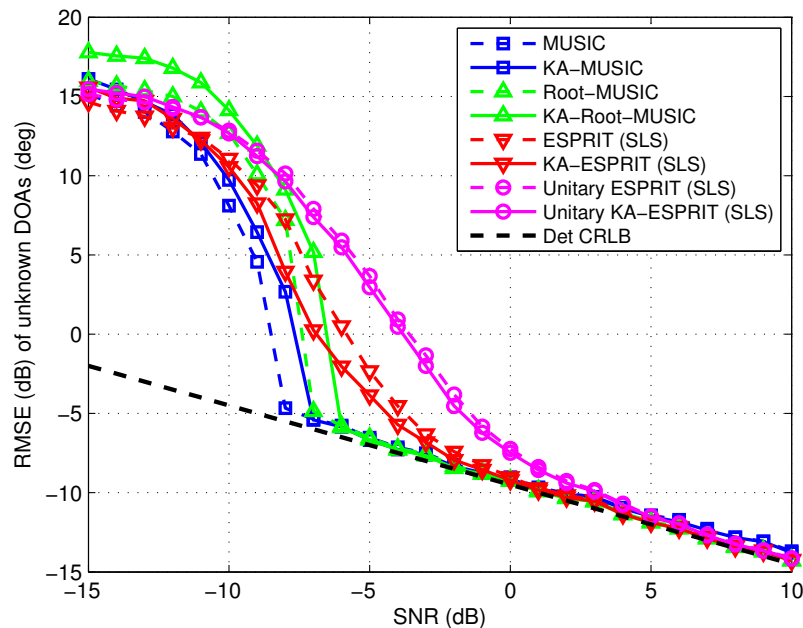


Fig. 5.13: Comparison of the proposed KA algorithms regarding the RMSE versus the SNR for widely-spaced sources with $M = 30$, $N = 10$, $d = 2$ sources at $\boldsymbol{\theta} = [-40^\circ, 40^\circ]^T$, $k = 1$ sources at $\theta_1 = -40^\circ$ considered known.

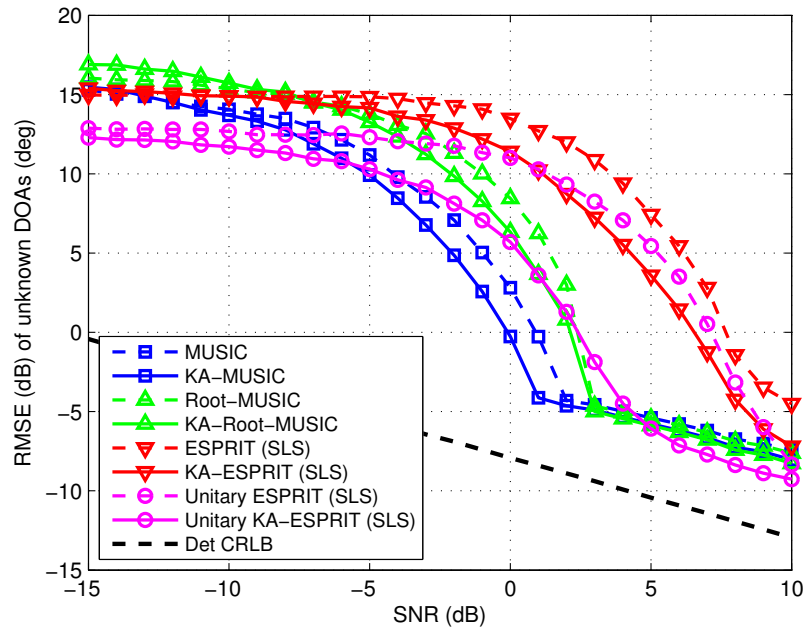


Fig. 5.14: Comparison of the proposed KA algorithms regarding the RMSE versus the SNR for correlated sources with $M = 30$, $N = 10$, $d = 5$ sources at $\boldsymbol{\theta} = [-50^\circ, -10^\circ, 10^\circ, 20^\circ, 70^\circ]^T$, $k = 2$ sources at $\theta_1 = -50^\circ$ and $\theta_5 = 70^\circ$ considered known and $\rho = 0.9$.

5.7 Simulations with inaccurate *a priori* knowledge

It was shown in the previous section that incorporating *a priori* knowledge by using the proposed KA scheme leads to substantial performance gains in terms of the estimation accuracy of all the proposed algorithms. However, our assumption was based on the precise knowledge of the signal directions. In this section, we extend this presumption to the case of imprecise knowledge and analyze the influence of those errors on the performance.

For the simulations, we assume again that there are $d = 5$ signal sources at $\boldsymbol{\theta} = [-50^\circ, -10^\circ, 10^\circ, 20^\circ, 70^\circ]^T$, but we allow an error of 1° for the known directions θ_1 and θ_5 , so that $\theta_1 = -51^\circ$ and $\theta_5 = 69^\circ$. Figure 5.15 depicts the curves and it is evident that compared to Figure 5.10 the perturbed knowledge of the DOAs only results into a small performance degradation. Thus, for reasonably small errors, the proposed KA scheme provides a certain robustness against imprecise knowledge. However, larger errors cause the estimation performance of the KA algorithms to be less accurate than their conventional counterparts. Furthermore, the proposed algorithms exhibit a performance degradation in the presence of inaccurate knowledge. A solution to this problem needs to be developed so that the combination weights of the covariance

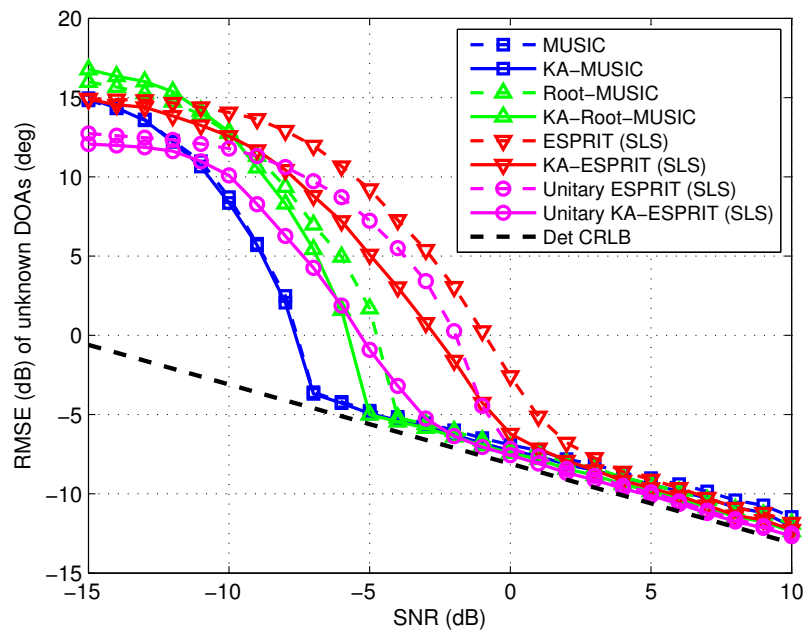


Fig. 5.15: Comparison of the proposed KA algorithms regarding the RMSE versus the SNR with inaccurate knowledge and $M = 30$, $N = 10$, $d = 5$ sources at $\boldsymbol{\theta} = [-50^\circ, -10^\circ, 10^\circ, 20^\circ, 70^\circ]^T$, $k = 2$ sources at $\theta_1 = -51^\circ$ and $\theta_5 = 69^\circ$ considered known.

matrices are automatically adjusted in a way that only the sample covariance matrix is used if the knowledge exceeds a certain level of impreciseness. Nevertheless, this is an issue for future work.

5.8 Conclusion

In this chapter, a novel way of incorporating *a priori* knowledge of a subset of the DOAs to improve the estimation accuracy under severe conditions is proposed and extensively discussed. After introducing the problem statement for cases when only a limited data record is available and the sample covariance matrix is a poor estimate, the idea of using prior knowledge for space-time adaptive processing (STAP) is effectively applied to DOA estimation. The concept of a weighted combination of a covariance matrix containing the knowledge and of the sample covariance matrix is formulated as an optimization problem, which is solved for the weight factors using two different ways. Having analyzed the general structure of the proposed knowledge-aided (KA) scheme, the KA-ESPRIT-type algorithms based on standard ESPRIT and Unitary ESPRIT and the KA-MUSIC-type algorithms based on MUSIC and Root-MUSIC are presented as methods which incorporate this KA concept. The estimation performance of these

proposed algorithms is then evaluated via computer simulations. It is shown that the exploitation of *a priori* knowledge is translated into a substantially better performance for situations with a shorter data record and a low SNR. In particular, the performance advantage depends on the direction finding methods and is more pronounced for KA-ESPRIT-type algorithms, especially when structured least squares (SLS) is used to solve the shift invariance equations. A comparison to previously developed knowledge-aided MUSIC-type algorithms, such as constraint MUSIC [45], reveals that the proposed KA-MUSIC-type methods outperform the constrained MUSIC and perform identically to the constrained Root-MUSIC. Furthermore, it is demonstrated that the effect of prior knowledge is considerably larger in the case of closely-spaced signal sources compared to widely-spaced sources. Also, it is shown that the gains for uncorrelated sources can be maintained if the signals are highly correlated. To conclude the study, it is illustrated that the proposed KA direction finding scheme exhibits a certain robustness for reasonably small errors, and only large deviations from the true DOA degrade the estimation accuracy.

Regarding the practical relevance of the proposed KA DOA estimation scheme, it should be emphasized that several scenarios exist where *a priori* knowledge of static signal directions is available and can be exploited. Some examples are, signals from base stations or static users and radar applications, where the signal is backscattered by stationary objects with known positions. For these practical scenarios the proposed KA direction finding scheme is a powerful way of incorporating prior knowledge under severe conditions and can be applied to any direction finding algorithm, which relies on the estimate of the sample covariance matrix.

6. SUMMARY AND FUTURE WORK

In this work, advanced array signal processing algorithms for beamforming and direction finding are devised and discussed.

The first part is concerned with the development of widely-linear adaptive beamforming algorithms designed according to the minimum variance principle that can exploit the properties of non-circular sources for an improved performance. The recently proposed Krylov subspace-based adaptive algorithms apply either the AVF, the CG or the MCG algorithm to iteratively update the beamforming weight vector and avoid the costly computation of the covariance matrix inversion. After discussing the advantages of the widely-linear processing, the aforementioned Krylov-based methods are devised to make use of this concept. The proposed algorithms fully exploit the second-order statistics of the signals that are assumed to be strictly non-circular. These new methods are then compared to the existing adaptive algorithms in terms of the required computational complexity and the performance in stationary and non-stationary scenarios. As a result, it is shown that the widely-linear processing adopted for the proposed techniques provides significant performance gains over the conventional way of designing the beamforming weights. It is also outlined that among the proposed algorithms the WL-MCG method requires the lowest computational cost and the WL-AVF outperforms all the existing techniques in stationary scenarios. In future work, the assumption of the strict non-circularity will be generalized to the weak non-circularity of the signals.

In the second part, we develop innovative algorithms for direction finding that operate in the beamspace domain and achieve better performance while dealing with the increased dimensions of large systems. A novel class of subspace-based direction finding methods employing the AVF and the CG algorithm is shown to yield superior estimation performance for closely-spaced sources at a low SNR and a small sample size. By extending these concepts to the strategy of beamspace processing, two new Krylov subspace-based direction finding methods are developed for two different ways of designing the beamspace. The proposed algorithms are then analyzed through complexity and performance evaluations, and compared to previously developed methods. It is shown that operation in beamspace substantially enhances the resolution capa-

bility and the estimation accuracy of the proposed algorithms, where the CG-based method outperforms the AVF-based algorithm.

Finally, a novel way of incorporating prior knowledge for direction finding is proposed. Having knowledge of a subset of the signal directions to be estimated, the estimation performance of unknown directions can be substantially improved. Existing knowledge-aided methods apply projection and polynomial rooting techniques to exploit this information. The new strategy is developed for situations with a limited data record and is based on an enhanced covariance matrix estimate obtained by linearly combining the sample covariance matrix and a prior known covariance matrix in an automatic fashion. Therefore, MUSIC-type and ESPRIT-type algorithms are devised, which employ the proposed scheme. Extensive simulations assessing the performance illustrate that the exploitation of prior knowledge is translated into significantly better performance. In particular, it is shown that the performance advantage depends on the direction finding methods and is more pronounced for ESPRIT-type algorithms. A derivation of a Cramér-Rao lower bound for the proposed knowledge-aided scheme will be considered in future work.

Appendix A

DERIVATIONS

A.1 Proof of equation (3.8)

We start by inserting the optimal solution \mathbf{w}_{opt} for $\gamma = 1$ in equation (3.6) into (3.7), rewritten as

$$\text{SINR} = \frac{\sigma_1^2 \mathbf{w}^H \mathbf{a}(\theta_1) \mathbf{a}^H(\theta_1) \mathbf{w}}{\mathbf{w}^H \mathbf{R}_u \mathbf{w}}, \quad (\text{A.1})$$

which yields

$$\text{SINR} = \frac{\sigma_1^2 \left(\frac{\mathbf{R}^{-1} \mathbf{a}(\theta_1)}{\mathbf{a}^H(\theta_1) \mathbf{R}^{-1} \mathbf{a}(\theta_1)} \right)^H \mathbf{a}(\theta_1) \mathbf{a}^H(\theta_1) \left(\frac{\mathbf{R}^{-1} \mathbf{a}(\theta_1)}{\mathbf{a}^H(\theta_1) \mathbf{R}^{-1} \mathbf{a}(\theta_1)} \right)}{\left(\frac{\mathbf{R}^{-1} \mathbf{a}(\theta_1)}{\mathbf{a}^H(\theta_1) \mathbf{R}^{-1} \mathbf{a}(\theta_1)} \right)^H \mathbf{R}_u \left(\frac{\mathbf{R}^{-1} \mathbf{a}(\theta_1)}{\mathbf{a}^H(\theta_1) \mathbf{R}^{-1} \mathbf{a}(\theta_1)} \right)}. \quad (\text{A.2})$$

Taking into account that \mathbf{R}^{-1} is a Hermitian matrix, we have that

$$\text{SINR} = \frac{\sigma_1^2 \left(\frac{\mathbf{a}^H(\theta_1) \mathbf{R}^{-1}}{\mathbf{a}^H(\theta_1) \mathbf{R}^{-1} \mathbf{a}(\theta_1)} \right) \mathbf{a}(\theta_1) \mathbf{a}^H(\theta_1) \left(\frac{\mathbf{R}^{-1} \mathbf{a}(\theta_1)}{\mathbf{a}^H(\theta_1) \mathbf{R}^{-1} \mathbf{a}(\theta_1)} \right)}{\left(\frac{\mathbf{a}^H(\theta_1) \mathbf{R}^{-1}}{\mathbf{a}^H(\theta_1) \mathbf{R}^{-1} \mathbf{a}(\theta_1)} \right) [\mathbf{R} - \sigma_1^2 \mathbf{a}(\theta_1) \mathbf{a}^H(\theta_1)] \left(\frac{\mathbf{R}^{-1} \mathbf{a}(\theta_1)}{\mathbf{a}^H(\theta_1) \mathbf{R}^{-1} \mathbf{a}(\theta_1)} \right)}, \quad (\text{A.3})$$

where the interference-plus-noise covariance matrix \mathbf{R}_u is expressed by the difference of the covariance matrix and the signal covariance matrix. Rearranging the expression (A.3), we obtain

$$\text{SINR} = \frac{\sigma_1^2 \mathbf{a}^H(\theta_1) \mathbf{R}^{-1} \mathbf{a}(\theta_1) \mathbf{a}^H(\theta_1) \mathbf{R}^{-1} \mathbf{a}(\theta_1)}{\mathbf{a}^H(\theta_1) \mathbf{R}^{-1} \mathbf{a}(\theta_1) - \sigma_1^2 \mathbf{a}^H(\theta_1) \mathbf{R}^{-1} \mathbf{a}(\theta_1) \mathbf{a}^H(\theta_1) \mathbf{R}^{-1} \mathbf{a}(\theta_1)} \quad (\text{A.4})$$

$$= \frac{\sigma_1^2 \mathbf{a}^H(\theta_1) \mathbf{R}^{-1} \mathbf{a}(\theta_1) \mathbf{a}^H(\theta_1) \mathbf{R}^{-1} \mathbf{a}(\theta_1)}{\mathbf{a}^H(\theta_1) \mathbf{R}^{-1} \mathbf{a}(\theta_1) [1 - \sigma_1^2 \mathbf{a}^H(\theta_1) \mathbf{R}^{-1} \mathbf{a}(\theta_1)]} \quad (\text{A.5})$$

$$= \frac{\sigma_1^2 \mathbf{a}^H(\theta_1) \mathbf{R}^{-1} \mathbf{a}(\theta_1)}{1 - \sigma_1^2 \mathbf{a}^H(\theta_1) \mathbf{R}^{-1} \mathbf{a}(\theta_1)}, \quad (\text{A.6})$$

which is the desired result.

A.2 Real-valued source symbols for strict non-circularity

The proof starts with rewriting the augmented array output matrix in (3.11) as

$$\tilde{\mathbf{X}} = \begin{bmatrix} \mathbf{A}(\boldsymbol{\theta})\mathbf{S} \\ \mathbf{A}^*(\boldsymbol{\theta})\mathbf{S}^* \end{bmatrix} + \begin{bmatrix} \mathbf{N} \\ \mathbf{N}^* \end{bmatrix} \in \mathbb{C}^{2M \times N} \quad (\text{A.7})$$

$$= \begin{bmatrix} \mathbf{A}(\boldsymbol{\theta}) \\ \mathbf{0} \end{bmatrix} \mathbf{S} + \begin{bmatrix} \mathbf{0} \\ \mathbf{A}^*(\boldsymbol{\theta}) \end{bmatrix} \mathbf{S}^* + \begin{bmatrix} \mathbf{N} \\ \mathbf{N}^* \end{bmatrix}. \quad (\text{A.8})$$

According to [21], the complex conjugate signal matrix \mathbf{S}^* can be decomposed by an orthogonal projection onto \mathbf{S} as

$$\mathbf{S}^* = \boldsymbol{\Psi}^* \mathbf{S} + [\mathbf{P} (\mathbf{I}_d - |\boldsymbol{\Psi}|^2)]^{\frac{1}{2}} \mathbf{S}', \quad (\text{A.9})$$

where $\boldsymbol{\Psi} = \text{diag}\{\rho_1, \dots, \rho_d\}$ contains the non-circularity coefficients of the d signal sources on its diagonal and $\mathbf{P} = \text{diag}\{\sigma_1^2, \dots, \sigma_d^2\}$ contains the signal powers on its diagonal. The matrix \mathbf{S}' is the part that is orthogonal to \mathbf{S} . Inserting (A.9) into (A.8), we obtain

$$\tilde{\mathbf{X}} = \begin{bmatrix} \mathbf{A}(\boldsymbol{\theta}) \\ \mathbf{0} \end{bmatrix} \mathbf{S} + \begin{bmatrix} \mathbf{0} \\ \mathbf{A}^*(\boldsymbol{\theta}) \end{bmatrix} [\boldsymbol{\Psi}^* \mathbf{S} + [\mathbf{P} (\mathbf{I}_d - |\boldsymbol{\Psi}|^2)]^{\frac{1}{2}} \mathbf{S}'] + \begin{bmatrix} \mathbf{N} \\ \mathbf{N}^* \end{bmatrix}, \quad (\text{A.10})$$

which can be expressed as

$$\tilde{\mathbf{X}} = \begin{bmatrix} \mathbf{A}(\boldsymbol{\theta}) \\ \mathbf{A}^*(\boldsymbol{\theta})\boldsymbol{\Psi}^* \end{bmatrix} \mathbf{S} + \begin{bmatrix} \mathbf{0} \\ \mathbf{A}^*(\boldsymbol{\theta}) \end{bmatrix} [\mathbf{P} (\mathbf{I}_d - |\boldsymbol{\Psi}|^2)]^{\frac{1}{2}} \mathbf{S}' + \begin{bmatrix} \mathbf{N} \\ \mathbf{N}^* \end{bmatrix}. \quad (\text{A.11})$$

Now we assume that all the signals are strictly non-circular, i.e., $|\rho| = 1$ and that the phase is $\psi = 0$, which is given for, e.g., BPSK-modulated signals. Thus (A.11) simplifies to

$$\tilde{\mathbf{X}} = \begin{bmatrix} \mathbf{A}(\boldsymbol{\theta}) \\ \mathbf{A}^*(\boldsymbol{\theta}) \end{bmatrix} \mathbf{S} + \begin{bmatrix} \mathbf{N} \\ \mathbf{N}^* \end{bmatrix}. \quad (\text{A.12})$$

It is event from (A.12) that the source symbol matrix \mathbf{S} is real-valued, which completes the proof.

A.3 Proof of equation (3.23)

In order to prove equation (3.23), we start by inserting (3.19) into (3.22), which gives

$$\mathbb{E} \left[|\tilde{\mathbf{w}}_k^H \tilde{\mathbf{r}}|^2 \right] = \tilde{\mathbf{w}}_k^H \tilde{\mathbf{R}} \tilde{\mathbf{w}}_k \quad (\text{A.13})$$

$$= \left(\tilde{\mathbf{w}}_{k-1}^H - \mu_k \tilde{\mathbf{g}}_k^H \right) \tilde{\mathbf{R}} \left(\tilde{\mathbf{w}}_{k-1} - \mu_k \tilde{\mathbf{g}}_k \right) \quad (\text{A.14})$$

$$= \tilde{\mathbf{w}}_{k-1}^H \tilde{\mathbf{R}} \tilde{\mathbf{w}}_{k-1} - 2\mu_k \tilde{\mathbf{g}}_k^H \tilde{\mathbf{R}} \tilde{\mathbf{w}}_{k-1} + \mu_k^2 \tilde{\mathbf{g}}_k^H \tilde{\mathbf{R}} \tilde{\mathbf{g}}_k. \quad (\text{A.15})$$

Taking the gradient with respect to μ_k and equating it to zero, yields

$$\frac{\partial \left(\tilde{\mathbf{w}}_k^H \tilde{\mathbf{R}} \tilde{\mathbf{w}}_k \right)}{\partial \mu_k} = 2\tilde{\mathbf{g}}_k^H \tilde{\mathbf{R}} \tilde{\mathbf{w}}_{k-1} + 2\mu_k \tilde{\mathbf{g}}_k^H \tilde{\mathbf{R}} \tilde{\mathbf{g}}_k \stackrel{!}{=} 0. \quad (\text{A.16})$$

After a simple rearrangement, the step size μ_k can be computed by

$$\mu_k = \frac{\tilde{\mathbf{g}}_k^H \tilde{\mathbf{R}} \tilde{\mathbf{w}}_{k-1}}{\tilde{\mathbf{g}}_k^H \tilde{\mathbf{R}} \tilde{\mathbf{g}}_k}. \quad (\text{A.17})$$

A.4 Proof of equation (3.43)

We start the derivation by inserting (3.42) and (3.36) into the expression

$$\tilde{\mathbf{g}}(i) = \tilde{\mathbf{a}}(\theta_1) - \hat{\tilde{\mathbf{R}}}(i) \tilde{\mathbf{v}}(i), \quad (\text{A.18})$$

resulting in

$$\tilde{\mathbf{g}}(i) = \tilde{\mathbf{a}}(\theta_1) - \left(\lambda \hat{\tilde{\mathbf{R}}}_{\text{dl}}(i-1) + \tilde{\mathbf{r}}(i) \tilde{\mathbf{r}}^H(i) + \xi \mathbf{I}_{2M} \right) \left(\tilde{\mathbf{v}}(i-1) + \alpha(i) \tilde{\mathbf{p}}(i) \right). \quad (\text{A.19})$$

Rearranging the terms, we get

$$\begin{aligned} \tilde{\mathbf{g}}(i) &= \tilde{\mathbf{a}}(\theta_1) - \left(\lambda \hat{\tilde{\mathbf{R}}}_{\text{dl}}(i-1) \tilde{\mathbf{v}}(i-1) + \tilde{\mathbf{r}}(i) \tilde{\mathbf{r}}^H(i) \tilde{\mathbf{v}}(i-1) \right) \\ &\quad - \left(\xi \mathbf{I}_{2M} \tilde{\mathbf{v}}(i-1) + \hat{\tilde{\mathbf{R}}}(i) \alpha(i) \tilde{\mathbf{p}}(i) \right), \end{aligned} \quad (\text{A.20})$$

which can be further simplified by applying an algebraic manipulation, leading to

$$\begin{aligned} \tilde{\mathbf{g}}(i) &= \tilde{\mathbf{a}}(\theta_1) - \lambda \tilde{\mathbf{a}}(\theta_1) + \lambda \left(\tilde{\mathbf{a}}(\theta_1) - \hat{\tilde{\mathbf{R}}}_{\text{dl}}(i-1) \tilde{\mathbf{v}}(i-1) \right) \\ &\quad - \tilde{\mathbf{r}}(i) \tilde{\mathbf{r}}^H(i) \tilde{\mathbf{v}}(i-1) - \xi \mathbf{I}_{2M} \tilde{\mathbf{v}}(i-1) - \hat{\tilde{\mathbf{R}}}(i) \alpha(i) \tilde{\mathbf{p}}(i). \end{aligned} \quad (\text{A.21})$$

Again, equation (3.42) is used to obtain the desired result

$$\tilde{\mathbf{g}}(i) = (1 - \lambda)\tilde{\mathbf{a}}(\theta_1) + \lambda\tilde{\mathbf{g}}(i - 1) - \left(\tilde{\mathbf{r}}(i)\tilde{\mathbf{r}}^H(i) + \xi\mathbf{I}_{2M}\right)\tilde{\mathbf{v}}(i - 1) - \alpha(i)\hat{\tilde{\mathbf{R}}}(i)\tilde{\mathbf{p}}(i). \quad (\text{A.22})$$

A.5 Proof of equation (5.30)

Applying the Cauchy-Schwarz inequality for matrices introduced in Lemma 5.2.4 to the Hermitian matrices $\mathbf{C} \in \mathbb{C}^{M \times M}$ and $\mathbf{R} \in \mathbb{C}^{M \times M}$ gives

$$|\langle \mathbf{R}, \mathbf{C} \rangle_F| \leq \|\mathbf{C}\|_F^2 \cdot \|\mathbf{R}\|_F^2 \quad (\text{A.23})$$

This expression can be formulated according to Lemma 5.2.2 as

$$\text{Tr}^2\{\mathbf{C}^H \mathbf{R}\} \leq \|\mathbf{C}\|_F^2 \cdot \|\mathbf{R}\|_F^2. \quad (\text{A.24})$$

After rearranging the terms, i.e.,

$$0 \leq \|\mathbf{C}\|_F^2 \cdot \|\mathbf{R}\|_F^2 - \text{Tr}^2\{\mathbf{C}^H \mathbf{R}\} \quad (\text{A.25})$$

and writing out the Frobenius norms and the trace, we obtain

$$0 \leq \sum_{i=1}^M \sum_{j=1}^M |c_{ij}|^2 \sum_{i=1}^M \sum_{j=1}^M |r_{ij}|^2 - \sum_{i=1}^M \sum_{j=1}^M (c_{ij}r_{ij})^2, \quad (\text{A.26})$$

which is always greater than zero as the first term contains the second term. The expression in (A.26) is only zero if the matrices \mathbf{C} and \mathbf{R} are identity matrices. However, this is not the case for the KA scheme.

The equation for γ is defined as

$$\gamma = \frac{\|\mathbf{R}\|_F^2 \|\mathbf{C}\|_F^2 - \text{Tr}^2\{\mathbf{C}^H \mathbf{R}\}}{\|\mathbf{C}\|_F^2}. \quad (\text{A.27})$$

From the above relations, we can conclude that the numerator is always greater than zero and thus, $\gamma > 0$, which concludes the proof.

ACRONYMS

ASK	Amplitude-Shift K eying
AVF	Auxiliary V ector F iltering
BPSK	Binary P hase S hift K eying
BS	Beam S pace
CG	Conjugate G radient
CRLB	Cramér-Rao L ower B ound
DFT	Discrete F ourier T ransform
DOA	Direction O f A rrival
DPSS	Discrete P rolate S pheroidal S equences
ESPRIT	Estimation of S ignal P arameters via R otational Invariance T echniques
EVD	Eigen V alue D ecomposition
FIR	Finite I mpulse R esponse
KA	Knowledge-Aided
LCMV	Linearly C onstrained M inimum V ariance
LC	Linear C ombination
LMS	Least M ean S quares
LS	Least S quares
MCG	Modified C onjugate G radient
ML	Maximum L ikelihood
MSE	Mean S quare E rror
MUSIC	M ultiple S ignal C lassification
MVDR	Minimum V ariance D istortionless R esponse
QPSK	Quadrature P hase-Shift K eying
RLS	Recursive L east S quares
RMSE	Root M ean S quare E rror
SINR	Signal-to-Interference-plus-Noise R atio
SLS	Structured L east S quares
SNR	Signal-to-Noise R atio
SOI	Source O f I nterest

STAP	Space-Time Adaptive Processing
SVD	Singular Value Decomposition
TLS	Total Least Squares
ULA	Uniform Linear Array
WL-CMV	Widely-Linearly Constrained Minimum Variance
WL	Widely-Linear

SYMBOLS AND NOTATION

Frequently used symbols

M	Number of sensor elements of the array
N	Number of snapshots
d	Number of incident signals
θ	Direction of arrival
\mathbf{I}_M	The $M \times M$ identity matrix
$\mathbf{\Pi}_M$	The $M \times M$ exchange matrix having only ones on its anti-diagonal and zeros elsewhere

Notation and operators

a, b, c	Scalars
$\mathbf{a}, \mathbf{b}, \mathbf{c}$	Column vectors
$\mathbf{A}, \mathbf{B}, \mathbf{C}$	Matrices
\mathbf{x}^*	Complex conjugate of \mathbf{x}
\mathbf{A}^T	Transpose of matrix \mathbf{A}
\mathbf{A}^H	Hermitian transpose of \mathbf{A}
$\text{Re}\{x\}$	Real part of x
$\text{Im}\{x\}$	Imaginary part of x
$\mathbb{E}\{\mathbf{x}\}$	Expected value of the random vector \mathbf{x}
$\ \mathbf{a}\ $	The Euclidean norm of the vector \mathbf{a}
$\ \mathbf{A}\ _F$	The Frobenius norm of the matrix \mathbf{A}
$\langle \mathbf{A}, \mathbf{B} \rangle_F$	The Frobenius norm inner product of \mathbf{A} and \mathbf{B}
$\text{Tr}\{\mathbf{A}\}$	The trace of the matrix \mathbf{A}
$\text{diag}\{\mathbf{x}\}$	Square matrix with the elements of the vector \mathbf{x} on its diagonal
$\text{span}\{\mathbf{A}\}$	Vector space spanned by the columns of the matrix \mathbf{A}

BIBLIOGRAPHY

- [1] H. V. Trees, *Optimum Array Processing: Part IV of Detection, Estimation, and Modulation Theory*, John Wiley & Sons, 2002.
- [2] D. G. Manolakis, V. K. Ingle, and S. M. Kogon, *Statistical and Adaptive Signal Processing: Spectral Estimation, Signal Modeling, Adaptive Filtering and Array Processing*, Artech House, 2005.
- [3] B. D. Van Veen and K. M. Buckley, "Beamforming: a versatile approach to spatial filtering," *IEEE ASSP Magazine*, vol. 5, no. 2, pp. 4–24, Apr. 1988.
- [4] O. L. Frost III, "An algorithm for linearly constrained adaptive array processing," *Proceedings of the IEEE*, vol. 60, no. 8, pp. 926–935, Aug. 1972.
- [5] S. Haykin, *Adaptive Filter Theory, 4th ed.*, Englewood Cliffs, New Jersey, USA: Prentice Hall Inc, 2002.
- [6] G. H. Golub and C. F. Loan, *Matrix Computations, 3rd ed.*, Baltimore, MD: Johns Hopkins Univ. Press, 1996.
- [7] G. K. Boray and M. D. Srinath, "Conjugate gradient techniques for adaptive filtering," *IEEE Transactions on Circuits and Systems I: Fundamental Theory and Applications*, vol. 39, no. 1, pp. 1–10, Jan. 1992.
- [8] P. S. Chang and Jr. A. N. Willson, "Analysis of conjugate gradient algorithms for adaptive filtering," *IEEE Transactions on Signal Processing*, vol. 48, no. 2, pp. 409–418, Feb. 2000.
- [9] D. A. Pados and G. N. Karystinos, "An iterative algorithm for the computation of the mvdr filter," *IEEE Transactions on Signal Processing*, vol. 49, no. 2, pp. 290–300, Feb. 2001.
- [10] H. Krim and M. Viberg, "Two decades of array signal processing research: parametric approach," *IEEE Signal Processing Magazine*, vol. 13, no. 4, pp. 67–94, July 1996.
- [11] J. Capon, "High-resolution frequency-wavenumber spectrum analysis," *Proceedings of the IEEE*, vol. 57, no. 8, pp. 1408–1418, Aug. 1969.
- [12] R. O. Schmidt, "Multiple emitter location and signal parameter estimation," *IEEE Transactions on Antennas and Propagation*, vol. 34, no. 3, pp. 276–280, Mar. 1986.
- [13] A. Barabell, "Improving the resolution performance of eigenstructure-based direction-finding algorithms," in *IEEE International Conference on Acoustics, Speech, and Signal Processing*, Apr. 1983, pp. 336–339.

- [14] R. H. Roy and T. Kailath, "ESPRIT-estimation of signal parameters via rotational invariance techniques," *IEEE Transactions on Acoustics, Speech, and Signal Processing*, vol. 37, no. 7, pp. 984–995, July 1989.
- [15] M. Haardt and J. A. Nosske, "Unitary ESPRIT: how to obtain increased estimation accuracy with a reduced computational burden," *IEEE Transactions on Signal Processing*, vol. 43, no. 5, pp. 1232–1242, May 1995.
- [16] R. Grover, D. A. Pados, and M. J. Medley, "Subspace direction finding with an auxiliary-vector basis," *IEEE Transactions on Signal Processing*, vol. 55, no. 2, pp. 758–763, Feb. 2007.
- [17] H. Semira, H. Belkacemi, and S. Marcos, "High-resolution source localization algorithm based on the conjugate gradient," *EURASIP Journal on Advances in Signal Processing*, vol. 2007, no. 2, pp. 1–9, June 2007.
- [18] I. Ziskind and M. Wax, "Maximum likelihood localization of multiple sources by alternating projection," *IEEE Transactions on Acoustics, Speech and Signal Processing*, vol. 36, no. 10, pp. 1553–1560, Oct. 1988.
- [19] P. J. Schreier and L. L. Scharf, "Second-order analysis of improper complex random vectors and processes," *IEEE Transactions on Signal Processing*, vol. 51, no. 3, pp. 714–725, Mar. 2003.
- [20] T. McWhorter and P. J. Schreier, "Widely-linear beamforming," in *Thirty-Seventh Asilomar Conference on Signals, Systems and Computers*, 2003, vol. 1, pp. 753–759.
- [21] P. Chevalier, J. P. Delmas, and A. Oukaci, "Optimal widely linear MVDR beamforming for noncircular signals," in *IEEE International Conference on Acoustics, Speech and Signal Processing*, 2009, pp. 3573–3576.
- [22] S. C. Douglas, "Widely-linear recursive least-squares algorithm for adaptive beamforming," in *IEEE International Conference on Acoustics, Speech and Signal Processing*, 2009, pp. 2041–2044.
- [23] L. Wang and R. C. de Lamare, "Constrained adaptive filtering algorithms based on conjugate gradient techniques for beamforming," *IET Signal Processing*, vol. 4, no. 6, pp. 686–697, Dec. 2010.
- [24] P. J. Schreier and L. L. Scharf, *Statistical Signal Processing of Complex-Valued Data: The Theory of Improper and Noncircular Signals*, Cambridge University Press, 2010.
- [25] F. Römer, "Advances in subspace-based parameter estimation: Tensor-ESPRIT-type methods and non-circular sources," Diploma thesis, Technische Universität Ilmenau, 2006.
- [26] B. D. Carlson, "Covariance matrix estimation errors and diagonal loading in adaptive arrays," *IEEE Transactions on Aerospace and Electronic Systems*, vol. 24, no. 4, pp. 397–401, July 1988.
- [27] H. Cox, R. M. Zeskind, and M. H. Owen, "Robust adaptive beamforming," *IEEE Transactions on Acoustics, Speech and Signal Processing*, vol. ASSP-35, pp. 1365–1376, Oct. 1987.

- [28] R. C. de Lamare, L. Wang, and R. Fa, "Adaptive reduced-rank LCMV beamforming algorithms based on joint iterative optimization of filters: design and analysis," *Elsevier Signal Processing*, vol. 90, no. 2, pp. 640–652, Feb. 2010.
- [29] M. E. Weippert, J. D. Hiemstra, J. S. Goldstein, and M. D. Zoltowski, "Insights from the relationship between the multistage wiener filter and the method of conjugate gradients," in *Proceedings of IEEE Sensor Array and Multichannel Signal Processing Workshop*, 2002, pp. 388–392.
- [30] D. G. Luenberger, *Linear and Nonlinear Programming, 2nd ed.*, Reading, MA: Addison-Wesley, 1984.
- [31] G. Bienvenu and L. Kopp, "Decreasing high resolution method sensitivity by conventional beamformer preprocessing," in *IEEE International Conference on Acoustics, Speech, and Signal Processing*, Mar. 1984, pp. 714–717.
- [32] H. Lee and M. Wengrovitz, "Resolution threshold of beamspace MUSIC for two closely spaced emitters," *IEEE Transactions on Acoustics, Speech, and Signal Processing*, vol. 38, no. 9, pp. 1545–1559, Sept. 1990.
- [33] M. D. Zoltowski, G. M. Kautz, and S. D. Silverstein, "Beamspace root-MUSIC," *IEEE Transactions on Signal Processing*, vol. 41, no. 1, pp. 344–364, Jan. 1993.
- [34] G. Xu, S. D. Silverstein, R. H. Roy, and T. Kailath, "Beamspace ESPRIT," *IEEE Transactions on Signal Processing*, vol. 42, no. 2, pp. 349–356, Feb. 1994.
- [35] D. Slepian, "Prolate spheroidal wave functions, Fourier analysis, and uncertainty; v: the discrete case," *The Bell system Technical Journal*, vol. 57, no. 5, pp. 1371–1429, May 1978.
- [36] P. Forster and G. Vezzosi, "Application of spheroidal sequences to array processing," in *IEEE International Conference on Acoustics, Speech, and Signal Processing*, Apr. 1987, pp. 2268–2271.
- [37] W. Chen, U. Mitra, and P. Schniter, "On the equivalence of three reduced rank linear estimators with applications to DS-CDMA," *IEEE Transactions on Information Theory*, vol. 48, no. 9, pp. 2609–2614, Sept. 2002.
- [38] W. L. Melvin and J. R. Guerci, "Knowledge-aided signal processing: a new paradigm for radar and other advanced sensors," *IEEE Transactions on Aerospace and Electronic Systems*, vol. 42, no. 3, pp. 983–996, July 2006.
- [39] W. L. Melvin and G. A. Showman, "An approach to knowledge-aided covariance estimation," *IEEE Transactions on Aerospace and Electronic Systems*, vol. 42, no. 3, pp. 1021–1042, July 2006.
- [40] J. S. Bergin, C. M. Teixeira, P. M. Techau, and J. R. Guerci, "Improved clutter mitigation performance using knowledge-aided space-time adaptive processing," *IEEE Transactions on Aerospace and Electronic Systems*, vol. 42, no. 3, pp. 997–1009, July 2006.
- [41] P. Stoica, J. Li, X. Zhu, and J. R. Guerci, "On using a priori knowledge in space-time adaptive processing," *IEEE Transactions on Signal Processing*, vol. 56, no. 6, pp. 2598–2602, June 2008.

- [42] X. Zhu, J. Li, and P. Stoica, “Knowledge-aided adaptive beamforming,” *IET Signal Processing*, vol. 2, no. 4, pp. 335–345, Dec. 2008.
- [43] R. Fa, R. C. de Lamare, and V. H. Nascimento, “Knowledge-aided STAP algorithm using convex combination of inverse covariance matrices for heterogenous clutter,” in *IEEE International Conference on Acoustics, Speech, and Signal Processing*, Mar. 2010, pp. 2742–2745.
- [44] R. Fa and R. C. de Lamare, “Knowledge-aided reduced-rank STAP for MIMO radar based on joint iterative constrained optimization of adaptive filters with multiple constraints,” in *IEEE International Conference on Acoustics, Speech, and Signal Processing*, Mar. 2010, pp. 2762–2765.
- [45] R. D. DeGroat, E. M. Dowling, and D. A. Linebarger, “The constrained MUSIC problem,” *IEEE Transactions on Signal Processing*, vol. 41, no. 3, pp. 1445–1449, Mar. 1993.
- [46] R. Boyer and G. Bouleux, “Oblique projections for direction-of-arrival estimation with prior knowledge,” *IEEE Transactions on Signal Processing*, vol. 56, no. 4, pp. 1374–1387, Apr. 2008.
- [47] M. Haardt, “Structured least squares to improve the performance of ESPRIT-type algorithms,” *IEEE Transactions on Signal Processing*, vol. 45, no. 3, pp. 792–799, Mar. 1997.
- [48] S. U. Pillai and B. H. Kwon, “Forward/backward spatial smoothing techniques for coherent signal identification,” *IEEE Transactions on Acoustics, Speech, and Signal Processing*, vol. 37, no. 1, pp. 8–15, Jan. 1989.
- [49] A. Lee, “Centrohermitian and skew-centrohermitian matrices,” *Linear Algebra and its Applications*, vol. 29, pp. 205–210, 1980.
- [50] M. Haardt, *Efficient One-, Two-, and Multidimensional High-Resolution Array Signal Processing*, Ph.D. thesis, Technische Universität München, Shaker Verlag, Aachen, 1997.
- [51] M. D. Zoltowski, M. Haardt, and C. P. Mathews, “Closed-form 2-D angle estimation with rectangular arrays in element space or beamspace via unitary ESPRIT,” *IEEE Transactions on Signal Processing*, vol. 44, no. 2, pp. 316–328, Feb. 1996.
- [52] L. Wang, R. C. de Lamare, and M. Haardt, “Reduced-rank DOA estimation based on joint iterative subspace recursive optimization and grid search,” in *IEEE International Conference on Acoustics, Speech, and Signal Processing*, Mar. 2010, pp. 2626–2629.
- [53] R. C. de Lamare, “Adaptive reduced-rank LCMV beamforming algorithms based on joint iterative optimisation of filters,” *Electronics Letters*, vol. 44, no. 9, pp. 565–566, Apr. 2008.
- [54] L. Wang and R. C. de Lamare, “Low-complexity adaptive step size constrained constant modulus SG algorithms for blind adaptive beamforming,” *Signal Processing*, vol. 89, no. 12, pp. 2503–2513, Dec. 2009.

THESES

- T1: The well-known Krylov-based adaptive beamforming algorithms employing the minimum variance principle are insufficiently designed if the signal sources are strictly non-circular.
- T2: By widely-linear processing, these adaptive algorithms can be advanced to fully exploit the strict non-circularity, providing significantly better convergence and steady-state performance.
- T3: The resolution performance of the existing Krylov subspace-based direction finding methods can be further improved by operation in the beamspace, which simultaneously reduces the computational complexity.
- T4: The beamspace transformation matrix applying discrete prolate spheroidal sequences constitutes a more adequate beamspace design and provides more accurate parameter estimates.
- T5: Incorporating prior knowledge in the direction finding procedure is an efficient way of enhancing the estimates of signal directions. Previously developed strategies to exploit this information break down in extreme conditions. A more robust approach developed in this work utilizes the prior knowledge to improve the covariance matrix and performs best under exactly those severe conditions.
- T6: The performance advantage of the proposed knowledge-aided direction finding scheme is more pronounced in combination with ESPRIT-type algorithms.

May 9, 2011

Jens Steinwandt

ERKLÄRUNG

Die vorliegende Arbeit habe ich selbstständig ohne Benutzung anderer als der angegebenen Quellen angefertigt. Alle Stellen, die wörtlich oder sinngemäß aus veröffentlichten Quellen entnommen wurden, sind als solche kenntlich gemacht. Die Arbeit ist in gleicher oder ähnlicher Form oder auszugsweise im Rahmen einer oder anderer Prüfungen noch nicht vorgelegt worden.

Ilmenau, den 9. Mai 2011

Jens Steinwandt